Chair of Reservoir Engineering

Master's Thesis

Wettability Changes due to Nanomaterials and Alkali in Spontaneous Imbibition Experiments

Samhar Saleh, BSc

November 2020

MONTANUNIVERSITÄT LEOBEN

MASTER THESIS

Wettability Changes due to Nanomaterials and Alkali in Spontaneous Imbibition Experiments

---

Author:
Samhar SALEH

Supervisors:
Univ.-Prof. Dr. Holger OTT
Dr. Rafael E. HINCAPIE
Dr. Elisabeth NEUBAUER
Dr. Torsten CLEMENS

A thesis submitted in fulfillment of the requirements
for the degree of Master of Science

in the

Department of Petroleum Engineering
Chair of Reservoir Engineering

November 26, 2020

"To my beloved family for their endless love and support..
To Verena who motivated me during this work..
To every one who taught me a word..
To all my friends who supported me alongside this journey.."

Samhar Saleh

MONTANUNIVERSITÄT LEOBEN
www.unileoben.ac.at

EIDESSTATTLICHE ERKLÄRUNG

Ich erkläre an Eides statt, dass ich diese Arbeit selbständig verfasst, andere als die angegebenen Quellen und Hilfsmittel nicht benutzt, und mich auch sonst keiner unerlaubten Hilfsmittel bedient habe.

Ich erkläre, dass ich die Richtlinien des Senats der Montanuniversität Leoben zu "Gute wissenschaftliche Praxis" gelesen, verstanden und befolgt habe.

Weiters erkläre ich, dass die elektronische und gedruckte Version der eingereichten wissenschaftlichen Abschlussarbeit formal und inhaltlich identisch sind.

Datum 23.11.2020

Unterschrift Verfasser/in
Samhar Saleh

Acknowledgements

I would like to thank my family who never stopped supporting me in good and bad times. Furthermore, I would like to express my gratitude OMV for sponsoring this thesis and giving me opportunity to work in state-of-the-art research facility.

I owe a huge dept of gratitude Dr.-Ing. Rafael Hincapie and Elisabeth Neubauer who supervised my thesis. I am also very thankful for *Tech Center and Lab* team especially to Ante Borovina and Magdalena Biernat who supported me a lot alongside the entire road. I would also like to thank Dr. Torsten Clemens for the insightful discussions during my journey with OMV. Finally, I am expressing my gratitude to my professor and supervisor Prof. Holger Ott for his support and supervision during my studies and for his valuable input all over this work.

Abstract

Nanomaterials gained a lot of attention in the past few years. Recent studies revealed that silica nanomaterials can be a very promising agent in enhanced oil recovery (EOR) operations. Previous researches discussed the potential synergy between nanomaterials and other EOR agents like surfactants or polymers and substantial impact on key EOR mechanisms like emulsion stabilization and wettability alteration.

In this work, the usage of silica nanomaterials and alkali in enhanced oil recovery was investigated through spontaneous imbibition tests, IFT measurements and phase behavior. The additional recovery was assessed for different rock/oil systems. The main goal was to evaluate the wettability alteration induced by the synergy between nanomaterials and alkali. Moreover, numerical analysis of the results by the means of inverse Bond number and capillary diffusion coefficient was carried out.

In the experimental part, two types of nanomaterials with different surface modification were tested. The influence of rock type on the recovery process was investigated by using Berea and Keuper outcrop materials. The influence of oil composition was examined by using two crude oil samples with different total acid numbers (TAN). Sodium carbonate (Na_2CO_3) was used as an alkaline agent and two types of synthetic brine were utilized in order to investigate the effect of brine composition on the recovery. Interfacial tension (IFT) measurements showed that nanomaterials are very effective in terms of IFT reduction. The surface charge of the nanomaterials plays an important role in this process. A good synergy with alkali lead to very low IFT values ($0.04\,\mathrm{mN\,m^{-1}}$). This effect was also seen in the phase behavior tests, where brine/oil systems with lower IFT exhibited better emulsification. Nanomaterials contribution to the phase behavior was mainly the stabilization of the emulsion mid-phase. The influence of TAN number on the IFT and the phase behavior was very prominent, especially when combined with alkali. Rock-fluid interactions were assessed using Amott tests which rely on spontaneous imbibition mechanism. This mechanism is very sensitive to wettability changes.

The enhancements observed within fluid-fluid interactions - especially IFT reduction - resulted in additional recovery ranging from 4 to 50% on top of the baseline under spontaneous imbibition, which was confirmed by inverse Bond number analysis. Promising results (97.7% of OOIP) were achieved using novel EOR formulations of alkali and nanomaterials. These values were attributed to wettability alteration that accelerated the imbibition kinetics as shown in capillary diffusion coefficient analysis.

Rock-fluid interactions are very complex and require a deeper understanding for the initial wettability state of each rock-oil system. This opens the door for future investigation, which might include contact angle measurements and forced imbibition.

Zusammenfassung

Nanomaterialien erhielten in den letzten Jahren viel Aufmerksamkeit. Neueste Studien zeigten, dass Silica-Nanomaterialien ein vielversprechendes Mittel für EOR-Operationen (Verbesserte Ölgewinnung) sein können. in früheren Studien wurden die möglichen Synergien zwischen Nanomaterialien und anderen EOR-Mitteln wie Tensid oder Polymer diskutiert. Nanomaterialien ein wesentlicher Einfluss auf wichtige EOR-Mechanismen wie Emulsionsstabilisierung und Umbenetzung zugeschrieben.

In dieser Arbeit wurde die Verwendung von Silica-Nanomaterialien und Alkali zur verbesserten Ölgewinnung durch spontane Imbibitionstests, Grenzflächenspannungsmessung und Phasenverhalten untersucht. Die zusätzliche Gewinnung wurde für verschiedene Gesteins- / Ölsysteme ausgewertet. Das Hauptziel war die Untersuchung der durch die Synergie zwischen Nanomaterialien und Alkali hervorgerufenen Änderung der Benetzbarkeit. Darüber hinaus wurde eine numerische Analyse der Ergebnisse mittels inverser Bond-Zahl und kapillarem Diffusionskoeffizienten durchgeführt. Im experimentellen Teil wurden zwei Arten von Nanomaterialien mit unterschiedlicher Oberflächenmodifikation getestet. Der Einfluss des Gesteinstyps auf den Ölgewinnungsprozess wurde durch zwei Gesteinstypen (Berea und Keuper) getestet. Keuper unterscheidet sich von Berea durch den höheren Tongehalt und die höhere Durchlässigkeit. Der Einfluss der Ölzusammensetzung wurde durch die Verwendung zweier Rohölproben mit unterschiedlichem Säuregehalt (TAN) bestimmt. Natriumcarbonat (Na_2CO_3) wurde als alkalisches Mittel verwendet, und zwei Arten von synthetischer Salzlösung wurden verwendet, um den Effekt der Solenzusammensetzung auf die Ölgewinnung zu untersuchen.

Messungen der Grenzflächenspannung (IFT) zeigten, dass Nanomaterialien hinsichtlich der IFT-Reduktion sehr effektiv sind. Die Oberflächenladung der Nanomaterialien spielt dabei eine wichtige Rolle. Partikeln mit neutral geladener Oberfläche können einfacher as der Grenzflächen zwischen Liquidphasen adsorbieren. Eine gute Synergie mit Alkali führt zu sehr niedrigen IFT-Werten ($0.04\,\mathrm{mN\,m^{-1}}$). Dieser Effekt wurde auch im Phasenverhalten beobachtet, bei denen Chemikalien/Öl-Systeme mit niedrigerer IFT eine bessere Emulgierung zeigten. Der Beitrag von Nanomaterialien zum Phasenverhalten war hauptsächlich die Stabilisierung der Emulsionsmittelphase. Der Einfluss der TAN-Zahl auf die IFT und das Phasenverhalten war besonders in Kombination mit Alkali sehr ausgeprägt.

Die bei Fluid-Fluid-Wechselwirkungen beobachteten Verbesserungen - insbesondere die IFT-Reduktion - führten zu einer zusätzlichen Ölgewinnung in den spontanen Imbibitionstests durch inverse Bond-Zahlsanalyse bestätigt. In unterschiedlichem Maße jedoch. Die Wechselwirkungen zwischen Gestein und Flüssigkeit sind sehr komplex und erfordern ein tiefes Verständnis der spezifischen Öl / Gesteins-Systeme und der Faktoren, die zu ihrem anfänglichen Benetzungszustand beitragen. Vielversprechende Ergebnisse (97.7% OOIP) wurden mit neuartigen EOR-Rezepturen mit Alkali und Nanomaterialien erzielt. Die erhöhte Entölung wurde auf eine Änderung der Benetzbarkeit zurückgeführt, die die Kinetik der spontanen Imbibition beschleunigte, wie in der Analyse des kapillaren Diffusionskoeffizienten gezeigt. Weitergehende Untersuchungen der Gesteins-Fluid Wechselwirkungen sollten Kontaktwinkelmessung und erzwungene Imbibition umfassen.

Contents

Affidavit v

Acknowledgements vii

Abstract ix

Zusammenfassung xi

1 Introduction 1
- 1.1 Background . . . 1
- 1.2 Research Objective . . . 2
- 1.3 Outline . . . 2

2 Fundamentals 3
- 2.1 Enhanced Oil Recovery . . . 3
- 2.2 Wettability . . . 3
- 2.3 Interfacial Tension . . . 8
- 2.4 Phase Behavior . . . 9
- 2.5 Mobility Ratio . . . 11
- 2.6 Alkaline Flooding . . . 12
- 2.7 Spontaneous Imbibition . . . 14

3 State of the Art 19
- 3.1 Nanotechnology . . . 19
- 3.2 Recovery Mechanisms . . . 21

4 Materials and Methods 31
- 4.1 Materials . . . 31
- 4.2 Experimental Procedure . . . 37

5 Results and Discussion 49
- 5.1 Interfacial Tension . . . 49
- 5.2 Phase Behavior . . . 52
- 5.3 Spontaneous Imbibition . . . 57
- 5.4 Dean-Stark Extraction . . . 70
- 5.5 Numerical Analysis . . . 72

6 Final Conclusions **77**
6.1 Summary . . . 77
6.2 Overall Conclusion . . . 79
6.3 Future Work . . . 80

Bibliography **81**

List of Figures

2.1 Contact angle . . . 5
2.2 Wettability measurement and capillary pressure . . . 6
2.3 Schematic of sessile drop . . . 8
2.4 Capillary desaturation curve . . . 9
2.5 Schematic of surfactant molecule . . . 10
2.6 *Winsor*'s classification of microemulsions . . . 11
2.7 Schematic of alkali reaction . . . 13
2.8 Co-current vs counter-current spontaneous imbibition . . . 15

3.1 sweep efficiency as a function of pore volumes (PV) (Singh et al. 2017) . . . 22
3.2 Pore plugging mechanisms . . . 25
3.3 Effect of structural disjoining pressure on meniscus profile (Chengara et al. 2004) . . . 26
3.4 Disjoining Pressure Parameters . . . 27
3.5 Pore scale view of wettability . . . 28

4.1 Photo of both rock types . . . 31
4.2 Berea thin section . . . 32
4.3 Phi vs K for Berea . . . 32
4.4 Phi vs K for Keuper . . . 33
4.5 ζ-potential and specific conductivity . . . 34
4.6 SEM imaging of both nanomaterials . . . 35
4.7 Helium Porosimeter . . . 38
4.8 Anton Paar DMA 5000 M (Anton Paar 2020) . . . 39
4.9 Tensiometer . . . 40
4.10 Spinning Drop . . . 41
4.11 Schematic of prestauration setup . . . 42
4.12 Mean grain size of core plug Keuper 123 . . . 44
4.13 ΔP vs time for different rates - Keuper 123 . . . 44
4.14 Permeability to water, measured vs fitted . . . 45
4.15 Amott Cell . . . 46
4.16 Amott cells in the oven . . . 46
4.17 Dean-stark apparatus . . . 47

5.1 Interfacial tension vs time - High TAN oil . . . 50
5.2 Interfacial tension vs time - Low TAN oil . . . 51
5.3 Sedimentation . . . 53
5.4 Emulsion volume vs time - High TAN oil . . . 54
5.5 Formed emulsion with alkali and nanomaterials - High TAN oil . . . 55

5.6 Emulsion volume vs time - Low TAN oil 56
5.7 Formed emulsion with alkali and nanomaterials - Low TAN oil 57
5.8 Baseline 58
5.9 Oil droplets on Keuper core plug 59
5.10 Baseline-Berea cores 60
5.11 Baseline Keuper High TAN 61
5.12 Oil recovery from Berea core plugs using nanomaterials 62
5.13 Oil recovery from Keuper core plugs using nanomaterials 63
5.14 Oil recovery from Berea cores using nanomaterials only 64
5.15 Oil recovery from Keuper cores using nanomaterials only 65
5.16 Oil recovery from core plugs using nanomaterials 66
5.17 Oil recovery from Berea cores - High TAN oil 67
5.18 Oil recovery from Berea cores - Low TAN oil 68
5.19 Oil recovery from Keuper cores - High TAN oil - Alkali 69
5.20 Oil recovery from Keuper cores - Low TAN oil - Alkali 70
5.21 Recovery curve comparison 72
5.22 Recovery vs $N_B^{-}1$ - Literature 73
5.23 Ultimate recovery vs $N_B^{-}1$ 74
5.24 Relative oil saturation vs square root of time 75

List of Tables

2.1 Contact angle values for different wettability systems (McPhee et al. 2015) 5
2.2 Amott Wetting Indices (McPhee et al. 2015) 7

3.1 Critical properties of CO_2 (Linstrom, 2020) 21

4.1 Properties of Berea core plugs 32
4.2 Properties of Keuper core plugs 33
4.3 Properties of the utilized nanomaterials 34
4.4 Properties of crude oil samples 36
4.5 Composition of synthetic brine 36
4.6 Properties of the utilized fluids 37
4.7 Regression Parameters 45

5.1 Summary of IFT values of various oil/brine systems 52
5.2 Investigated parameters using SI tests 57
5.3 Summary of oil ultimate recoveries in Berea core plugs 68
5.4 Summary of oil ultimate recoveries in Keuper core plugs 70
5.5 Dean-Stark results 71
5.6 Results of the computations performed on each core 75

List of Abbreviations

HSE	**H**ealth **S**afety **E**nvironment
NP	**N**ano- **P**articles
EOR	**E**nhanced **O**il **R**ecovery
ASP	**A**lkali **S**urfactant **P**olymer
IFT	**I**nter- **F**acial **T**ension
SI	**S**pontaneous **I**mbibition
PV	**P**ore **V**olume
SEM	**S**canning **E**lectron **M**icroscopy
AFM	**A**tomic **F**orce **M**icroscopy
CT	**C**omputed **T**omography
WIP	**W**ater- **I**n **P**lace
OIP	**O**il **I**n **P**lace
OOIP	**O**riginal **O**il **I**n **P**lace
ppm	**P**arts **P**er **M**illion

List of Symbols

S	Saturation	%
ϕ	Porosity	%
K	Permeability	mD
ζ	Zeta-potential	mV
σ	Interfacial tension	$\mathrm{mN\,m^{-1}}$
ω	Angular velocity	rpm
ρ	Density	$\mathrm{kg/m^3}$
μ	Viscosity	cP
P_c	Capillary pressure	Pa
$N_B^{-}1$	Inverse Bond number	-
N_C	Capillary number	-
M	Mobility ratio	-
L_D	Characteristic length	-
t_D	Dimensionless time	-

Chapter 1

Introduction

1.1 Background

As the wheel of the oil industry turns to fulfill the growing global demand, keeping a secure energy supply became a vital mission for the industry worldwide. Despite the growing concerns regarding global warming, fossil fuel especially oil and gas is still the cornerstone in today's energy portfolio [1]. Reservoir engineers are confronted with crucial task, namely, to exploit the current resources in the most efficient way using environment-friendly techniques in order to adapt to the environmental policies. Enhanced oil recovery (EOR) became an important research area for oil companies. Unlocking the potential of oil fields which have reached their plateau or started showing a productivity decline can extend the life of the existing resources and provide promising prospective for meeting the global energy demand.

Enhanced oil recovery can be conducted by chemical, thermal or solvent means. Chemical EOR (CEOR) includes injecting certain chemicals like polymers, surfactant or alkali to tune key reservoir properties and maximize the ultimate recovery. Alkali flooding is one of the most common chemical EOR methods. It takes advantage of the reaction of acidic components in the oil with injected alkali to form insitu surfactants (soap) (Sheng 2013).

Nanotechnology has attracted an increasing interest since the 1980s. It was the driving force behind revolutionizing some industries e.g. pharmaceutics, biotechnology, and material science. These achievements draw the attention of petroleum industry to utilize this technology and find novel applications in upstream as well as in downstream. Health, safety and environment (HSE) are some of the main concerns of nanotechnology. Despite their toxicology the base of many environmental and medical applications (e.g., adsorption contaminant, green nanotechnology and nanosensors, etc.) (Taghavi et al. 2013), nanomaterials can have very hazardous effects on the living matter and their toxicology can be reduced or increased by the surface modification and the particle size (Yang et al. 2005). Therefore, an environmental risk assessment is vital before any roll out of nanotechnology (Taghavi et al. 2013).

In addition to their low cost and availability (Ali et al. 2018), research proved that silica nanoparticles can significantly improve key EOR mechanisms like emulsion stability or wettability alteration (Almahfood et al. 2018). Thus, researchers started to investigate the nano-EOR potential using silica nanoparticles as a standalone EOR agent or evoke the synergy between nanoparticles and other EOR agents like surfactants or polymers.

---

[1] See Enerdata 2019

However, there has been a little effort on the synergy between nanoparticles and in situ generated surfactant during alkali flooding.

1.2 Research Objective

This research tries to shed some light on the role of nanoparticles during alkali flooding. The study considers two groups of interactions: fluid-fluid and rock-fluid interactions. The focus of this work is wettability alteration potential which is mainly evaluated by spontaneous imbibition test. It is also a part of EOR screening workflow that investigates several EOR agents under various conditions. This will help screening the future EOR candidates.

1.3 Outline

This work consists of six chapters. The focus of each them is briefly as follows:

Chapter 1 previews the motivation behind this work and briefly discusses the role of nanotechnology and EOR.

Chapter 2 reviews the fundamental concepts which are vital for this study.

Chapter 3 reviews other experimental works that have been conducted in this field and presents the state of the art knowledge.

Chapter 4 describes the materials and experimental approaches, which were used in the course of this thesis.

Chapter 5 depicts the results obtained from the experimental work and analyses them by the means of different numerical approaches.

Chapter 6 summarizes the conclusions drawn in the course of this study.

Chapter 2

Fundamentals

This chapter handles the basic concepts which this work is trying to approach.

2.1 Enhanced Oil Recovery

Enhanced oil recovery (EOR) processes include altering the properties of oil/rock/brine system in order to improve the displacement process (Ezekwe 2011).

EOR agents interact with the reservoir rock/oil/brine system, possibly leading to reduction of the interfacial tensions (IFT), oil swelling, favorable mobility ratio, wettability modification, favorable phase behavior or optimized mobility ratio. EOR techniques are generally classified into four main categories:

- chemical
- thermal
- gas/solvent
- other methods

2.2 Wettability

In multiphase flow, porous media exhibit a certain tendency towards one of the phases to adsorb on the rock surface. This material property is called *wettability* (Blunt 2017).

2.2.1 Wettability States Related to Oil Recovery

Water-Wet State

In water/oil/rock system, the rock is considered to be *water-wet* when more than 50% of its pore surface is covered by water. As a result, water forms a thin film that coats pore walls allowing it to occupy small pores. The oleic phase in the system occupies larger pores in form of droplets at the center that rest on the water film (Schön et al. 2015). Therefore, the water phase is continuous throughout the pore space while oil flows discontinuously unless the water saturation is close to initial water saturation S_{wi}. Note that in such a case, remaining or irreducible water saturation is high.In this case, water is called *Wetting Phase* (Donaldson et al. 2010). When a water-wet rock saturated with oil gets into contact with water, the water spontaneously displaces the oil. This phenomenon is called *Spontaneous Imbibition* and the driver is capillary forces. The displacement process takes place until an equilibrium between surface and capillary forces is established. Spontaneous imbibition is a crucial recovery mechanism especially in naturally fractured reservoirs, where most of the oil is stored in the tight matrix (Morrow et al. 2001). Spontaneous imbibition will be discussed more thoroughly in section 2.7. As a matter of background, most of sandstone reservoirs are neutral to water-wet (Lyons 2009).

Fractional Wettability State

This wettability state prevails when a random distribution of the preferential wetting is observed throughout the rock. This can be explained by the rock heterogeneity and the random distribution of some minerals that promotes a specific wetting state (Tiab et al. 2012).

Mixed-wet State

This state occurs when the small pores of the rock shows a water-wet behavior and filled with water while the larger pores are oil-saturated and are preferentially oil-wet (Tiab et al. 2012). The reason behind this condition is probably linked to the reservoir formation conditions. When oil migrates into the reservoir and displaces the connate water, oil droplets can easily occupy large pores, while the capillary entry pressure of smaller pores cannot not be overcome. Thus, these pores contain the connate water and remain water-wet. Afterwards, oil in the larger pores displaced the original connate water film from the pore walls and renders the wettability state towards oil-wet (Donaldson et al. 2010).

In mixed-wet state, oil prefers to flow via ganglion mechanism unlike water-wet state where the flow is mainly governed by oil filling and snap-off events (Rücker et al. 2019).

Oil-wet State

At this wettability state, smaller pores are filled with oil while water is located only in the larger pores in form of big droplets laying on an oil film that coats pore surfaces. Oil and water in this case are called wetting phase and nonwetting phase respectively. At high water saturation, water can flow as continuous phase through the pore network. However, at any oil saturation greater than residual oil saturation (S_{or}), oil becomes the continuous phase (Donaldson et al. 2010). The wettability of most carbonate reservoirs ranges between neutral to strongly oil wet (Narr 2011).

2.2.2 Initial Wettability State

Numerous factors that can contribute to the wettability state of a rock, e.g. oil polar components, asphaltene precipitation and clay minerals. Some of sandstone reservoirs are oil-wet when the oil is rich of polar components that got attached on the mineral surface (Donaldson et al. 2010). Asphaltene precipitation on the mineral surface can occur due to either colloidal instability or polar interaction depending on the rock mineralogy (Buckley 1998, Buckley 1995). Clay minerals in sandstone reservoirs - despite their low content - can strongly affect the initial wettability state. Moreover, higher clay content promotes more oil wetness at low to moderate salinity formations (Sayyouh et al. 1990).

2.2.3 Evaluation and Characterization of Wettability

Quantitative Evaluation

Contact angle: Contact angle measurements are a widely used tool to assess the wettability of a mineral surface. The main advantage is the ability to measure wettability on a clean surface eliminating factors like sample contamination by mud filtration, etc. (Peters 2012). A mineral surface (quartz/glass, clay or calcite) or a clean rock sample can be used.

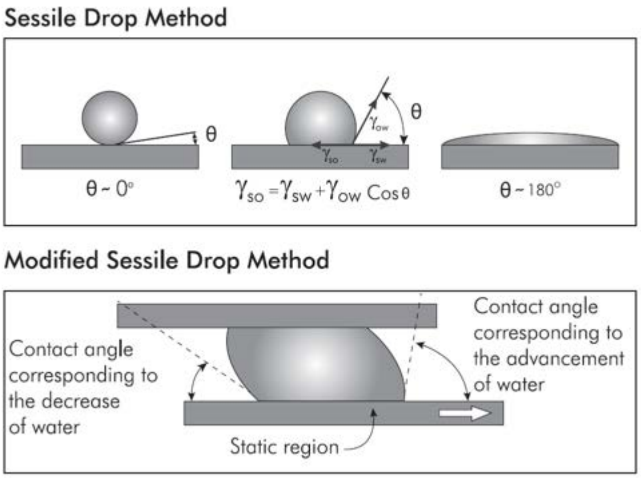
Sessile Drop Method
θ
θ ~ 0°
γ_{ow}
θ
γ_{so}
γ_{sw}
$\gamma_{so} = \gamma_{sw} + \gamma_{ow} \cos\theta$
θ ~ 180°
Modified Sessile Drop Method
Contact angle corresponding to the advancement of water
Contact angle corresponding to the decrease of water
Static region

FIGURE 2.1: Contact angle measurement using sessile drop and modified sessile drop (McPhee et al. 2015)

Despite that the contact angle method provides a reliable assessment at a small scale, upscaling the results might be challenging especially in case of heterogeneous reservoir. Surface roughness might cause deviation from the ideal behavior. In a dynamic state, one can distinguish between advancing and receding contact angle. The deviation from advancing to receding contact angle is called *Contact Angle Hysteresis* (Blunt 2017).

TABLE 2.1: Contact angle values for different wettability systems (McPhee et al. 2015)

	Water-wet	**Neutrally-wet**	**Oil-wet**
Min	0	60-75	105-120
Max	60-75	105-120	180

Amott-Harvey: A technique considers two different processes: 1) Imbibition: Invasion of the wetting phase and 2) Drainage: Invasion of the nonwetting phase. These processes are carried out spontaneously and under force. A common convention is to call an increase in water saturation an *Imbibition* and an increase in oil saturation a *Drainage* as shown in figure 2.2.

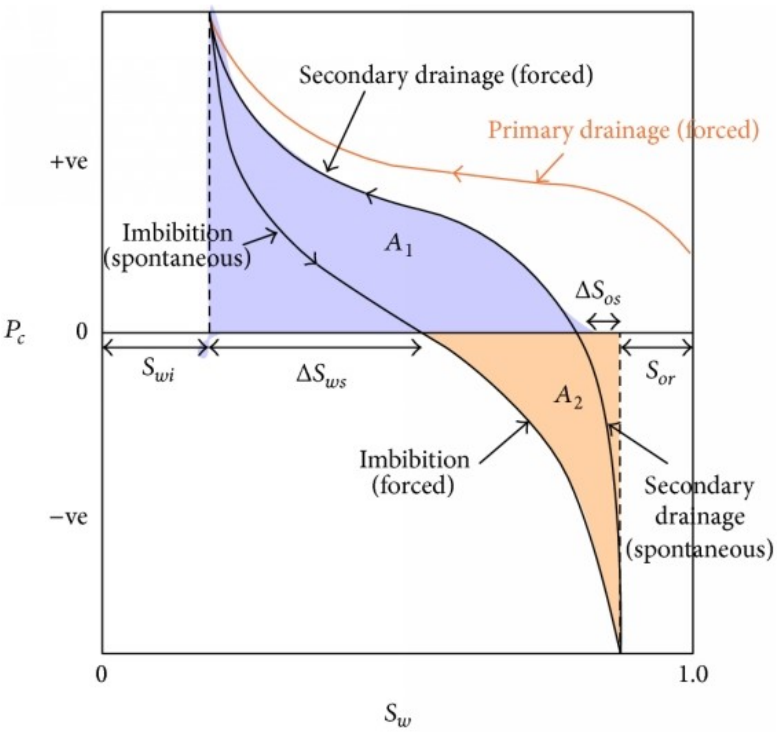

FIGURE 2.2: Capillary pressure curve during drainage and imbibition (Falode et al. 2014)

According to McPhee et al. 2015, the Amott-Harvey Procedure after is as follow:

1.cAmott A A core plug is saturated initially with oil until S_{wir} (irreducible water saturation) undergoes a spontaneous brine imbibition. Textbooks recommend 480 hours (McPhee et al. 2015) until the equilibrium is reached. The water saturation change is ΔS_{ws} (see figure 2.2)

2. **Amott B** Forced imbibition of water using centrifuge or Hassler cell. This step is carried out until S_{or} is reached.

3. **Amott C** Spontaneous Oil imbibition. The produced water volume is recorder over time and this step is carried out until the system is at equilibrium state. For an oil-wet core, the imbibed oil volume will be significantly high. The oil saturation change is indicated by ΔS_{os}

4. **Amott D** Forced oil imbibition. This step is carried out until S_{wir} is reached.

I_o and I_w are the Amott indices for oil and water respectively and can be calculated according to 2.1:

$$I_o = \frac{\Delta S_{os}}{1 - S_{wi} - S_{or}}, \quad I_w = \frac{\Delta S_{ws}}{1 - S_{wi} - S_{or}} \tag{2.1}$$

Afterwards, Amott-Harvey index (AJWI)can be determined according to 2.2:

$$AHWI = I_w - I_o \tag{2.2}$$

Amott-Harvey index determines the average wettability of the core can be estimated by comparing ot to the values in 2.2

TABLE 2.2: Amott Wetting Indices (McPhee et al. 2015)

	Water-wet	**Neutrally-wet**	**Oil-wet**
I_w	positive	0	0
I_o	0	0	positive
AHWI	+0.3 to +1.0	+0.3 to -0.3	-0.3 to -1.0

Amott Harvey index determines the average wettability in the core. The duration of the spontaneous imbibition phase should be long enough. Moreover, the pressure applied during the forced displacement stages should be equal (McPhee et al. 2015). SI alone can be a strong qualitative indicator of the wettability state. When the wettability state is tuned towards water-wet, more water will imbibe into the core leading to a higher ultimate recovery. In an oil rock, water cannot spontaneously imbibe into the core due to the negative capillary pressure (Standnes 2004)

USBM This method is named after the *U.S. Bureau of Mines*. The wettability index is determined from the area bounded between the drainage and imbibition capillary pressure curves as shown in figure 2.2.

The capillary pressure value is determined by forced displacement under centrifugal (gravitational) force. The gravitational force should overcome the capillary pressure in order to displace a certain amount of oil. The wettability index is determined by the equation 2.3:

$$USBM = \log(\frac{A_1}{A_2}) \tag{2.3}$$

This method does not require a spontaneous displacement phase. USBM index ranges between positive for water-wet to negative for oil-wet. Values close to zero indicate a neutral wettability state. Amott-Harvey index is more sensitive towards neutrally wet rocks (McPhee et al. 2015).

Qualitative Evaluation

Advanced Pore-scale imaging Li et al. 2019 used interferograms of an oil drop resting on a nanoparticle-treated glass surface to analyze the effect of nanoparticles on wettability followed by Atomic Force Microscopy (AFM) to characterize the structure of nanoparticles covering a glass surface. By determining the nature of the thin film coating the grains, an understanding for the wettability behavior could be developed.

Relative Permeability Curve This approach can offer an indicator whether the core is strongly oil-wet or strongly water-wet but they might fail to distinguish between strongly water-wet and weakly water-wet (León-Pabón et al. 2014).

2.3 Interfacial Tension

This phenomenon is caused by intramolecular interactions. In an air-water system (i.e. water droplet), the molecules far from the interface are in a force equilibrium. For the molecules situated at the fluid-fluid interface, the attraction of liquid molecules to each other (due to cohesion) is greater than to air molecules (due to adhesion), resulting in an inward force at the surface. Consequently, the interface tends to shape itself into a sphere in order to maintain the smallest contact area. The force acting on the interface between two immiscible fluids is referred to as *Interfacial Tension* (*IFT*). However, when the second fluid is in gaseous phase, the term *Surface Tension* is used (Blunt 2017).

Common symbol of IFT in the literature is σ and the unit is energy per surface area which is reduced to Newton per meter or $\mathrm{mN\,m^{-1}}$. Interfacial tension is strongly dependent on temperature and less dependent on the pressure (Pinder et al. 2008).

2.3.1 Measurement Methods

An IFT measurement relies on the droplet shape of an immiscible fluid within another fluid. The shape of the droplet is an equilibrium between gravity forces (or any other forces acting on the droplet) and interfacial tension. By analyzing the droplet's dimensions, IFT can be estimated. Base on the range of the expected IFT value one can choose between the sessile drop, pendant drop, and spinning drop method (Gennes et al. 2004). Figure 2.3 shows the curvature caused by surface free energy in a sessile drop.

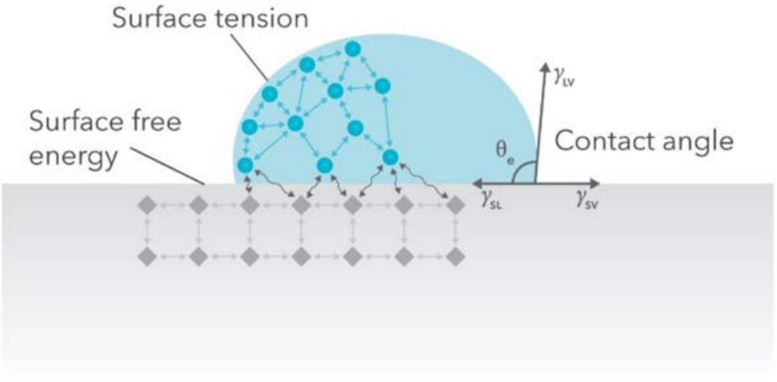

FIGURE 2.3: Sessile drop schematic and surface tension (Nanoscience Instruments 2020)

2.3.2 IFT and Oil Recovery

Capillary Number (N_c) is a dimensionless parameter that represents the ratio of capillary to viscous forces (Yeganeh et al. 2016). N_c can be computed through equation 2.4.

$$N_c = \frac{v\mu}{\sigma} \tag{2.4}$$

Where: v is the interstitial velocity, μ is dynamic viscosity σ is interfacial tension Figure 2.4 illustrates the *Capillary Desaturation Curve* (*CDC*). CDC describes the relationship between the capillary number and residual oil saturation (S_{or}).

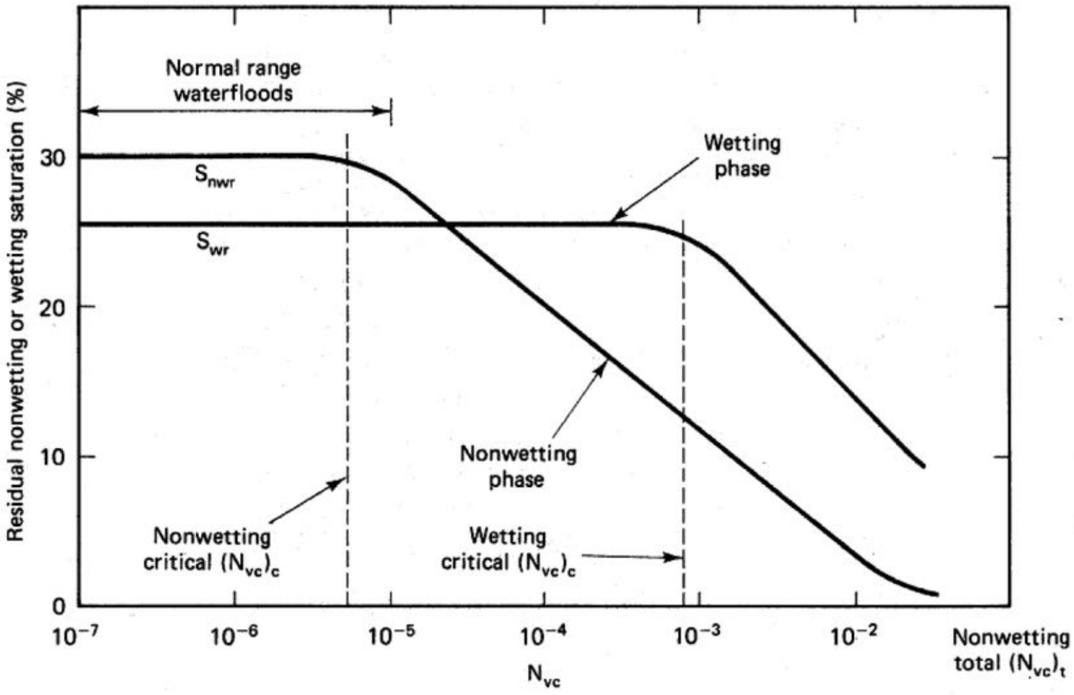

FIGURE 2.4: Capillary desaturation curve (Lake 1989)

According to the capillary desaturation curve, by increasing N_c, the residual oil saturation is consequently decreased and hence the ultimate recovery is higher. Increasing N_c means that the viscous forces exceed capillary forces and thus trapped oil ganglia can be mobilized (Youssef et al. 2015). The magnitude of v and μ is limited to the flow regime and downhole pressure. The most effective way to manipulate N_c is to reduce σ to ultra-low values ($1 \times 10^{-3}\,\mathrm{mN\,m^{-1}}$). When surfactant molecules or nanoparticles adsorb on the interface, IFT is lowered and emulsification process can take place.

2.4 Phase Behavior

Phase behavior test can be conducted in in small pipettes (5 or 10 mL) in order to investigate the stability, precipitation, optimal salinity, optimal surfactant concentration and oil type (Sheng 2011).

2.4.1 Surfactants

A surfactant (surface-active agent) is a chemical agent with the ability to adsorb onto the fluid/fluid interface. A surfactant molecule consists of two parts: a nonpolar (hydrocarbon) tail and an ionic/polar part which is called head. Figure 2.5 shows a schematic of a surfactant molecule.

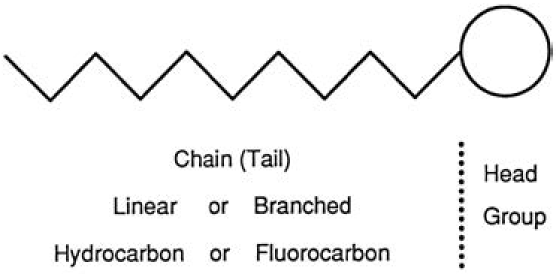

FIGURE 2.5: Schematic of surfactant molecule (Green et al. 2008)

The tail is generally hydrophobic which means that it is pushed due its nonpolar nature out towards the oleic phase. While the polar heads tend to stay within the water phase. At low concentration, this dual nature keeps the surfactant on the interface allowing it to alter the interfacial properties. By increasing the concentration of surfactant, IFT decreases sharply until surfactant concentration reaches the *Critical Micelle Concentration* (CMC).

At CMC, the surfactant molecules cover the entire interface. Beyond that, any additional surfactant molecules will form micelles in one of the phases (Lyons 2009). Based on the nature of the head group, surfactants can be classified into cationic, anionic or zwitterionic (Negin et al. 2017). Once IFT between two immiscible phases is lowered enough, emulsification can take place where droplets of one of the phases coated by a surfactant film can get entrained in the other phase forming a colloidal suspension (Speight 2016). Based on the droplet size we can differentiate between 3 types of emulsions:

Macroemulsion The droplet size is larger than 1 µm. the main characteristics are milky color, high turbidity and thermal instability (Sharma et al. 1985).

Two subcategories can be distinguished between:

Single emulsion A phase separation by a surfactant film controls the stability of dispersion and prevents the coalescence of droplets. Based on which phase is dispersed into the other, we can divide this category into two subtypes: *Water-in-Oil* (W/O) or *Oil-in-Water* (O/W).

Double emulsion When two or more emulsifier films separate two or more immiscible fluids. *Oil-Water-Oil* (O/W/O) and *Water-Oil-Water* (W/O/W) emulsions can be recognized as sub types.

Macroemulsions require high amount of excess energy to be generated. This energy can be supplied in form of agitation (Arab et al. 2018).

Microemulsion Unlike macroemulsions, microemulsions are thermodynamically stable systems. Their droplet size does not exceed 0.10 µm. They can form spontaneously and upon gentle mixing. The most common classification is the one suggested by Winsor 1956. Winsor showed that the type of microemulsion, which is formed has a strong dependency on a set of parameters like: salinity, temperature, initial phase ratios, emulsifier, oil type, etc. The three relevant types to EOR process can be seen in figure 2.6:

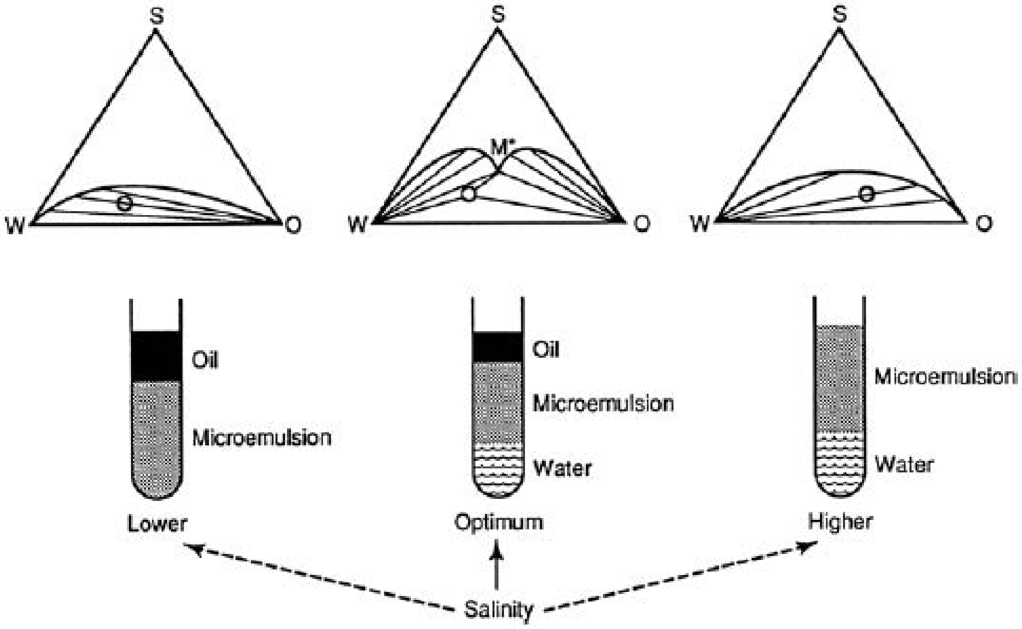

FIGURE 2.6: *Winsor*'s classification of microemulsions (Healy et al. 1975)

- **Type II+** Forms at low salinity. Consist of water external microemulsion and excess oil phase.
- **Type II-** At high salinity values, excess water rests at the on the bottom while an oil-external microemulsion forms on the top (Green et al. 2008).
- **Type III** At intermediate salinity, midphase microemulsions are formed. This phase is saturated by oil and water. This is considered to be an optimum due to the ultra-low IFT between oil and water.

Nanoemulsions The system is very heterogeneous. the droplet size ranges between 5 and 200 nm (Aboofazeli 2010).

2.5 Mobility Ratio

In viscous displacement process, the macroscopic displacement efficiency is strongly dependent on the mobility ratio. *Mobility* (λ) of one phase in a multiphase flow incorporates two attributes: the relative permeability of the phase (K_r) divided by its viscosity (μ). Mobility ratio during a water flooding process is defined as following:

$$M = \frac{\lambda_{displacing}}{\lambda_{displaced}} \tag{2.5}$$

In order to achieve a desired macroscopic sweep efficiency, a stable front and a mobility ratio close to one have to be established. At high values of **M**, piston-like displacement cannot be sustained, and viscous fingering occurs. As a result, a lot of oil remains unswept and viscous fingers can develop into an early water breakthrough (Ahmed 2010). Due to the significant viscosity contrast between oil and the injected fluid (brine) in some heavy oil reservoirs, thermal or solvent-based EOR techniques should be applied (Arab et al. 2018).

Polymer flooding targets λ_w, namely the water viscosity μ_w. Polymers of high molecular weight and good solubility in water can increase the viscosity of water even at low concentrations (few hundred ppms) and achieve conformance control (Gbadamosi et al. 2019).

Polymers are often liable to polymer retention and very sensitive to salinity of the reservoir (Firozjaii et al. 2019). Some studies showed that due to polymer retention and adsorption on the rock surface, wettability alteration might take place (Juarez-Morejon et al., 2017).

2.6 Alkaline Flooding

2.6.1 Soap Generation

Once injected, alkali interacts with the formation rock, oil and formation brine (Sheng 2013). Alkali's reaction with acidic components in the oil, namely carboxylic groups, yields to insitu surfactants generations. In order to distinguish between insitu surfactants and injected surfactant, literature refer to insitu generated surfactant by alkali-oil reaction as *soaps* (Sheng 2015). Soaps are able to reduce the interfacial tension and alter the wettability (Lake 1989).

The key parameter in this process is *Total Acid Number* (TAN). TAN is the mass of KOH (potassium hydroxide) in mg, which is needed to neutralize one gram of crude oil. (Sheng 2015). However, TAN parameter does not distinguish between carboxylic groups and weaker acidic components like phenolic.

Sodium carbonate Na_2CO_3 is among the most widely used alkali chemicals in EOR operations due to the following reasons (Sheng 2011):

- low-cost
- lower ion exchange and mineral dissolution than stronger alkali e.g. NaOH
- Weak alkalinity assists ASP floods in maintaining a near-neutral pH range.

The reactions taking place during alkali flooding are illustrated in figure 2.7 and consist of the following steps (Sheng 2015):

- HA_o is an acidic sub-component. A^- represents a carboxylic compound of the form ($RCOO^-$) soluble within the oelic phase is dissolved into the aqueous phase:

$$HA_o \rightleftharpoons HA_w \tag{2.6}$$

- HA_w dissociates within the aqueous phase by hydrolysis:

$$HA_w \rightleftharpoons H^- + A^+ \tag{2.7}$$

- Water dissociates as following:

$$\mathrm{H_2O} \rightleftharpoons \mathrm{H}^+ + \mathrm{OH}^- \tag{2.8}$$

- The overall reaction with NaOH as alkali:

$$HA_o + \mathrm{NaOH} \rightleftharpoons \mathrm{H_2O} + NaA \tag{2.9}$$

- Anionic surfactant A^- is generated.

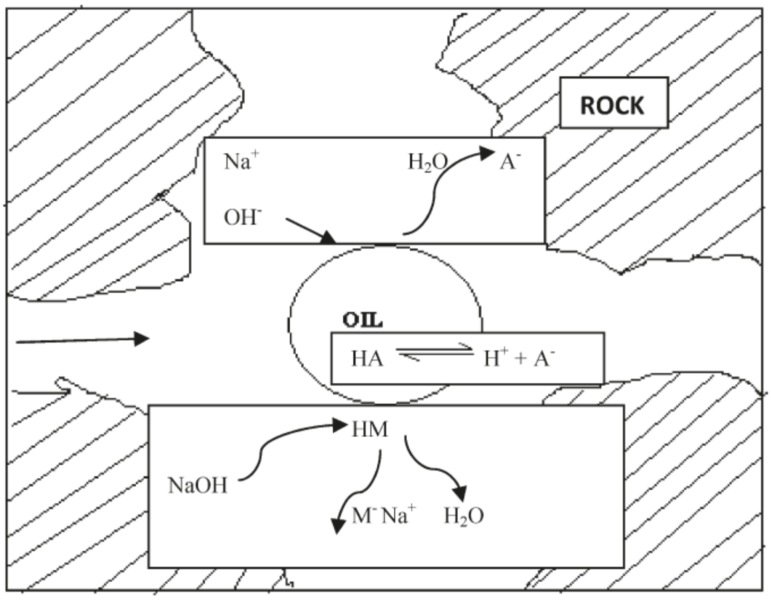

FIGURE 2.7: Schematic of alkali reaction (Samanta et al. 2011)

2.6.2 Alkali-Rock Interactions

Alkali interacts with the rock depending on its mineralogy. The interaction occurs in form of surface exchange and hydrolysis, congruent and incongruent dissolution reactions and insoluble salt formation (Ma et al. 1999). Strong alkali like NaOH could dissolve quartz mineral (Mohnot et al. 1987). Despite their low content, clay minerals consumed the injected alkali which lead to a drop in alkalinity of the medium (Mohnot et al. 1987) leading to pH lag (Delshad et al. 2011).

Ion exchange with clay minerals might result in a release of divalent cations which may cause unfavorable phase shift and solid precipitation (Somerton et al. 1983). Clay minerals are very susceptible to swelling. Clay swelling often results in permeability reduction and formation damage. High pH brine might trigger clay swelling. However, Salinity of the injected brine is more decisive factor in clay swelling process (Kazempour et al. 2013).

2.7 Spontaneous Imbibition

Spontaneous imbibition (SI) happens when the wetting phase flows into the porous medium increasing its saturation, and this flow is taking place under capillary forces without any viscous displacement or differential pressure applied. By this means, the nonwetting phase is produced (Abd et al. 2019). This process is considered an unsteady state flow (Nooruddin et al. 2016) and it can be approached as a piston-like displacement (Haugen et al. 2014). The imbibed volume is proportional to the square root of time (Alyafei et al. 2018).

$$q(t) = 2C\sqrt{t} \tag{2.10}$$

Where C is the imbibition constant and $q(t)$ is the imbibition rate.

The key factor that controls spontaneous imbibition process is the capillary pressure (P_c):

$$P_c = \frac{2\sigma}{r} \tag{2.11}$$

where σ is the interfacial tension and r is the capillary radius. While the velocity v can be described by the *Poissuille* equation 2.12:

$$v = \frac{\Delta P}{xr^2 8\mu} \tag{2.12}$$

Where μ is the fluid viscosity and ΔP is the pressure gradient which can be replaced by P_c from 2.11 yielding:

$$v = \frac{2\sigma}{r}\frac{1}{x}\frac{r^2}{8\mu} = \frac{\sigma r}{4\mu x} \tag{2.13}$$

Since $v = \frac{\delta x}{\delta t}$, 2.13 can be integrated to form:

$$x^2 = \frac{\sigma r t}{2\mu} \tag{2.14}$$

Which means that the front moves proportional to the square root of time (Abd et al. 2019).

Spontaneous imbibition involves two flow regimes which are illustrated in figure 2.8.

2.7.1 Counter-current SI

This term is used when the wetting phase flows into the rock through the same surface the nonwetting phase is produced from. In other words, both phases are passing through the same inlet surface but in opposing flow directions.

This leads to lower mobility for both phases due to the flow impedance. Consequently, the capillary backpressure is increased (Haugen et al. 2014). *Capillary backpressure* is the pressure required to be overcome in order to produce the nonwetting phase (oil) (Abd et al. 2019). Viscous forces have a negative impact on the flow (Nooruddin et al. 2016) In case of viscous oil, water enters the core at low saturation while oil flows oppositely at higher saturation. However, for lighter, less viscous oils, counter-current SI takes place under higher water saturation. This is due to the fact that SI under counter-current regime tries to equalize the mobility ratio under so-called *self-compensating effect* (Morrow et al. 2001). The flow is governed by the following equations (Nooruddin et al. 2016):

$$\frac{\delta}{\delta x}(D(S_w)\frac{\delta S_w}{\delta x}) = \frac{\delta S_w}{\delta t} \tag{2.15}$$

The net flow will be in this case equal to zero as shown in 2.16

$$q_o = -q_w \Rightarrow q_t = 0 \tag{2.16}$$

High IFT and low viscosity increases the recovery rate by counter-current SI (Al-Quraishi 2004). Even though the imbibition rate is significantly lower under counter-current SI tan under co-current SI, the recovery was found to be higher under counter-current SI (Kantzas et al., 1997).

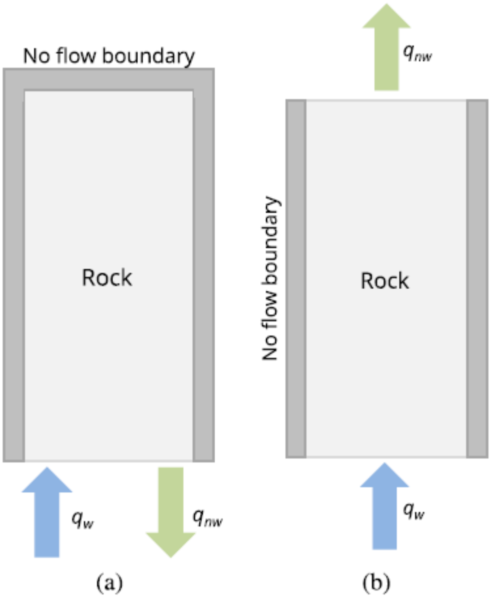

FIGURE 2.8: (a) Counter-current SI, (b) Co-current SI. *nw* indicates non-wetting phase, *n* stands for wetting phase (Alyafei et al. 2018)

2.7.2 Co-current SI

Co-current SI takes place when the wetting phase enters from the inlet displacing the nonwetting phase, which escapes in the same direction from the outlet (figure 2.8). At this case, the phases flow at higher mobility. Therefore, viscous forces can positively influence the displacement (Morrow et al. 2001). A faster and higher recovery can be obtained under this regime. Co-current SI is likely to dominate under low mobility of water and oil (Andersen et al. 2019). Under gravity segregation in fractured reservoirs, oil tends to flow out of the matrix through the surface that is in contact with oil (Morrow et al. 2001).

$$\frac{\delta}{\delta x}(D(S_w)\frac{\delta S_w}{\delta x} - q_t f(S_w)) = \Phi\frac{\delta S_w}{\delta t} \tag{2.17}$$

The above equation consists of two terms: an advective and a diffusive term.

In our work, it is noticed that both flow regimes occur simultaneously but to different extents. At the beginning, counter-current was more dominant since the surface area subjected to counter-current is larger (the whole core plug is exposed to water, and water imbibes into the rock through all surfaces). While water saturation inside the core increases by imbibition, gravity segregation promotes co-current SI.

2.7.3 Low IFT Spontaneous Imbibition

In section 2.3.2 we discussed the influence of IFT on the recovery from a viscous displacement perspective. However, in a mere spontaneous imbibition, the flow is governed by capillary pressure devoid of viscous pressure gradient. In this case, gravity forces can play an important role. Primarily in naturally fractured reservoirs (NFR), where the matrix height and the vertical connectivity is the key answer on the question which recovery mechanism will be dominant (Al-Quraishi 2004). The relationship between gravity an capillary forces is best described by *inverse Bond number* N_B^{-1}. Inverse Bond number represents the ratio capillary to gravity forces and can be calculated by the equation 2.18.

$$N_B^{-1} = C\frac{\sigma\sqrt{\frac{\phi}{k}}}{\Delta\rho g H} \tag{2.18}$$

Where: C = 0.4 for a capillary tube model, H is the core height [meter], σ is the interfacial tension [$\mathrm{mN\,m^{-1}}$], ϕ is the porosity [%], k is the absolute permeability [mD] $\Delta\rho$ is the density difference between the phases [$\mathrm{kg/m^3}$].

Higher density contrast between the phases triggers gravity drainage which can be translated in less contribution of capillary forces N_B^{-1} is low. This ratio can be affected by changing matrix height or reducing the IFT. Increasing inverse Bond number (i.e., SI occurs under low IFT), will lead to higher ultimate recovery. Nevertheless, under lower imbibition rate (Schechter et al. 1994). This was later attributed to the fact that low IFT increases the imbibition rates at late time or to wettability alteration process (Babadagli 2005). Imbibition rate is only affected in ultra-low IFT systems.

When IFT ranges between high and intermediate values, imbibition rate is not influenced by IFT (Al-Quraishi 2004). When IFT is reduced enough to enable the emulsification process, solublization factor can be used to correlate the recovery using SI and the formed emulsion (Chen et al. 2018) Solublization factor S_F can be computed by incorporating the oil solublization ratio SP_o and water solublization ratio SP_w into the equation 2.19 (Sheng 2011).

$$S_F = \sqrt{SP_w^2 + SP_o^2} \tag{2.19}$$

Since inverse Bond number as expressed in equation 2.18 does not take the wettability factor into account, other expressions of inverse Bond number were developed to include wettability-related parameter ($f(\theta)$) (Babadagli 2005) as shown in equation 2.20:

$$N_B^{-1} = C\frac{f(\theta)\sigma\sqrt{\frac{\phi}{k}}}{\Delta\rho g H} \tag{2.20}$$

2.7.4 Capillary Diffusion Coefficient

The capillary imbibition can be approached as diffusion mechanism after neglecting the convection and gravity effects (Chevalier et al. 2019).

$$\begin{array}{l} \Phi\frac{\delta S_w}{\delta t} = -\nabla[K\frac{K_w K_o}{K_t}\nabla P_c(S_w)] \; with: \\ K_o = \frac{K_{ro}}{\mu_o}, \\ K_w = \frac{K_{rw}}{\mu_w}, \\ K_t = K_o + K_w \end{array} \tag{2.21}$$

Where: K is the single phase permeability, S is the saturation, μ is the viscosity and o and w stand for the oil and phase respectively.

After introducing the imbibition capillary pressure $P_c(S_w)$, the equation 2.21 can be expressed by the means of the capillary diffusion coefficient (D_c) as following:

$$\frac{\delta S_w}{\delta t} = D_c \Delta(S_w) \tag{2.22}$$

In a cylindrical geometry the oil Saturation can be normalized as following

$$S_o^* = \frac{S_o - S_{of}}{S_{oi} - S_{of}} \tag{2.23}$$

S_o^* can be also expressed as a product of 2 solutions: C_{ps} for a plane sheet and C_{cyl} for a cylinder as follows:

$$S_o^* = C_{ps} C_{cyl} \tag{2.24}$$

With (Crank 1979):

$$C_{ps} = \sum_{n=1}^{\infty} \frac{8}{(2n+1)^2\pi^2} \exp(-D_c(2n+1)^2\pi^2\frac{t}{4l^2}) \tag{2.25}$$

$$C_{cyl} = \sum_{n=1}^{\infty} \frac{4}{r^2 q_n^2} \exp(-D_c q_n^2 t) \tag{2.26}$$

Where: l is the length of the plug, r the radius, q_n are the positive roots of the equation: $J_o(rq_n) = 0$, J_0 is zero order of the first type Bessel's function.

Chapter 3

State of the Art

3.1 Nanotechnology

3.1.1 Historical Overview

Nanotechnology has become a trend in the recent decades and it was cornerstone in revolutionizing some industries, i.e. pharmaceutics, medical industry, etc.

The oil and gas industry, especially the upstream sector, did not consider the nanotechnology as a promising research area at the beginning due because reservoirs are huge in terms of volume. Therefore, massive volumes of nanofluids would be required to treat a reservoir, which was considered unprofitable. In addition to that, the heterogeneity and downhole delivering techniques were believed to be an obstacle (Huh et al. 2019). In the last ten years, nanotechnology found its way into the petroleum industry after several advancement made by other industries.

3.1.2 The Uniqueness of Nanomaterials

The term *Nanomaterial* stands for solid composite, complex fluids or colloidal dispersion whose construction unit is at the nanometer scale [1]. The size of nanoparticles (NPs) ranges between 1-100 nm. The size of NPs is usually described in one dimension even though it might have different shapes.

The extremely tiny particle size allows the nanomaterial to possess a large surface area. Consequently, its properties differ from the original bulk material; i.e., low melting point, unique optical properties and unique magnetizing behavior (Hornyak 2009).

Due to their small dimensions, the surface area of NPs can be as high as several hundreds of m2/g. As an example: *AEROSIL 300* from EVONIK (hydrophilic fumed silica) have specific surface area of 300 m^2/g. Therefore, NPs are more exposed to the surroundings allowing them to be more reactive (Almahfood et al. 2018).

Different chemicals can be attached to the surface of NPs in order to modify its properties to take advantage of the high mobility of NPs (e.g., deliver chemicals to desired spot) (Huh et al. 2019).

---

[1] $1 Nanometer = 10^{-9} Meter$

3.1.3 Types of Nanoparticles

Nanoparticles can be classified based on the composition of their constructing units:

- Metal oxide
- Organic
- Inorganic

3.1.4 Nanofluids

When NPs are suspended in a liquid phase, NPs collide with water particles generating Brownian energy. Brownian diffusion governs the intra-particle forces. These forces might result in a repulsion or adhesion.

The resulting force is a sum of electrostatic force (U_{el}) and Lifshitz-Van der Waals force (U_{lw}). Both of these forces are dependent on the distance between particles. However, the presence of electrolytes affects only the electrostatic force, while Lifshitz-Van der Waals force is charge-independent. In order to deliver NPs and maintain their functionality, a dispersion within the liquid phase must be stable. Otherwise, NPs may adhere to each other forming clusters.

DLVO & XDLVO Theory

The *DLVO Theory* was named after the Russian scientists B. Derjaguin and L. Landau, and Dutch scientists E. Verwey and J. Overbeek). This theory describes the interaction of two NPs based on the distance between (Ohshima 2012).

The original version of DLVO theory considered only the electrostatic force and Lifshitz-Van der Waals force. In case of NPs it has been proven that non-DLVO forces are significant and cannot be neglected. *XDLVO* is an extension to DLVO and it is applied when one of the two studied particles has dimensions of the nanoscale (van Oss 2008). In XDLVO theory, the following forces are taken into account:

U_{el}	Electrostatic force
U_{lw}	Lifshitz-Van der Waals force
U_{m}	Magnetic force if NP has magnetic properties
U_{ab}	Acid-base interaction energy
U_{bo}	Born repulsion energy
U_{osm}	osmotic repulsion energy due to polymer coating
U_{elas}	elastic steric repulsion energy due to surface functionalization

Colloidal Stability

An instability of the colloidal suspension might lead to an aggregation of NPs forming clusters. Therefore, the functionality of NPs will be significantly affected due to the decrease of surface area. The growth of clusters might also results in pore plugging during the flow in a porous medium (Huh et al. 2019).

3.2 Recovery Mechanisms

3.2.1 NP-assisted EOR

Recent studies have introduced NPs as novel EOR agents. NPs can serve as a standalone EOR agent or as supplementary additive to chemical EOR agents (foam, surfactant, alkali). NPs became focal point in EOR field due to their high mobility and ability to tolerate harsh salinity and high temperature environments (Ali et al. 2018). NPs can be involved in several process in EOR, which are described in this section.

3.2.2 Foam Stabilization

CO_2 can be a very beneficial EOR agent due to its unique properties. Once it is injected in a supercritical state, CO_2 can be miscible with the oil at achievable pressure, causing the oil to swell which improves its mobility. CO_2 at super critical state is very mobile. Therefore, mobility control techniques should be deployed in order to prevent breakthrough and avoid excessive injection. Due to its low density in comparison to heavy oil, gravity override may occur while injecting CO_2.

TABLE 3.1: Critical properties of CO_2 (Linstrom, 2020)

T_C	30.9782	°C
ρ_C	467.6	kg/m^3
P_C	73.773	bar
μ	0.037334	cP

Foam is a dispersion of gaseous phase within the liquid phase and it can be generated on surface or by co-injecting a surfactant with the gas (Sheng 2013). This results in lower interfacial tension allowing the foam to be generated, and a significantly lower mobility than the mobility of each forming phase alone.

The main operational limitation when deploying foam on field scale is foam degradation. Foam degrades quickly in the reservoir when the thin liquid films collapse. This phenomena is related to the used surfactant and its ability to withstand formation conditions. In order to assure that foam will cover the targeted reservoir, liquid films must have long livability to deliver the EOR agent to targeted spot (Yekeen et al. 2018).

Singh et al. 2017 investigated the utilization of silica NPs with polyethylene glycol (PEG) surface modification to stabilize CO_2 foam in homogeneous sand packs. The recovery was compared to the cases of water flooding and surfactant-stabilized foam (figure 3.1). The utilization of NPs allowed a higher recovery in comparison to the normal foam at the early injection stages and outperform waterflooding which yielded however a high initial recovery. This improvement is due to the higher stability using NPs, allowing the foam to sweep better using less PV.

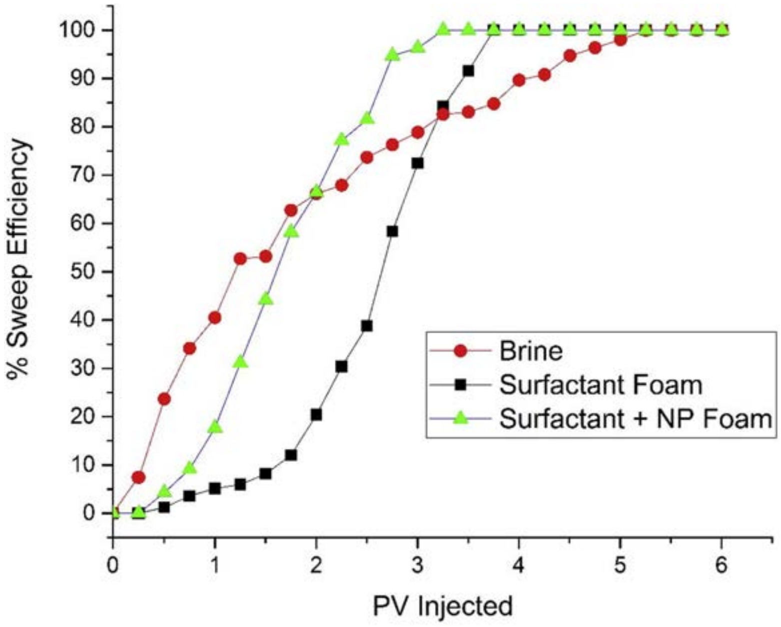

FIGURE 3.1: sweep efficiency as a function of pore volumes (PV) (Singh et al. 2017)

Rognmo et al. 2018 showed that surface-treated NPs could serve as foaming agent. a proportional relationship between NP concentration and oil recovery was suggested. Khajehpour et al. 2018 utilized surface-treated silica NPs with surfactants as a steam additive. They showed that synergy between silica NPs and surfactants provided higher foamability and long-livability.

3.2.3 Rheology Enhancement

Polymers, like other chemicals, are prone to degradation under harsh reservoir conditions. Consequently, the viscoelastic properties especially viscosity of the injected fluids will be altered which might influence the displacement efficiency (Xin et al. 2018).

Corredor et al. 2019 modified silica NPs towards more hydrophobic surface in order to improve their dispersivity into the polymer. Hydrophobic silica NPs can form a network with HPAM molecules and improve its viscoelastic properties through stronger polymer bridging which resulted in higher recovery in core floods. This enhancement was highly dependent on the surface modification of silica NPs.

3.2.4 IFT Reduction

Bare silica nanoparticles have no impact on interfacial tension (Jiang et al. 2017). However, functionalized silica nanoparticles can spontaneously adsorb onto the fluid-fluid interface, exhibiting a surfactant-like behavior. Nonetheless, NPs have a larger size and thereby lower diffusivity in the solution that makes the adsorption kinetics slower than the one with surfactant (Huh et al. 2019). The adsorption of NPs has two main mechanisms (Sofla et al. 2019):

Langmuir monolayer A particle film directly deposits onto the interface assisted by spreading solvent.

Gibbs monolayers Spontaneous adsorption of NPs onto the interface from the bulk suspension.

Another distinction from surfactant is the magnitude of IFT reduction. Modern surfactant can lower the IFT to ultra-low values ($1 \times 10^{-3}\,\mathrm{mN\,m^{-1}}$) while IFT reduction by NPs alone is significant but still modest compared to surfactant (ShamsiJazeyi et al. 2014).

Numerous researches investigated the IFT reduction caused by NPs. Sharma et al. 2016 observed that IFT was reduced in brine/oil system from $18\,\mathrm{mN\,m^{-1}}$ to $10.20\,\mathrm{mN\,m^{-1}}$ after adding 1 wt% of silica NPs. IFT was lowered to $4.80\,\mathrm{mN\,m^{-1}}$ by introducing surfactant-polymer mixture in addition to the nanofluid. An increase in IFT was reported when higher concentration of NPs was involved which can be explained as following: at high concentrations of NPs in the solution, oil/water interface will reach a state of saturation. After that. NPs will start replacing the surfactant molecules at the interface which are more effective in terms of IFT reduction. Ahmed et al. 2019 reported that IFT in oil/brine system was lowered from $17.10\,\mathrm{mN\,m^{-1}}$ to $6\,\mathrm{mN\,m^{-1}}$ after introducing surface treated silica NPs to the brine. They also reported that IFT reduction was more significant when the concentration of NPs was increased. Neubauer et al. 2020 observed that more negatively charged silica NPs were more effective in terms of IFT reduction than more neutrally charged silica. They also reported a strong dependency on the particle size. Particle with smaller size have higher specific area and the particles have higher diffusivity due to the electric repulsion and Brownian motion (Kim et al. 2016).

3.2.5 Emulsion Stabilization

Emulsion-Assisted Mobility Control

By reducing the interfacial tension in the oil/brine system, emulsification can occur. The formed emulsion can act as a flow barrier to divert the flow into unswept zones and block the highly permeable corridors.

Emulsion-based mobility control can be an adequate alternative to polymers especially for heavy oil reservoirs (Arab et al. 2018). An oil-in-water emulsion has higher viscosity than water but still less viscous than the oil. This slug-wise viscosity distribution helps achieving a flow conformance among the phases and a stable piston-like displacement.

The emulsification process can be achieved using surfactant, alkaline or both. The surfactant-based emulsion is liable to degradation under harsh reservoir conditions. Degradation can be in form of coalescence, Oswald ripening,sedimentation or creaming (Perazzo et al. 2018).

As a result, emulsions will decompose before reaching the preferred zones and the improvement will be only temporary (Shamekhi et al. 2013). Afterwards, the production mechanism is limited to oil entrainment within the emulsion phase instead of the plugging mechanism by the emulsion itself (Kumar et al. 2010). Hence, mobility control along the flooded reservoir cannot be sustained (Kim et al. 2016).

Nanoparticle-based Emulsification

When the emulsion is stabilized by solid particles, e.g. silica NPs, which accumulate on the interface between two immiscible fluids, this emulsion is called *Pickering Emulsion* and it was named after Pickering 1907. NPs can serve as a standalone emulsifier. Hydrophilic NPs yield oil-in-water microemulsions, while hydrophobic NPs yield water-in-oil (Huh et al. 2019). Binks et al. 2000 showed that surfactant-free emulsion could be stabilized by silica NPs.

Synergistic Effects

Binks 2002 suggested that nanoparticles have a surfactant-like behavior during the emulsification process. Based on their surface wettability they tend to accumulate onto water oil interface. The advantage of NP-stabilized emulsions over surfactant is the thermal stability and the ability to withstand harsh reservoir environment (Sharma et al. 2015). Binks et al. 2007 showed that Synergistic stabilization of O/W emulsions can be achieved by mixing oppositely charged NPs and surfactant.

Sharma et al. 2015 compared the thermal stability of Pickering emulsions stabilized solely by surfactant to the one stabilized by hydrophilic silica nanoparticles. They observed that emulsions stabilized by NPs and surfactant were highly stable and able to tolerate high temperature and very saline environments.

Kumar et al. 2017 studied the Pickering emulsions formed by light mineral oil surfactant and silica nanoparticles. Through droplet size analysis, they concluded that emulsion was more stable, and ζ-potential measurements exhibited a colloidal stability. The viscoelastic properties of the emulsions could be improved by adding polymers. Hence, nanoparticles can contribute to the emulsion-assisted mobility control process by stabilizing the emulsion and consequently plugging highly permeable channels and sustaining a stable displacement (Arab et al. 2018).

Kamkar et al. 2020 investigated the rheology of oil-in-water emulsion formed by combining surface-modified NPs and hydrolyzed polyacrylamide (HPAM) polymer. Their results revealed that partially hydrophobic silica NPs has more favorable mobility from the bulk phase towards the oil-water interface, which makes them more effective in lowering IFT and creating an elastic interfacial film. The addition of HPAM improved the bulk rheological properties of the nanofluids, nonetheless, acted as an emulsion destabilizer.

3.2.6 Pore Plugging

Pore channel-plugging helps to divert the flow into more desired zones. This effect can be attained by two mechanisms illustrated in figure 3.2: Mechanical entrapment or log-jamming (Raffa et al. 2019).

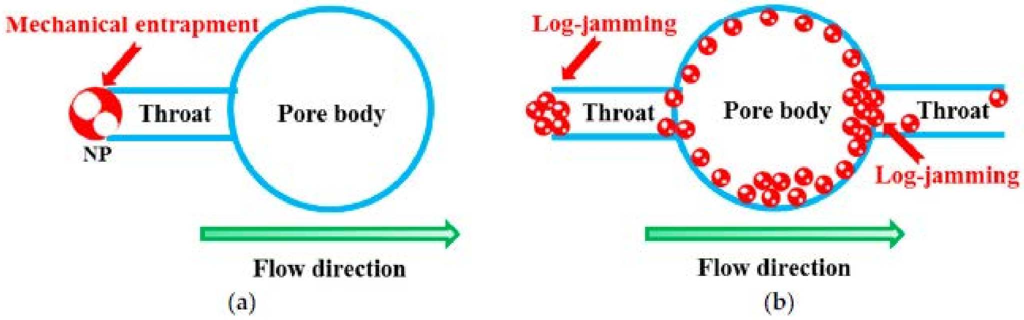

FIGURE 3.2: Pore Plugging mechanisms. (a): mechanical entrapment, (b): log jamming (Sun et al. 2017)

Mechanical entrapment happens when the particle's diameter exceeds the pore throat size that is often not the case with nanomaterials. As previously mentioned, nanoparticles are very mobile in the pore network (Denney 2011). Log-jamming occurs when water molecules passes through the pore channel with a velocity higher than the one of suspended nanoparticles leading to an aggregation at pore throats (Sun et al. 2017).

3.2.7 Wettability Alteration

Mechanism

Wettability alteration is a complex synergistic process. Polymers can alter the wettability by a reptation mechanism, which leads to detachment of trapped oil droplets (Juarez-Morejon et al., 2017).

Depending on their surface coating, NPs can alter the mineral surface properties towards super hydrophilic or super hydrophobic. Hydrophilicity promotes a water-wet surface (Huh et al. 2019) while hydrophobic silica nanoparticles have almost no impact on the wettability (Li et al. 2019).

Surface wettability is controlled by interfacial and surface energies. Spreading coefficient S of water on a solid surface in oil/water/solid system is determined as follows:

$$S = \gamma_{O/S} - \gamma_{W/S} - \gamma_{O/W} \tag{3.1}$$

Where: $\gamma_{O/S}, \gamma_{W/S}, \gamma_{O/W}$ are the interfacial energies between oil /surface, water/surface and oil/water respectively. Reducing IFT between oil and water will results in increasing the spreading coefficient and consequently promotes more water-wetness (ShamsiJazeyi et al. 2014).

Wettability of a mineral surface can be altered by adhesion of surfactant molecules on the rock surface. This leads to a reduction in surface energy. The adhesion of NPs to the mineral surface results in a change/reduction of surface energy and a change in surface roughness when the adhered layer acts as coating (Ganie et al. 2019).

Disjoining pressure

Disjoining Pressure is exerted by inter-molecular interactions of a thin liquid film at three phase region and it plays a major role in wettability control process (Yu et al.).

The forces that contribute to disjoining pressure are Electrostatic force (U_{el}), Lifshitz-Van der Waals force (U_{lw}) and Acid-base interaction energy (U_{ab}) (Chengara et al. 2004).

Chengara et al. 2004 studied the utilization of NPs to detach an oil drop from a solid surface. He suggested that the nanofluid forms a wedge-shaped thin film due the existence of disjoining pressure. Under the injection pressure, NPs accumulate in the front resulting in an increased entropy of the system due to Brownian motion and the previously mentioned forces. This new situation of NPs can create additional pressure (disjoining pressure). 3.3 shows the meniscus profile in the contact region in presence of NP. The contact line in the presence of fluid containing 20 nm particles is more advanced than the bulk fluid. As a result, the oil will be detached from the mineral surface as the nanofluid film spreads further.

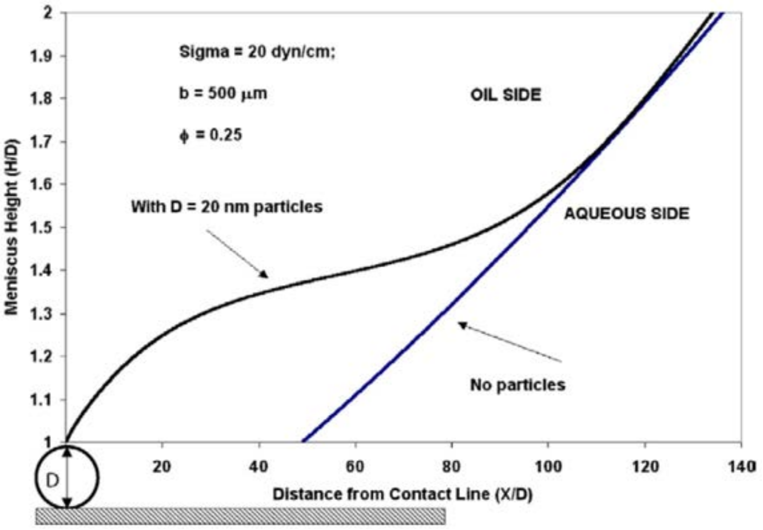

FIGURE 3.3: Effect of structural disjoining pressure on meniscus profile (Chengara et al. 2004)

Kondiparty et al. 2011 examined the spreading of a nanofluid on a solid surface and he defined key parameters that influence this process. Disjoining pressure can be affected by nanoparticle size, concentration, temperature, salinity and surface modification.

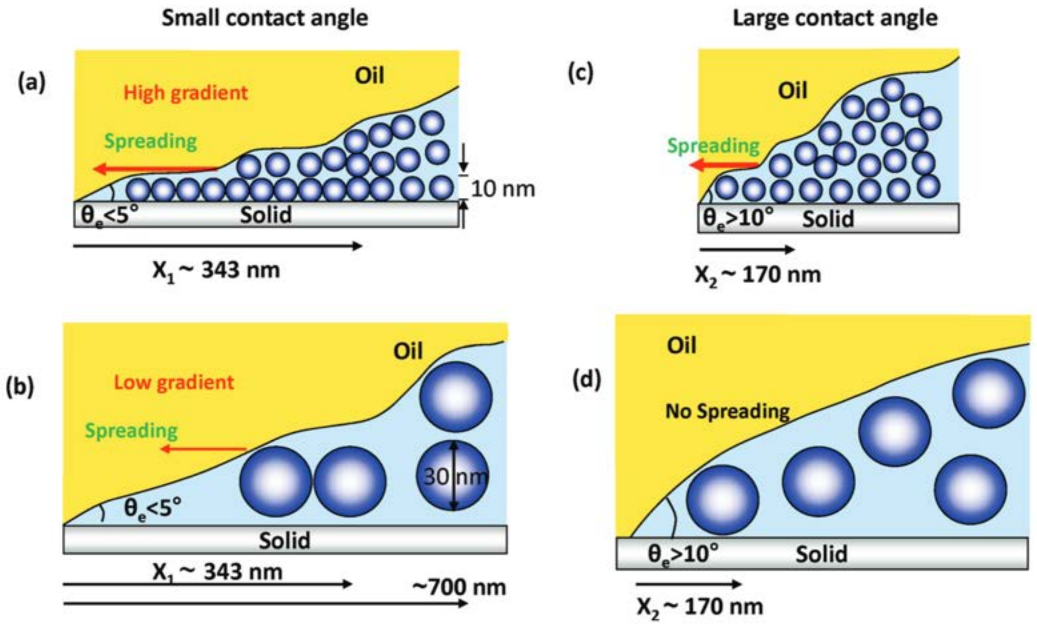
Small contact angle
Large contact angle
(a)
High gradient
Oil
Spreading
10 nm
θe<5°
Solid
X1 ~ 343 nm
(c)
Oil
Spreading
θe>10°
Solid
X2 ~ 170 nm
(b)
Oil
Low gradient
Spreading
30 nm
θe<5°
Solid
X1 ~ 343 nm
~700 nm
(d)
Oil
No Spreading
θe>10°
Solid
X2 ~ 170 nm

FIGURE 3.4: (a) Schematic showing multilayering of small particles at small contact angles. (b) shows large particles form mono layer for the same axial distance X1. (c) shows that axial distance for large contact angle X2 < X1. Small particles form layered structure over short distance due to size effect and result in nanofluid spreading. (d) Large particles cannot form ordered structures in such short distance X2 when confinement is wide. Thus spreading can not take place (Kondiparty et al. 2011)

It is worth mentioning that wettability alteration due to the spreading of nanofluid is a well observed phenomenon, but the mechanism behind it still a research topic and yet not clarified. Disjoining pressure requires high concentrations of nanoparticles at the interface (Wasan et al. 2003) and the nanoparticles should not adsorb on the rock surface (Kuang et al. 2018). Moreover, a water-wet rock surface is prerequisite for the 3-phase contact region (Sofla et al. 2019). Hence, structural disjoining pressure cannot solely serve as explanation for wetting behavior and recovery mechanism using nanofluids.

Nanoparticles as Wettability Modifiers

Ahmed et al. 2019 reported a reduction in contact angle from (80°) to $2-3^\circ$ accompanied with a reduction in IFT between oil/brine using surface modified silica NPs.

Rostami et al. 2019 observed a wettability alteration through silica NPs by conducting contact angle measurements and micro-models. A significant decrease in contact angle was observed after submerging the glass chip in nanofluid. In the micro-models, nanofluids adsorbed on the grains disrupting the initial thin oil film as shown in figure 3.5.

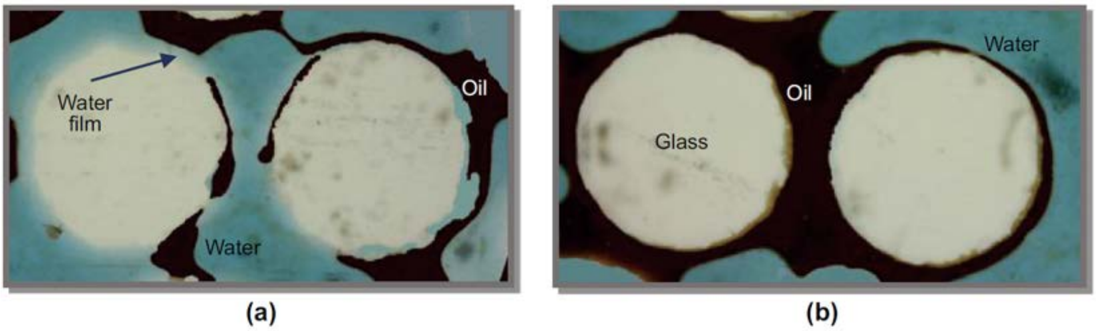

FIGURE 3.5: Pore scale view of wettability. (a): water-wet, (b): oil-wet (Rostami et al. 2019)

Alvarez-Berrios et al. 2018 investigated the effect of surface charge of silica NPs on the wettability alteration process. Contact angle measurements revealed that slightly negatively charged silica nanoparticles reduced the contact angle from 106.3 to 74 were negatively and positively charged scored 94,5 and 100.2 respectively. The wettability alteration was also investigated by series of spontaneous imbibition experiments. At low concentrations slightly negatively charged silica NPs achieved the highest ultimate recovery. However, at higher concentrations strongly negatively and positively charged NPs were more effective in terms of wettability alteration. While Jiang et al. 2017 found that bare silica NPs could alter the wettability at small enough sizes and sufficient concentrations.

Bila et al. 2019 performed core flood experiments using nanofluids containing polymer coated silica NPs at low concentrations on neutrally wet Berea core plugs followed by Amott-Harvey test. They showed that the highest additional recovery can be achieved by using NPs in the secondary flooding stage. They attributed that to different mechanisms like IFT reduction and the formation of micro emulsions by most importantly wettability alteration.

Nanoparticles adsorption is controlled by many factors: Li et al. 2019 observed by the mean of advanced surface wetting visualization an increase in NPs adsorption onto Berea sandstone when NPs concentration increased. The pH of nanofluids had also an impact on the adsorption process: low pH (pH=2.01) favors a uniform NPs adsorption. As the nanofluids pH increased to 4.84, more NPs adsorbed to the rock surface.

Xu et al. 2019 reported an improvement in recovery and imbibition rate after introducing silica NPs to the utilized brine during Amott test. The recovery showed a great dependency on NPs concentration. The incremental recovery was linked to IFT reduction and lower contact angle, which promoted more water-wetness. Wang et al. 2017 studied the imbibition of fluids with silica NPs into a capillary using molecular dynamic simulation. they concluded that the displacement of nanofluids was higher with increased hydrophilicity.

3.2.8 Silica NP Interactions with Mineral Surfaces

Clay minerals play a crucial role in the transport process of NPs in the porous media. Pham et al. 2014 showed that the utilization of PEG coated silica nanoparticles at low concentrations can inhibit clay swelling. A synergy between NPs and electrolytes is also observed.

Omurlu et al. 2016 studied the retention of silica nanoparticles of different surface modifications on the clay mineral surface. They showed that the adsorption is independent of the salinity (electrolyte concentration). However, the electrolyte type affected it. NPs showed lower adsorption in the presence of KCl than NaCl. PEG-coated silica nanoparticles exhibited higher adsorption on clay (montmorillonite). NPs adsorption was also independent of pH range.

Chapter 4

Materials and Methods

In this chapter, the materials used in this study are viewed. The experimental approaches and the overall methodology are discussed.

4.1 Materials

4.1.1 Core Plugs

In order to investigate the effect of rock properties on the recovery process, two rock types were selected for this study. Core plugs used for this study were drilled out of outcrops and are rather homogeneous. Berea and Keuper outcrops were selected based on their properties, which mimic to a certain extent the potential EOR candidates. 4.1

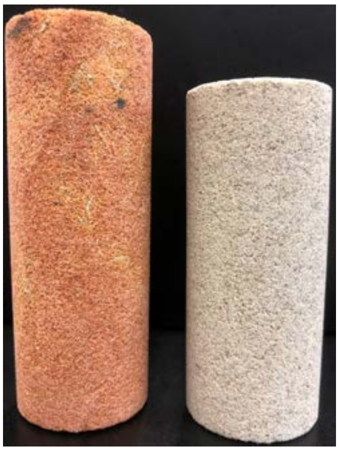

FIGURE 4.1: Core plugs (From left to right) Keuper - Berea

Berea

Berea outcrop is a yellowish grey sandstone. It consists of very homogeneous well-sorted sand with more than 85% quartz and approximately 6% feldspar. The degree of roundness varies between angular to sub-angular. The interparticle porosity governs the porosity system. The secondary porosity was reduced due to the crystal growth of quartz as shown in figure 4.2 which is SEM capture of a thin section from the same outcrop. In the center, heavily corroded feldspar can be spotted.

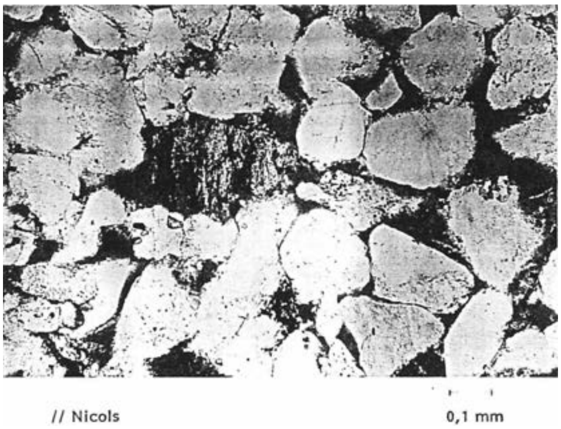

FIGURE 4.2: Thin section analysis - Berea

The measured porosity from RCA of the utilized core samples is plotted vs. the permeability to N_2 in figure 4.3.

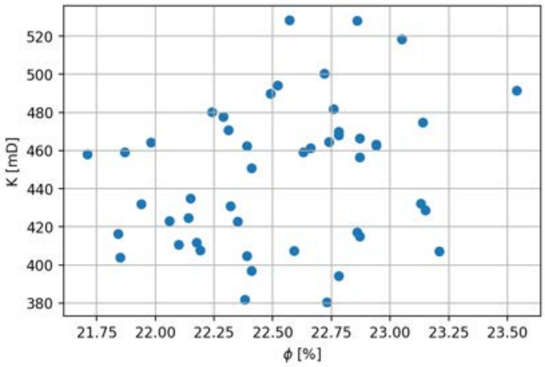

FIGURE 4.3: ϕ vs. K for Berea core plugs

Table 4.1 summarizes the main petrophysical properties of Berea core plugs [1]. Core plugs exhibit a good homogeneity.

TABLE 4.1: Properties of Berea core plugs

	$\phi[\%]$	**K [mD]**	$K_w[mD]$	$S_{wi}[\%]$
Mean	22.6	447.6	223.9	24.0
STD	0.4	37.4	17.9	8.0
Min	21.7	380.5	191.7	5.8
Max	23.5	528.4	262.6	43.9

---

[1] Data from 48 core plugs

Keuper

This sandstone is fine-grained and has a reddish-brownish color. Black dots or yellow intrusions can be spotted on some plugs. According to the thin-section analysis, the rock is a well-sorted sandstone arenite. Main minerals are quartz (88%), feldspar (1%), kaolinite (10%) and other minerals (1%). The governing porosity regime is interparticle porosity. Secondary porosity in feldspar contributes to minor part of the porous space. Iron oxide FeO.OH.nH$_2$O (limonite) covers the mineral grains and causes the reddish color.

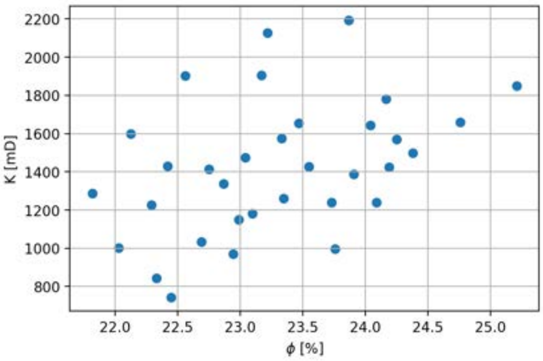

FIGURE 4.4: ϕ vs. K for Keuper core plugs

4.2 summarizes the main petrophysical properties of Keuper core plugs [2]. It can be seen that Keuper core plugs are less homogeneous than Berea core plugs. Keuper core plugs are more permeable despite having the same porosity range.

TABLE 4.2: Properties of Keuper core plugs

	$\phi[\%]$	$K[mD]$	$K_w[mD]$	$S_{wi}[\%]$
Mean	23.3	1425.2	890.0	21.4
STD	0.8	349.6	193.9	7.9
Min	21.8	743.1	511.8	4.7
Max	25.2	2193.5	1316.1	40.4

---

[2] Data from 33 core plugs

4.1.2 Fluids

Nanomaterials

Evonik Ressource Efficiency GmbH provided nanomaterials in the form of colloidal dispersion. Two Types of silica nanoparticles were tested. hereafter called material *A* and *B*, respectively (see figure 4.6). The base material of the particles is the same, but each type has undergone a different surface modification.

TABLE 4.3: Properties of the utilized nanomaterials

	A	*B*
Solid [wt %]	22.5	27.9
μ @ 10 1/s [mPas]	16	39
Particle Size (d50)	110	114
pH	9.5	3.2

Surface Modification Untreated silica nanoparticles have a strongly negative surface. In order to assure a stable dispersion, the ζ-potential should not be lower than $-25\,\mathrm{mV}$ (Huh et al. 2019). Nanomaterials surface can be modified through coating with metal cations, polymers or other organic components depending on field of application (Kim et al. 2014). ζ-potential varies with pH value of the solution. As demonstrated in figure 4.5a, ζ-potential varies slightly within the pH-range compared with type (*B*). Type (*B*) is more negatively charged and its ζ-potential changes within the same pH range as can be seen in figure 4.5b. This is due to the polar function (OH^-) of the surface coating material. ζ-potential measurements were carried out by the supplier of nanomaterials as well as the SEM imaging demonstrated in figure 4.6.

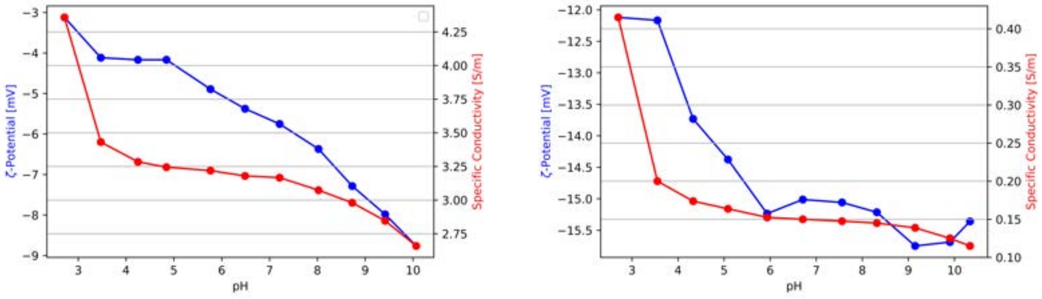

(A) Nanomaterial *A*

(B) Nanomaterial *B*

FIGURE 4.5: ζ-potential and specific conductivity

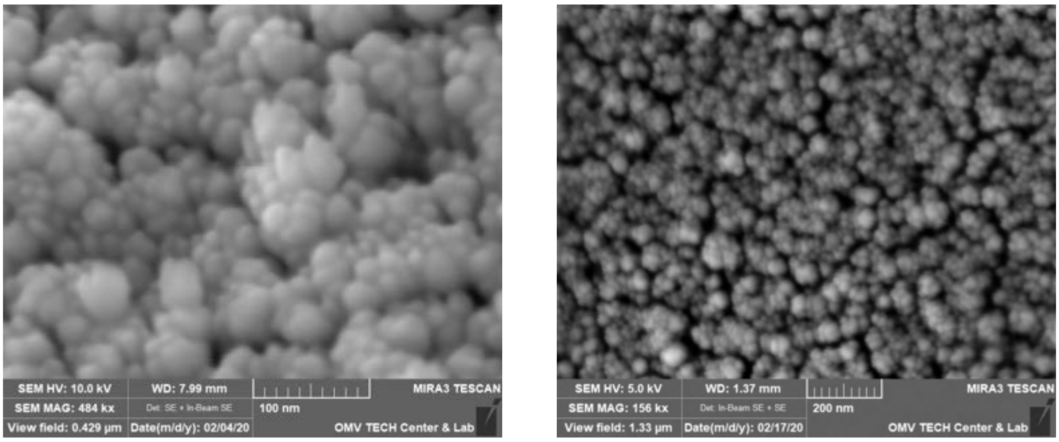
SEM HV: 10.0 kV
WD: 7.99 mm
MIRA3 TESCAN
SEM MAG: 484 kx
Det: SE + In-Beam SE
100 nm
View field: 0.429 μm
Date(m/d/y): 02/04/20
OMV TECH Center & Lab
SEM HV: 5.0 kV
WD: 1.37 mm
MIRA3 TESCAN
SEM MAG: 156 kx
Det: In-Beam SE + SE
200 nm
View field: 1.33 μm
Date(m/d/y): 02/17/20
OMV TECH Center & Lab

(A) Nanomaterial *A* (B) Nanomaterial *B*

FIGURE 4.6: SEM imaging of both nanomaterials

ζ-potential Titration ζ-potential was assessed using the device *DT-300* manufactured by *3P*. The colloidal dispersion was titrated over a pH range (3-10). The measurement is based on the following physical process:

- An ultrasonic wave vibrates the suspended particles within the liquid phase due to the density contrast.
- The electrostatic equilibrium is consequently disturbed and transient dipoles are formed.
- Hence, an alternating current is generated which can be measured as well as the specific conductivity.

As demonstrated in figure 4.5a, ζ- potential of material *A* decreases slightly from -3 mV to -9 mV when the pH increases from pH 3 to pH 10 slightly within the pH-range compared with type (*B*). *B* is more negatively charged and its ζ-potential changes drastically decreases from -12 mV at pH 3 to -15 mV at pH 10 (figure within the same pH range as can be seen in 4.5b). This is due to the polar functionality (OH –) of the surface coating material.

Crude Oil

In order to evaluate the effect of oil composition on the EOR, two oil samples were used. The main difference is total acid number, which is a crucial parameter for this study. Due to geochemical factors, other compositional and rheological properties varies. 4.4 summarizes the properties of both samples.

TABLE 4.4: Properties of crude oil samples

	High TAN	**Low TAN**
Reservoir	16 TH	Flysch
Well	Bockfliess 112	St. Ulrich 65
TVD top [m]	1622	1060
TAN [mg KOH/g]	1.55	0.39
Saturates [%]	39	55
Aromatics [%]	20	25.6
Resins [%]	39	18.6
Asphaltene [%]	2	0.8
μ @ 60 °C [cP]	11.9	6
ρ @ 20 °C [g/cm^3]	0.917	0.866
ρ @ 60 °C [g/cm^3]	0.884	0.842

Brine

In order to investigate the effect of divalent cations, two synthetic brines were used, and the composition of both brine is listed in table 4.5.

- Softened injection brine (TW)
- Synthetic formation brine (FW)

TABLE 4.5: Composition of synthetic brine

	TW	**FW**
$NaCl$ [g/L]	18.96	19.75
$NaHCO_3$ [g/L]	1.96	-
$CaCl_2 \cdot 2\,H_2O$ [g/L]	-	0.4
$MgCl_2 \cdot 6\,H_2O$ [g/L]	-	0.66
NH_4Cl [g/L]	-	0.17
$SrCl_2 \cdot 6\,H_2O$ [g/L]	-	0.06
$BaCl_2 \cdot 2\,H_2O$ [g/L]	-	0.03

Chemical Combinations for EOR

Different fluid combinations were prepared. Solutions with 0.1 wt% of nanomaterials were prepared as common practice. Alkaline solutions were prepared with concentration of 3000 ppm of Na_2CO_3. According to the study conducted by Lüftenegger et al. 2017 using 16TH oil, any higher alkali concentration will not result in further reduction of interfacial tension.

TABLE 4.6: Properties of the utilized fluids

Fluid	Density [Kg/m^3] Avg	Density [Kg/m^3] Std	pH Avg	pH Std
TW	0.9943	0.00	8.93	0.00
FW	0.9955	0.00	NA	NA
0.1 wt% Type (A) in TW	0.9977	0.00	8.56	0.02
0.1 wt% Type (B) in TW	0.9848	0.01	8.76	0.02
0.1 wt% Type (A) + 3000 ppm Na_2CO_3 in TW	0.9926	0.00	9.93	0.00
0.1 wt% Type (B) + 3000 ppm Na_2CO_3 in TW	1.0007	0.00	9.92	0.01
3000 ppm Na_2CO_3 in TW	0.9982	0.00	9.98	0.02

4.2 Experimental Procedure

4.2.1 Overall Methodology

In order to evaluate the potential impact of nanomaterials on the recovery process, the following workflow was adopted:

- Characterization of the utilized materials (RCA, density measurements, pH measurements, etc.).
- Dispersion stability by monitoring the prepared brine for any flocs or indication of colloidal instability
- Fluid/Fluid interactions through:
  - IFT measurement to examine the impact of nanomaterials on the interfacial properties.
  - Phase behavior test in order to investigate different combinations.
- Rock/Fluid interactions using spontaneous imbibition test.
- Dean-Stark extraction.
- Results analysis by the means of *inverse Bond number* and *capillary diffusion coefficient*.

4.2.2 Routine Core analysis

Porosity and Pore Volume

Porosity was measured according to Boyle's law. The helium technique was employed to determine the pore volume, which yields the effective porosity. 4.7 represents a schematic of the porosimeter.

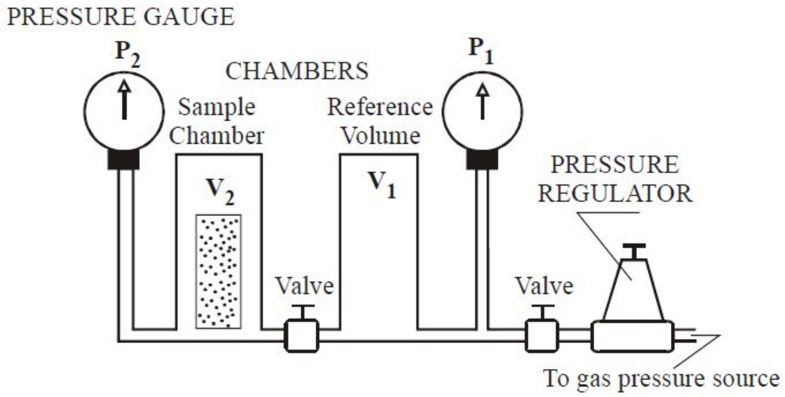

FIGURE 4.7: Schematic of helium porosimeter (Torsæter et al. 2003)

Helium is injected into a chamber that contains the sample. After pressure stabilization, a valve leading to a reference chamber with known volume is opened, and the pressure drop is measured. The volume of gas is determined using the equation of state. Triplicate measurements ensure a good data quality Pore volume (PV) can be determined as following:

$$p_1 V_1 + p_2 V_2 = p(V_1 + V_2) \tag{4.1}$$

In order to determine the pore volume V_2:

$$V_2 = \frac{p - p_1 V_1}{p_2 - p} \tag{4.2}$$

The bulk volume was determined by measuring the sample dimensions (length, diameter). Measurements were carried out on triplicate in order to insure reproducibility.

Permeability to Gas

Permeability was measured using Nitrogen by placing the core plug a Hassler cell connected to differential pressure transducer. N_2 is injected from the inlet at a rate of 400-800 $\mathrm{mL\,min^{-1}}$ and the outlet is at atmospheric pressure. After pressure stablization, Darcy's law4.3 is applied to estimate the permeability. Results is corrected for Klingenberg effect.

$$q = -\frac{KA}{\mu L}\Delta P \tag{4.3}$$

4.2.3 Density measurements

Fluid densities were measured using *Anton Paar DMA 5000 M* density meter demonstrated in figure 4.8.

The device relies on the oscillating U-tube principle. A U-shaped tube oscillates at its characteristic frequency. The characteristic frequency varies depending on the density of measured fluid.

All the measurements were performed in triplicates in order to capture the uncertainty. The average value was considered for further calculations.

FIGURE 4.8: Anton Paar DMA 5000 M (Anton Paar 2020)

4.2.4 Phase Behavior

The phase behavior was assessed using the procedure described by Sheng 2011. Glass pipettes with a capacity of 10 ml a manufactured by *Fisher* were filled with the aqueous phase and the oil at a ratio 1:1. Subsequently, the pipettes sealed with a CH_4/O_2 flame. The pipettes were shaken for 70 hours before they were placed into the oven under 60 °C. volumes of each phase (brine, oil and emulsion) were read for the next 100 days. This time was chosen because it is believed that an equilibrium is reached within this period.

4.2.5 IFT

IFT was measured using a spinning drop tensiometer **SDT** manufactured by *Krüss*.

KRÜSS
Spinning Drop Tensiometer

FIGURE 4.9: Spinning drop tensiometer SDT (Krüss Scientific 2018)

The device relies on shape analysis of the oil drop. The geometry of the oil drop was analyzed throughout the experiment. The length and diameter of the drop were determined using image recognition.

Measurement Conditions

All the measurements were conducted under reservoir temperature at 60 °C. A rotational speed of 7000 rpm was maintained during all measurements. With total observation time of 300 min, 900 data points were collected, and the time interval was with 20 s.

Procedure

An oil droplet is suspended in brine within a silica glass capillary. When the capillary starts to spin, the centrifugal force pushes out the heavy phase (aqueous phase) more strongly than the lighter phase (oleic phase) due to its higher density. This results in pushing the oil droplet towards the center of the capillary and eventually elongating it. Based on droplet's shape, one of the following fits is applied to obtain the IFT at each step (Viades-Trejo et al. 2007).

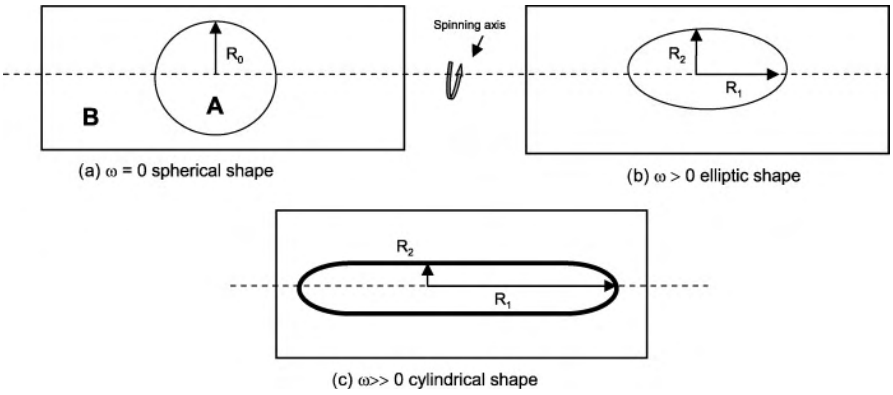

FIGURE 4.10: geometry of the spinning drop (Viades-Trejo et al. 2007)

Young-Laplace Fit Before applying any centrifugal force, the droplet has a spherical shape. For high to medium IFT values, the droplet elongates into an elliptic form upon spinning.

$$\Delta P = \sigma(\frac{1}{r_1} + \frac{1}{r_2}) \tag{4.4}$$

Where ΔP is the differential pressure on the inner and outer side of the curved surface, σ the interfacial tension and r_2, r_1 are the radii of curvature as shown in figure 4.10.

Vonnegut's Fit When the IFT drops to low values and the ratio $\frac{r_2}{r_1} > 4$ *Young-Laplace* fit is not valid.

Vonnegut's fit is applicable for cylindrically-shaped droplets

$$\sigma = \frac{\Delta\rho\omega^2 R^3}{4} \tag{4.5}$$

where $\Delta\rho$ is density difference between the phases, ω is the rotational speed and R is the droplet radius.

4.2.6 Pre-Saturation

Figure 4.11 illustrates the flooding setup that was used to pre-saturate the core plugs with water and oil and determine the endpoint relative permeability for each phase.

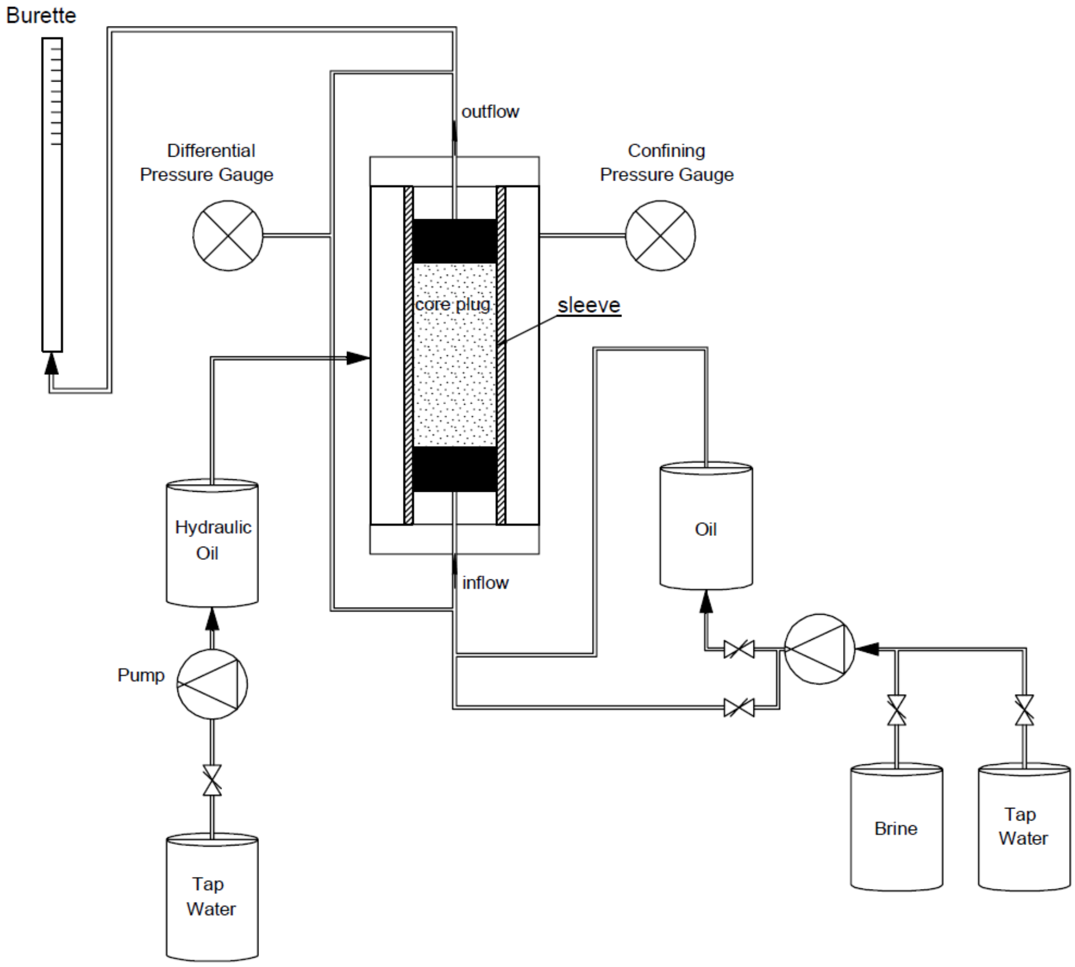
Burette
outflow
Differential Pressure Gauge
Confining Pressure Gauge
core plug
sleeve
Hydraulic Oil
Oil
inflow
Pump
Brine
Tap Water
Tap Water

FIGURE 4.11: Schematic of prestauration setup

Workflow

- The core plugs were initially placed in a vacuum glass cell and connected to an vacuum pump. The cell was vacuumed until 1 µbar was reached and then saturated with synthetic brine.
- Once the core plug was fully saturated with brine, the plug was placed into the core holder (Hassler Cell) and a confining pressure of 40 bar was applied to ensure that injected fluid does not bypass the plug.
- After flushing the cores with 2 PV of brine to insure a complete water saturation, differential pressure was recorded for different flow rates.
- The permeability to water at 100% water saturation is measured by flooding at different rates and measuring differential pressure. Data was inputted in equation 4.3o determine permeability to water by Darcy's Law.

- Subsequently, oil is connected to the inflow. The core plug was flushed by oil overnight at a very low rate $0.10\,\mathrm{mL\,min^{-1}}$.
- The displaced water was collected in burette, and the volume was recorded to determine the water saturation.
- In order to overcome the capillary end effect, bump rates were applied.
- Oil at bump rates up to $7\,\mathrm{mL\,min^{-1}}$ is pumped until no additional water is displaced.
- Water saturation in the core plug was calculated and assumed to be the irreducible water saturation.
- The permeability to oil was measured at the irreducible water saturation.
- Finally, core was dismounted and placed in a vial submerged in oil.
- Core plug was aged in an oven at 60 °C for 3-4 weeks.

4.2.7 Endpoint Permeability

After flushing the cores with 2 PV of brine to insure a complete water saturation, differential pressure is recorded for different flow rates. The flow rates were selected so that Reynolds number was maintained below 1in order to maintain a laminar flow regime (Bear 2013).

$$Re = \frac{\rho q d}{\mu} \tag{4.6}$$

Where: Re : Reynolds Number [dimensionless], ρ : Fluid density [$\mathrm{kg/m^3}$], q: interstitial velocity [$\mathrm{m\,s^{-1}}$], d: the mean grain diameter [meter], μ: dynamic viscosity [$\mathrm{kg\,s^{-1}\,m^{-1}}$].

The mean grain diameter was estimated using the empirical relationship from Berg 1970 The same procedure is followed to calculate the oil end-point permeability at irreducible water saturation.

Example: Keuper 123

The core plug has a porosity $\phi = 22.56\%$ and permeability to gas $K = 1906mD$. An average grain diameter of 375 µm was estimated based on based on figure 4.12. For the highest flow rate ($10\,\mathrm{ml\,min^{-1}}$), an interstitial velocity of $10.45 \times 10^{-4}\,\mathrm{m\,s^{-1}}$ was calculated.

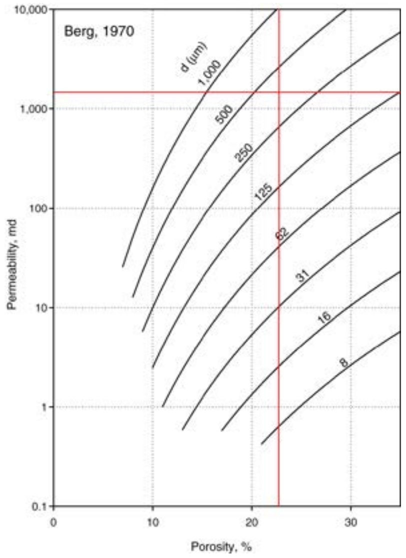

FIGURE 4.12: Relating permeability to porosity with varying median grain size (Berg 1970). Permeability and porosity of core plug Keuper 123 are marked with red lines

By applying the equation 4.6, the value of Reynolds number is 0.39. This indicates that laminar flow regime is dominating and it is safe to apply Darcy's law to estimate the water permeability at 100 % water saturation. Figure 4.13 shows the differential pressure response for the various flow rates for core plug K123,

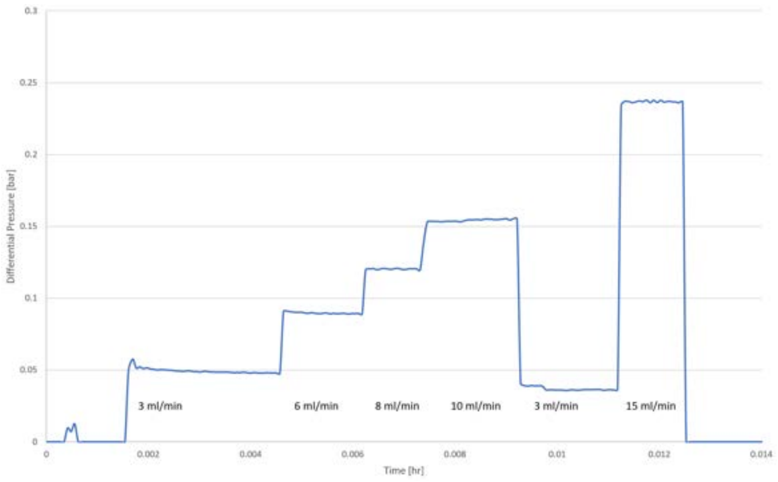

FIGURE 4.13: ΔP vs time for different rates - Keuper 123

Linear Regression

In order to save time, end-point permeability measurements were collected from different cores and a multi linear regression was ran to estimate the endpoint permeability to water, using the porosity and permeability to N_2. A linear fit for each rock type was conducted. Table 4.7 summarizes the fitting parameter as shown in figure 4.14; the predicted values were plotted against the measured values to ensure the accuracy of the prediction.

TABLE 4.7: Regression Parameters

	Berea	**Keuper**
Slope	0.55	0.21
Intercept	122	133

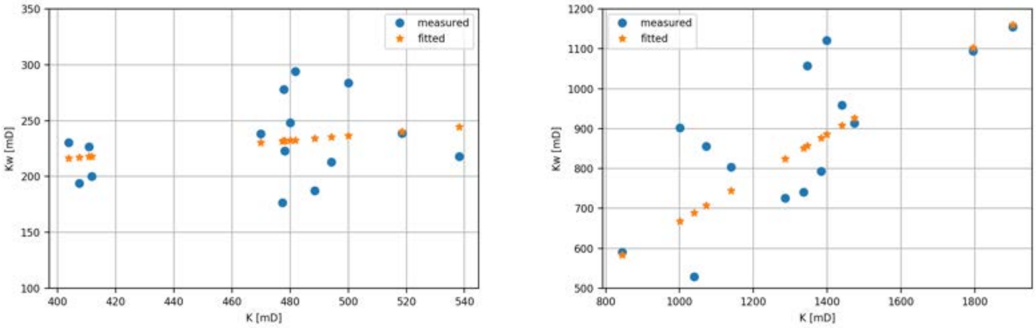

(A) Berea

(B) Keuper

FIGURE 4.14: Permeability to water, measured vs fitted

4.2.8 Spontaneous Imbibition

Amott cells (shown in 4.15) of temperature-resistant glass manufactured by *PanTerra* were used to perform spontaneous imbibition tests.

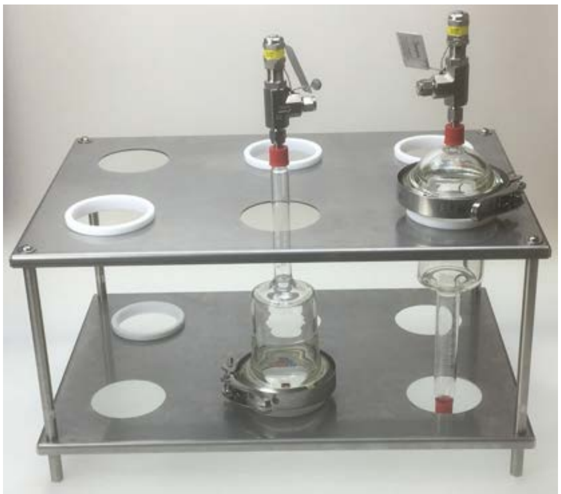

FIGURE 4.15: Amott cell for imbibition (left) and drainage (right) (PanTerra 2020)

The core was placed into the cell submerged in the tested brine. The oil was spontaneously produced by the capillary imbibition mechanism. As produced oil was collected in a graduated tube, the volume was read in short time intervals at the beginning (hourly on the first day) and larger time intervals (daily) once the imbibition process slowed down. The test cells were placed in an oven as shown in figure 4.16 under the reservoir temperature 60 °C.

The cells were occasionally shaken before readings in order to release the droplets attached on the core. The test was run until a production plateau was observed.

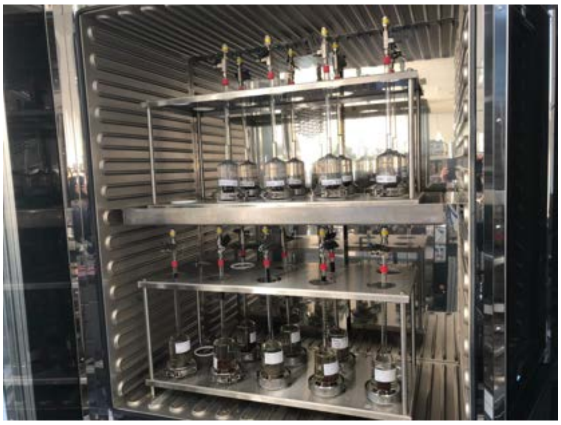

FIGURE 4.16: Amott cells in the oven

4.2.9 Dean-Stark extraction

Dean-Stark extraction was conducted after the spontaneous imbibition test. In order to quality-control the recovery values obtained from spontaneous imbibition tests and assure the final water saturation values.

Setup and Workflow

A schematic of Dean-Stark apparatus shows the measurement principle (figure 4.17).

Toluene (1) is used as solvent at lab grade according to McPhee et al. 2015. By heating the solvent in a flask (2) until boiling point, toluene vapor passes through the sample (3) evaporating the water. the toluene/water mixture passes through the condenser (5) which is cooled down by a water stream (6,7). Due to cooling, the mixture condenses and falls down into the burette (8). Due to gravity segregation, water separates from toluene. The process is performed for 48 hours and the extracted water volume is recorded.

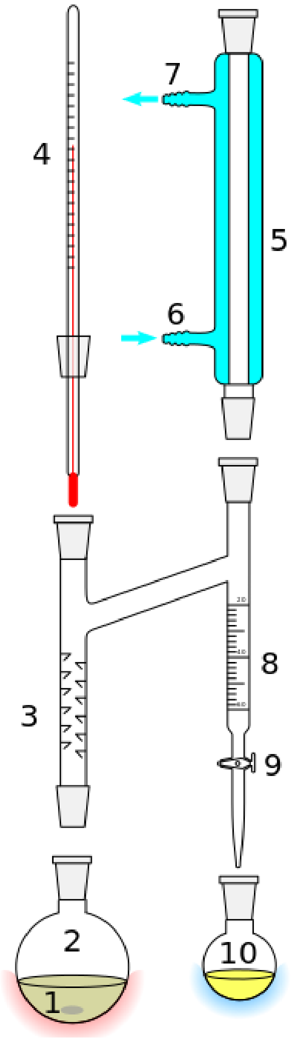

FIGURE 4.17: Dean-stark apparatus (McPhee et al. 2015)

Chapter 5

Results and Discussion

In this chapter, experimental data obtained from; interfacial tension measurements, phase behavior experiments and spontaneous imbibition tests will be reviewed and discussed.

5.1 Interfacial Tension

In order to investigate the effect of type of nanomaterial, alkali and oil acidity on interfacial tension, IFT measurements were carried out between different EOR fluids and high and low TAN oil.

5.1.1 High TAN Oil

Nanomaterials as standalone EOR agent

The interfacial tension in oil/brine system stabilized at 8.4 mN/m. As can be seen in figure 5.1a, nanomaterial *B* could lower the IFT compared to the base case (softened injection brine). The IFT reduction is attributed to adsorption of particles onto the oil-water surface. The adsorption is limited by the hydrophobicity of the particles surface. Hydrophilic particles tend to remain suspended within the aqueous phase instead of traveling towards the interface. Despite the fact that both nanomaterials share the same base composition (SiO_2) and approximately the same dimensions, nanomaterial *B* performed better than *A* in terms of IFT reduction. The more neutrally-charged surface makes *A* more preferable accumulate onto the interface. However, the large particle size results in a lower specific surface area. With nanomaterial *B*, the surface was modified to increase its hydrophobicity. Nevertheless, figure 4.5 revealed that *B* is more negatively-charged, thus the electrostatic repulsion becomes more effectual (Vatanparast et al., 2018).

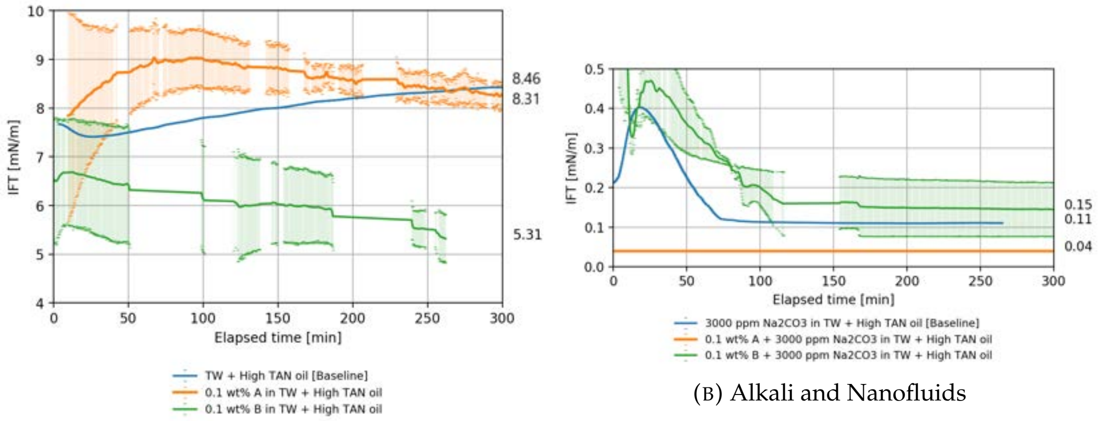

(B) Alkali and Nanofluids

(A) Nanofluids

FIGURE 5.1: Interfacial tension vs time - High TAN oil

Nanomaterials and Alkali

IFT between combinations of nanomaterials and 3000 ppm of sodium carbonate (Na_2CO_3) and high TAN oil was measured. The utilization of alkali leads to a drastic reduction of IFT as shown in figure 5.1b. Alkali reacts with acidic components of the oil producing in situ surfactants (soap) which contribute mainly to the IFT reduction (Schumi et al. 2019). An interesting behavior was a slight increase in the IFT at the beginning if the measurement followed by a steep drop and a stabilization. Neubauer et al. 2020 observed a similar behavior. Sharma et al. 1989 explained that by the shielding of the newly formed surfactants at the interface. Thus, the consumption of alkali is decelerated. Due to convective diffusion at the interface, surfactant molecules migrate towards the aqueous phase allowing the reaction to occur until an equilibrium has been reached. In comparison with the base case (softened injection brine with 3000 ppm of Na_2CO_3), nanomaterial *B* had no substantial effect on the interfacial tension (0.15 vs. $0.11\,\mathrm{mN\,m^{-1}}$, see also table 5.1). This can be explained as following: The electrostatic repulsion between the anionic surfactant molecules and silica particles is very prominent. However, surfactant molecules are the main player in IFT reduction. Vhen nanomaterials replace the surfactant molecules at the interface, the IFT is less reduced (Huh et al. 2019). However, a synergistic effect between nanomaterial *A* and the alkali can be noticed and it resulted in IFT reduction to $0.04\,\mathrm{mN\,m^{-1}}$.

It is seen that the IFT reduction took place at the early stage of the measurement. Hence, due to the short time scale of this mechanism in comparison with other recovery mechanisms (e.g. imbibition or wettability alteration) we can safely assume a constant IFT value for the whole procedure.

5.1.2 Low TAN Oil

Nanomaterials as standalone EOR agent

The addition of nanomaterial *A* resulted in a slight IFT reduction compared to the base case (from 3.3 to $2.60\,\mathrm{mN\,m^{-1}}$) (figure 5.2a and table 5.1). Nanomaterial *B* performed better and reduced the IFT to $1\,\mathrm{mN\,m^{-1}}$ due to the more negatively charged surface. IFT reduction is attributed here to the accumulation of particles at the fluid/fluid interface.

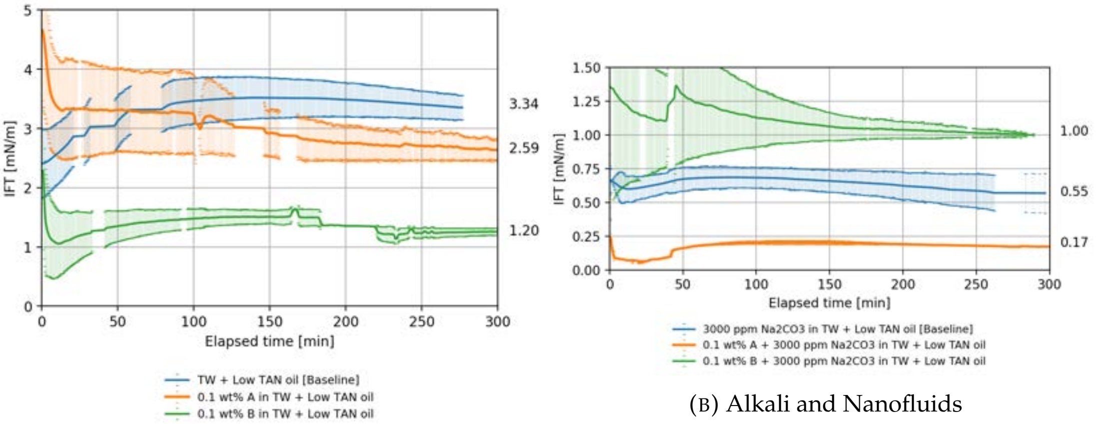

(B) Alkali and Nanofluids

(A) Nanofluids

FIGURE 5.2: Interfacial tension vs time - Low TAN oil

Nanomaterials and Alkali

The addition of alkali to the synthetic softened water had a significant impact on the IFT despite the low TAN number of the oil. As in high TAN case, *A* outperformed *B* when combined with alkali.

IFT was measured between a solution of 3000 ppm of Na_2CO_3 and low TAN oil at $0.55\,\mathrm{mN\,m^{-1}}$. The addition of nanomaterial (*B*) did not result in further IFT reduction which can be mainly attributed to alkali acid reaction. Nevertheless, nanomaterial *A* exhibited a strong synergy with alkali and IFT was lowered to $0.17\,\mathrm{mN\,m^{-1}}$ as shown in figure 5.2b. This can be explained by its more neutrally charged surface as discussed in chapter 4.

The reaction between alkali and acidic components of the oil takes place but the oil does not contain enough acids to sustain the reaction and lower the IFT further. Therefore, the IFT was reduced to lower values for high TAN oil than for low TAN oil.

5.1.3 Summary

Nanomaterials were effective in terms of IFT reduction. Combined with alkali, very low IFT values as low as $0.04\,\mathrm{mN\,m^{-1}}$ can be achieved.

TABLE 5.1: Summary of IFT values of various oil/brine systems

Brine	**Oil**	**AVG** [$mN\,m^{-1}$]	STD	**Oil**	**AVG** [$mN\,m^{-1}$]	STD
Baseline(TW)	High TAN	8.40	-	Low TAN	3.40	0.50
0.1 wt% A + TW	High TAN	8.30	0.15	Low TAN	2.60	0.13
0.1 wt% B + TW	High TAN	5.31	0.49	Low TAN	1.26	0.06
3000 ppm Na_2CO_3 + TW	High TAN	0.11	0.00	Low TAN	0.55	0.15
0.1 wt% A + 3000 ppm Na_2CO_3 + TW	High TAN	0.04	0.00	Low TAN	0.17	0.00
0.1 wt% B + 3000 ppm Na_2CO_3 + TW	High TAN	0.15	0.06	Low TAN	1.00	0.01

It can be observed that for oil-brine systems with high IFT, the measurements were hardly reproducible. Thus, it is important to note that the IFT measurements of high IFT cases cannot offer a conclusive quantification but rather a qualitative comparison of the IFT trends.

The following issues were observed and might have contributed to the uncertainty in the measurements.

- Junction of oil droplets that leads to change in dimensions and hence, a new IFT value.
- Switching the fitting algorithm during the measurement
- Under low IFT values, separation of oil droplet occurred leading to a new dimension and hence new IFT value.
- Connection to the camera was occasionally lost due to memory issues leading to a discontinuity of the measured IFT.
- Spinning drop method works better for low IFT systems (below 1 $mN\,m^{-1}$). Above this value, other techniques are more suitable (pendant drop).
- Pendant drop measurements were not possible under 60 °C only at room temperature because the droplet was detached before IFT stabilized.
- IFT value with distilled water should be around 20-30 $mN\,m^{-1}$. Nonetheless, the measured value with synthetic injection brine (TW) was significantly lower. This is presumably due to the presence of carbonate buffer[1] which reacts to a certain extent with acidic components of the oil.

5.2 Phase Behavior

The goal of phase experiments is to study the emulsification process and emulsion stability over time.

---

[1] See table 4.5

5.2.1 Compatibility Test

During fluid preparation, white sediment deposited in the solutions that contain nanomaterials and alkali, which were prepared using synthetic formation brine rich in divalent cations [2]. Nevertheless, this precipitation did not occur in the nanomaterials suspension diluted with formation brine. A solution of 3000 ppm Na_2CO_3 was prepared using formation brine and monitored for a few hours. As shown in figure 5.3, precipitation similar to the previously mentioned one was observed, however, to a lower extent. The precipitation is triggered by the reaction of dissolved calcium with alkali due to supersaturation of calcium carbonate at a specific pH range (Spanos et al. 1998). In the presence of nanomaterials, hetero aggregation of calcium carbonate flocs and the nanomaterials (Liesegang et al. 2017) or incorporation of nanoparticles in calcium carbonate (Magnabosco et al. 2019) is believed to occur. Hence, it is not recommended to use alkali when the formation brine is rich in divalent cations.

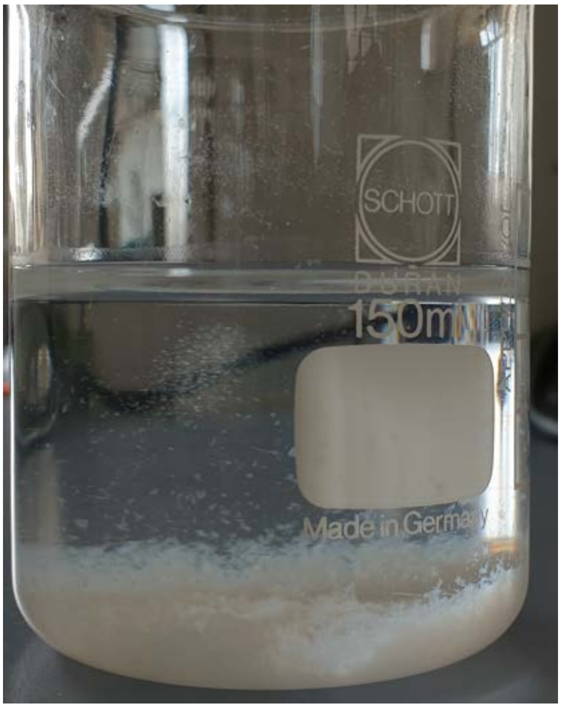

FIGURE 5.3: Precipitation in the formation brine/alkali solution

5.2.2 High TAN Oil

It can be concluded that the emulsification process was mainly driven by the alkali-acid reaction. Nanomaterials alone were not able to emulsify a significant amount of oil. However, a thin emulsion layer was observed at the oil/brine interface, and it was stable throughout the measurement period. Figure 5.4 shows that the emulsions formed under the presence of nanomaterials and alkali were very stable compared to alkali alone.

---

[2] See table 4.5 for brine composition

In previous work from Neubauer et al. 2020, nanomaterial *B* produced more stable emulsions, which had also better rheological properties after 100 days. The difference between out work and the previously conducted work by Neubauer et al. 2020 can be attributed to the initial energy input that may have differed from the previous study (Arab et al. 2018) or differences in the experimental setup.

Figure 5.5 shows the middle-phase macroemulsion. it can be observed that the emulsions obtained with nanomaterial *B* have a slightly darker color, which indicates higher oil content. To explain that, two questions have to be answered. Firstly: How do phase separation occur. secondly: How emulsions are stabilized. The main mechanism of phase separation is droplets junction. emulsions are created when oil droplets are coated with hydrophilic layer and dispersed within the aqueous phase. Binks et al. 2007 suggested that the synergy between is triggered when the oppositely-charged surfactant molecules are attached to nanoparticles surface changing their wettability. In our case, the oil droplets, which are covered by anionic surfactants (soaps), are sterically hindered from coagulation due to the electrostatic repulsion. The dispersion of negatively charged particles in the medium enhances this repulsive interaction.

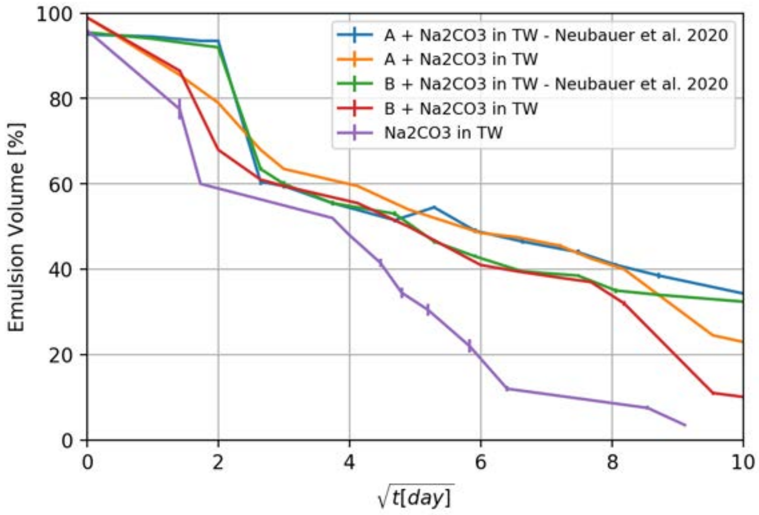

FIGURE 5.4: Emulsion volume vs time - High TAN oil

Emulsion Type

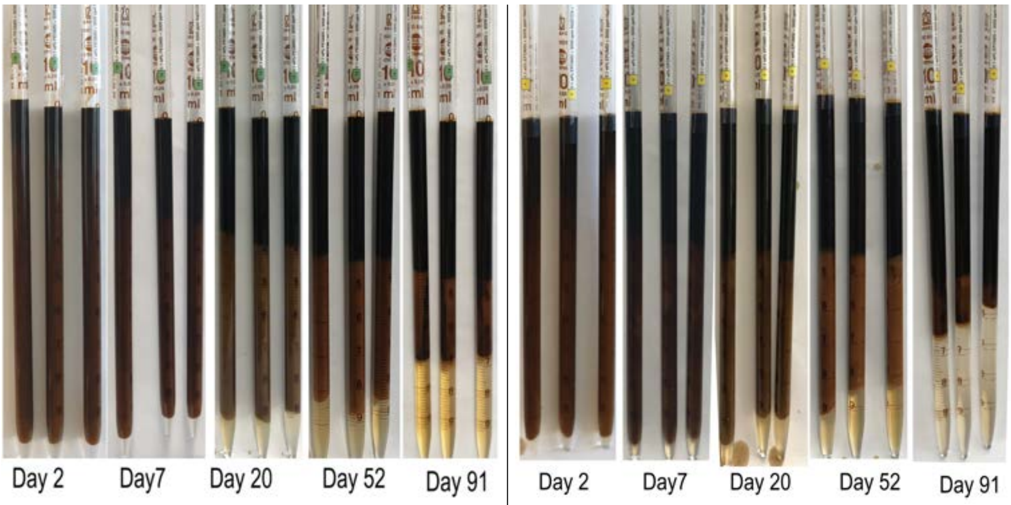

(A) 0.1 wt%A + 3000 ppm Na_2CO_3 (B) 0.1 wt%B + 3000 ppm Na_2CO_3

FIGURE 5.5: Formed emulsion with alkali and nanomaterials - High TAN oil - Softened injection brine (Triplicates)

Solublization Factor

S_F was reviewed in section 2.7.3. S_F was computed for the solutions containing nanoparticles only and they were treated as surfactant molecules. This was not applicable to alkaline solutions since the mass of generated soap is unknown. After 100 days S_F using nanomaterial (A) was $\underline{13.3}$ while for (B) was $\underline{35.2}$

5.2.3 Low TAN Oil

In case of low TAN oil, high emulsion volume was observed directly after mixing.

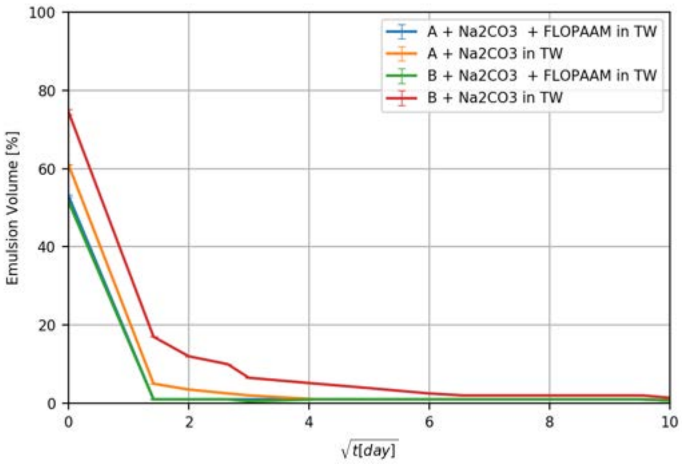

FIGURE 5.6: Emulsion volume vs time - Low TAN oil

Despite the low TAN number, high initial emulsion volume was obtained using alkali. Figure 5.6 shows that nanomaterial *B* resulted in a better emulsification with alkali. In general, alkali, together with the acidic components of the oil, provided the necessary medium for emulsification, while nanomaterials stabilized the emulsion.

Both nanomaterials showed the same emulsification behavior with low TAN oil in the absence of alkali. A thin film was developed at the interface and was stable throughout the measurement period.

Figure 5.7b shows the formed emulsion using alkali and nanomaterial *B* with low TAN oil. A middle phase of macroemulsion can be recognized. In comparison with figure 5.7a, we can see that the emulsion phase for both nanoparticles shows similar optical properties (Dark milky color).

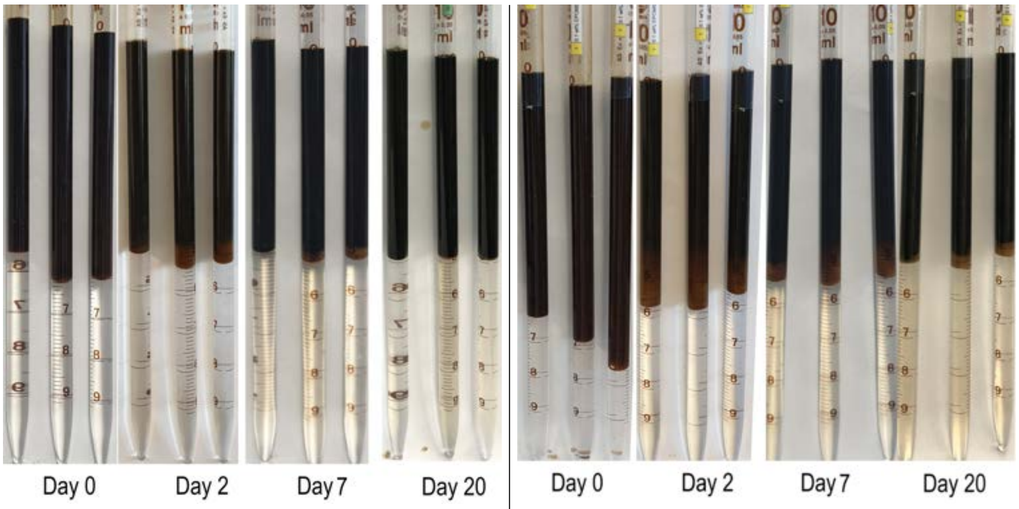

(A) 0.1 wt%A + 3000 ppm Na_2CO_3 (B) 0.1 wt%B + 3000 ppm Na_2CO_3

FIGURE 5.7: Formed emulsion with alkali and nanomaterials - Low TAN oil (Triplicates)

5.3 Spontaneous Imbibition

This section evaluates the rock-fluid interactions by observing the oil recovery by the spontaneous imbibition of the brine. In order to capture the various effects and parameters that control this process, different cases were tested as following:

TABLE 5.2: Investigated parameters using SI tests

Oil	High TAN Low TAN
Rock Type	Berea Keuper
Nanomaterials	Type A Type B
Alkali	no alkali 3000 ppm Na_2CO_3
Divalent Cations	Softened injection brine (TW) Synthetic formation brine (FW)

5.3.1 Baseline Experiments

The baseline experiments consist of four different oil/rock combinations soaked in softened injection brine. These tests are crucial to assess the additional recovery by utilizing EOR fluids. Figure 5.8 shows the oil recovery versus square root of time.

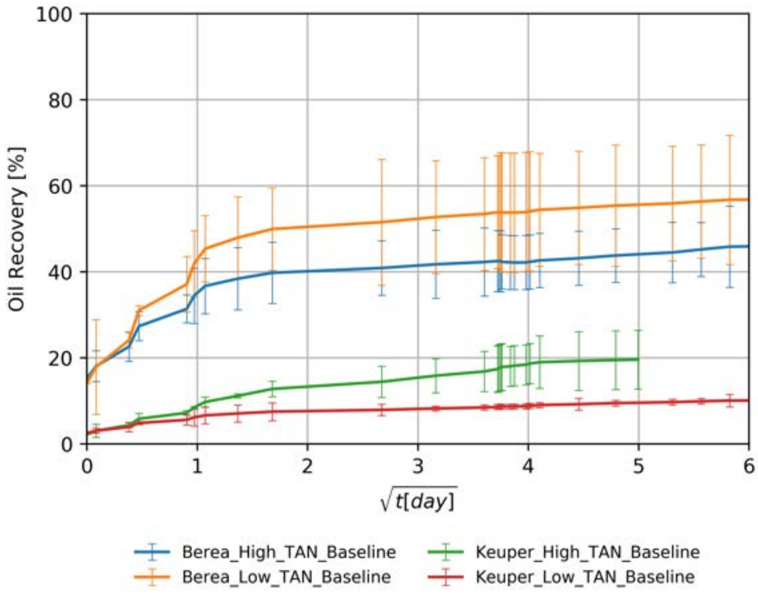

FIGURE 5.8: Oil recovery using softened injection brine (Baseline)

The following observations can be made:

Initial wettability state The high recoveries from Berea samples for both oil types can be attributed to a mixed-wet state.

Core plugs permeability Since the spontaneous imbibition is a capillary driven mechanisms, the recovery was higher/faster in the cores with lower permeability where the capillary forces tend to be more significant (Morrow et al. 2001).

IFT From 5.9 we can observe the relatively large volume of the produced oil droplets, which indicates a high IFT regime between the oil and brine , which is in accordance with the IFT measurements.

Oil viscosity Low TAN oil has significantly lower viscosity than high TAN oil (6 mPa s and 11.90 mPa s for low and high TAN oil respectively). In core plugs with low permeability, the recovery values were higher for the low TAN oil, which is in agreement with the results of Zhou et al. 2002 and Meng et al. 2017 who observed a similar behavior in low-perm dolomite. They attributed that proportionality between ultimate oil recovery to the square root of dimensionless time $\sqrt{t_D}$. t_D is given by the equation 5.1. Under the same capillary pressure and wettability it is directly dependent on the mobility ratio M [3].

$$t_D = t\sqrt{\frac{K}{\phi}}\frac{\sigma}{L_D^2}\sqrt{\lambda_{rw}^*\lambda_{rnw}^*}\frac{1}{\sqrt{M^*}+\frac{1}{\sqrt{M^*}}} \tag{5.1}$$

Where: K, ϕ are the rock permeability and porosity, σ is the interfacial tension, L_D is the characteristic length, λ_{rnw} and λ_{rw} are the characteristic mobilities for non-wetting and wetting phase respectively and M^* is the characteristic mobility ratio.

Imbibition mechanisms Counter current SI was more dominant especially at the early stage of the process. This can be concluded from the observation that most of the produced oil droplets were accumulating on the walls of core plugs.

Clay content Keuper core plugs with clay content higher than 10% are believed to be more oil wet according to Sayyouh et al. 1990 who suggested that under low to moderate salinity the tendency towards oil-wet increases with increasing clay content. More oil wetness makes the water less favorable to imbibe into the core, and thus the recovery under SI will be lower.

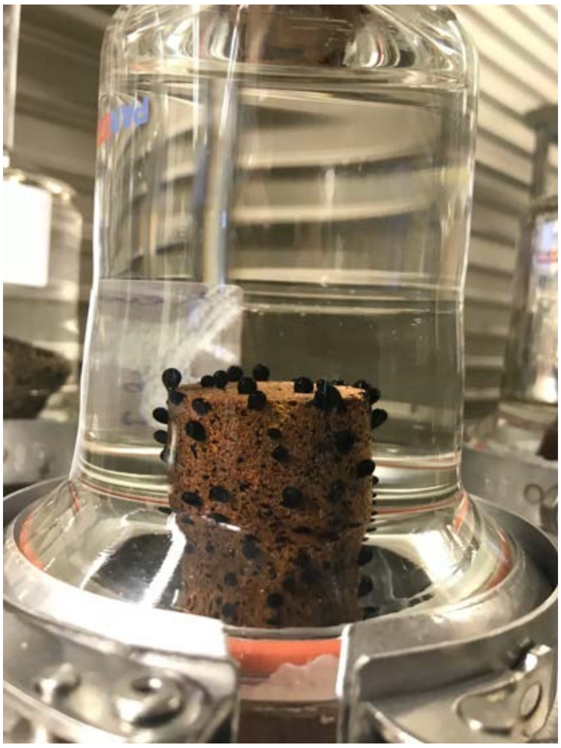

FIGURE 5.9: Oil droplets on Keuper core plug

---

[3] See equation 2.5

Berea Samples

Figure 5.10 depicts the recovery from individual core plugs.

The baseline experiments using high TAN oil was run in duplicates. Core plugs 5-114 and 5-147 were submerged in softened injection brine (TW). Both core plugs followed the same recovery curve and the end recoveries were 41.1 % and 53.3% respectively.

For low TAN oil, core plugs 5-184 and 5-179 were used. Core plug 5-179 exhibited more rapid imbibition, and the final recoveries were 67% and 47% respectively.

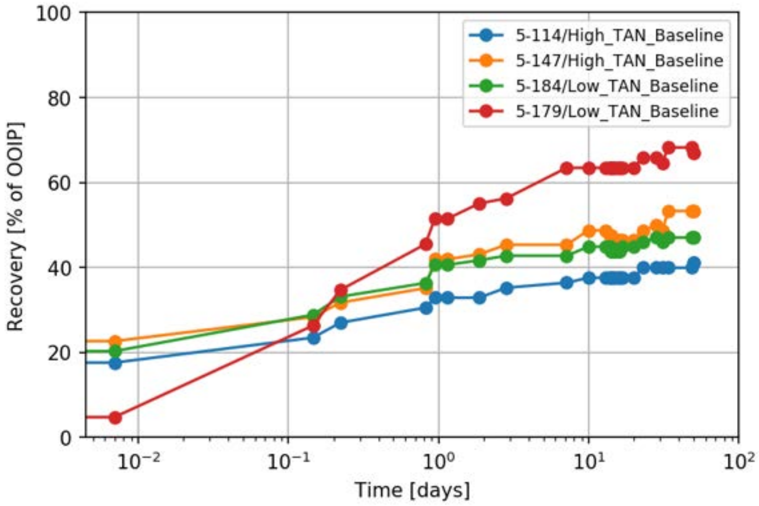

FIGURE 5.10: Oil recovery from Berea core plugs (Baseline)

Keuper Samples

For the baseline experiments in Keuper with high TAN oil, the test was conducted in triplicates. Core plugs (K103, K98 and K108) were tested using Amott cells. Figure 5.11 illustrates oil recovery from the selected cores.

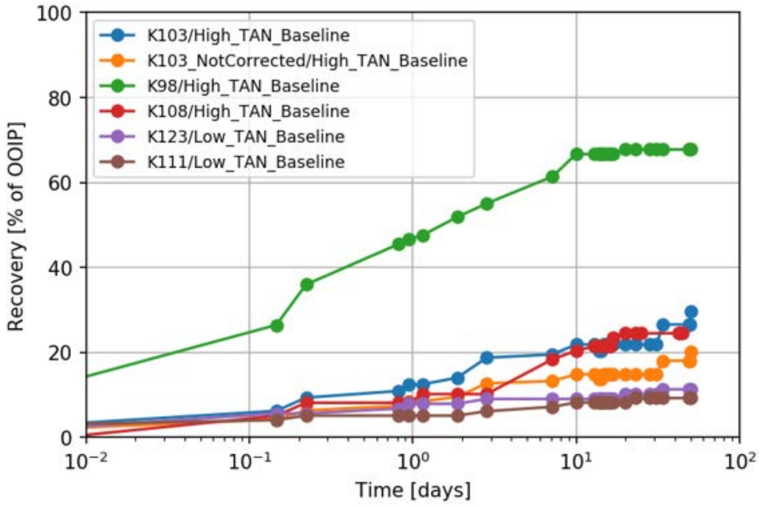

FIGURE 5.11: Oil recovery from Keuper core plugs (Baseline - High TAN oil)

The following observations can be made:

K103 This core achieved a recovery of 29.7% of OOIP. Dean-Stark extraction showed that the extracted water volume exceeded the estimated volume (imbibed brine + initial water saturation) by 3 mL. The reason behind could be that the initial water saturation was underestimated or the more water imbibed into the core during dismounting. The initial water saturation was corrected to match Dean-Stark value.

K98 This core plug experienced mechanical shaking during the mounting process. The recovery was abnormally high (70%) compared to the other replicates.

K108 due to time restrictions, Dean-Stark extraction was not performed on this core. However, due to the consistency with the results obtained from K103, K108 was selected to be the baseline for the later experiments performed in Keuper with high TAN oil.

Core plugs for Keuper with low TAN oil showed a consistent behavior. Core plugs K123 and K111 followed the same recovery trend with very little standard deviation (figure 5.8) and 11.3% and 9.2% of OOIP was recovered.

5.3.2 The Influence of Nanomaterials

Berea Samples

Figure 5.12 demonstrate that the utilization of nanomaterials resulted in additional recoveries up to 20% for both oil types.

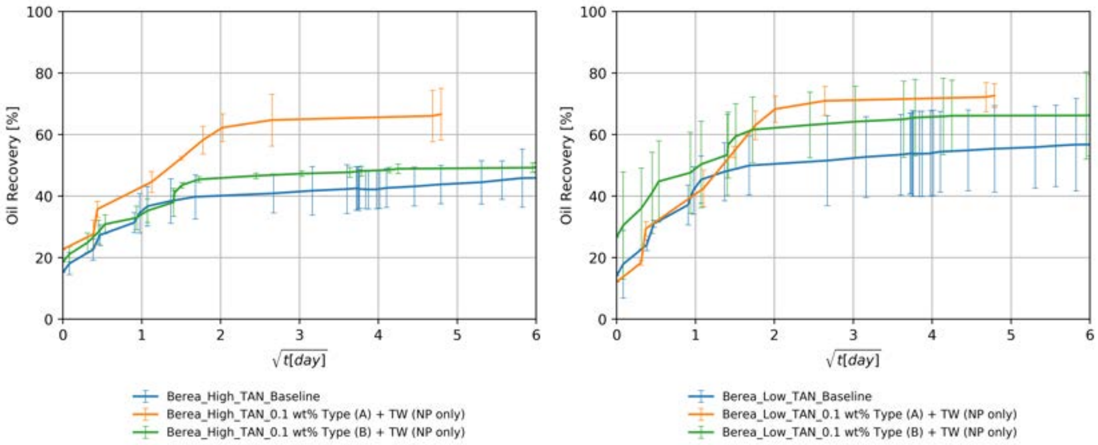

(A) High TAN oil

(B) Low TAN oil

FIGURE 5.12: Oil recovery from Berea core plugs using nanomaterials

As shown in figure 5.12a, nanomaterial *A* could achieve higher recovery than nanomaterial *B*. This can be explained by the more neutrally charged surface. In addition, one potential factor is the solublization factor S_F which is lower for nanomaterial *A* than for nanomaterial *B* (13.3 vs 35.2, see section was mentioned in 5.2.2). A lower solublization factor would lead to higher recovery under SI (Chen et al. 2018).

Figure 5.12b indicates that the recoveries with low TAN oil were higher than with high TAN oil. This can be explained by the lower viscosity of low TAN oil. The lower IFT, which was achieved using low TAN oil nanomaterial *A* could also contribute to the higher/faster recovery of nanomaterial *A* than what was achieved using nanomaterial *B*.

Keuper Samples

Figure 5.13 shows that the contribution of nanomaterials to additional recovery varied depending on the nanomaterial type and the oil, which was used.

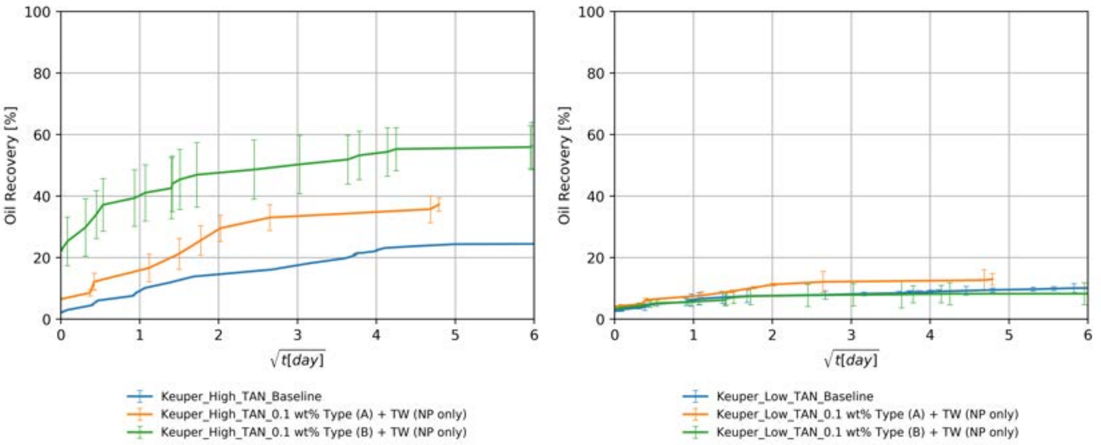

(A) High TAN oil

(B) Low TAN oil

FIGURE 5.13: Oil recovery from Keuper core plugs using nanomaterials

As shown in figure 5.13a, Type B was more effective with high TAN oil in terms of recovery in contrary to what was observed in Berea core plugs. The more negatively charged silica NPs tend to adhere better on the pore walls that are coated by ferric oxide which promotes more positively charged surface (Omurlu et al. 2016). Due to this adhesion, the mineral surface will be tuned towards more favorable wettability state (Alvarez-Berrios et al. 2018).

Figure 5.13b indicates that the recoveries with low TAN oil were lower than the ones obtained with high TAN oil. Nanomaterial *A* could achieve slightly higher recovery than *B* which did not show any improvement compared to the baseline. This can be attributed to tho more neutral surface charge of nanomaterial *A*.

The recovery mechanisms in Keuper are more complicated due to the presence of clay minerals and iron (hydr)oxides. Higher clay content promotes oil wetness (Sayyouh et al. 1990). Thus, wettability alteration of the mineral surface would be the most effective mechanism.

5.3.3 The Effect of TAN Number

Berea Samples

Figure 5.14 demonstrates that for all aqueous solutions that do not contain alkali, the recoveries with low TAN oil were higher than the ones with high TAN oil. This can be due to two reasons:

- The lower viscosity of low TAN oil.
- The higher asphaltene and polar components content in high TAN oil (2% vs. 1%), which promotes more oil wetness (Buckley 1995).

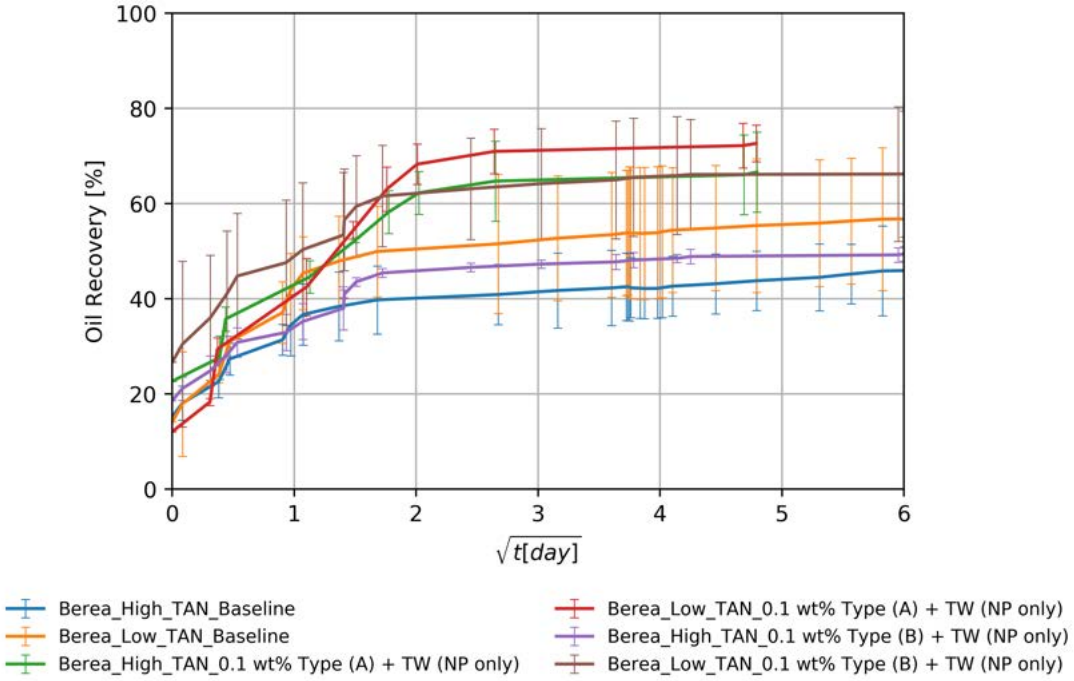

FIGURE 5.14: Oil recovery from Berea cores using nanomaterials only

Keuper Samples

Figure 5.15 shows the opposite behavior was observed for Keuper cores, i.e. higher recoveries for high TAN oil than for low TAN oil. Keuper core plugs saturated with high TAN oil exhibited higher recoveries compared to the ones with low TAN oil.

Due to the high permeability of Keuper core plugs, the viscosity of oil does not play a major role in the spontaneous imbibition process (Meng et al. 2017). Hence, the capillary forces are also weaker.

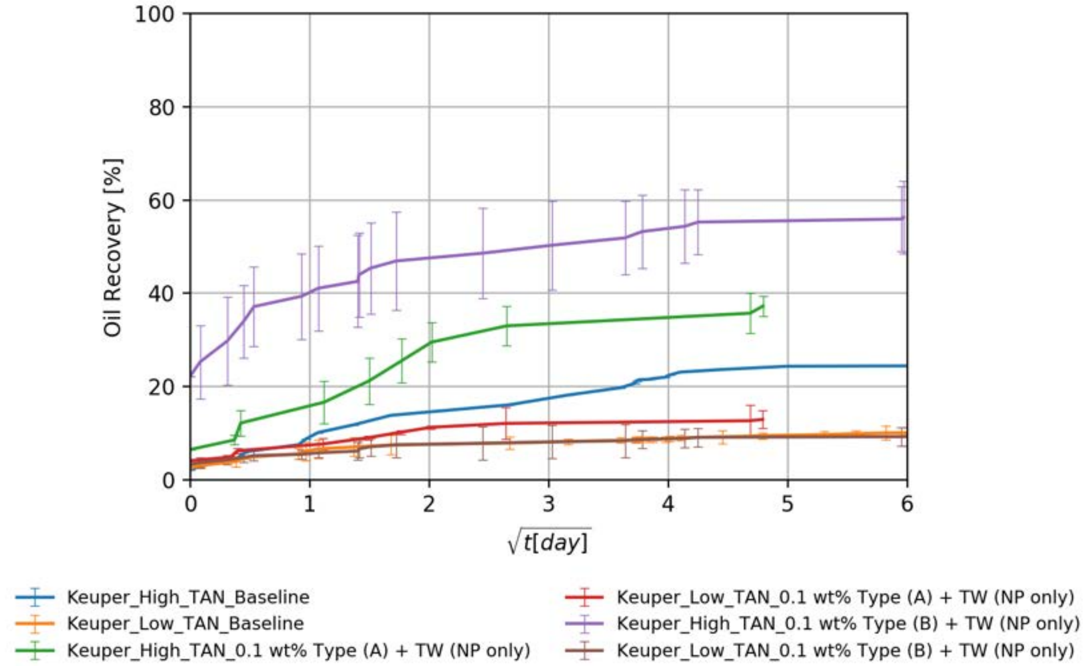

FIGURE 5.15: Oil recovery from Keuper cores using nanomaterials only

5.3.4 The Effect of Divalent Cations

Core plugs of both rock types were pre-saturated with synthetic formation brine, which is rich in divalent cations. However, EOR fluids were prepared using synthetic injection brine (TW) [4]. Figure 5.16a shows that, in the baseline for Berea, recoveries were slightly higher in the core plugs saturated with formation brine (58.3% of OIIP). Nevertheless, nanomaterials had a negative impact on the recovery in the presence of divalent cations (49 ± 3% of OIIP). Metin et al. 2011 investigated the effect divalent cations on colloidal stability. Divalent cations like calcium or magnesium trigger the aggregation of silica nanomaterials. This could result in pore throat plugging and formation damage. Figure 5.16b revealed that for the baseline for Keuper core plugs saturated with formation brine, lower recovery values were achieved (6.3% vs. 9.2% of OOIP). This could be explained by the fact that the presence of divalent cations promotes more oil-wetness (Haagh et al. 2017). In contrary to the Berea case, the use of nanomaterials in EOR fluids succeeded to slightly enhance the recovery. The larger pore throat in the Keuper cores and the higher clay content and mineralogical heterogeneity that involves mechanisms that are more complex, can explain these observations.

---

[4] For brine composition see table 4.5

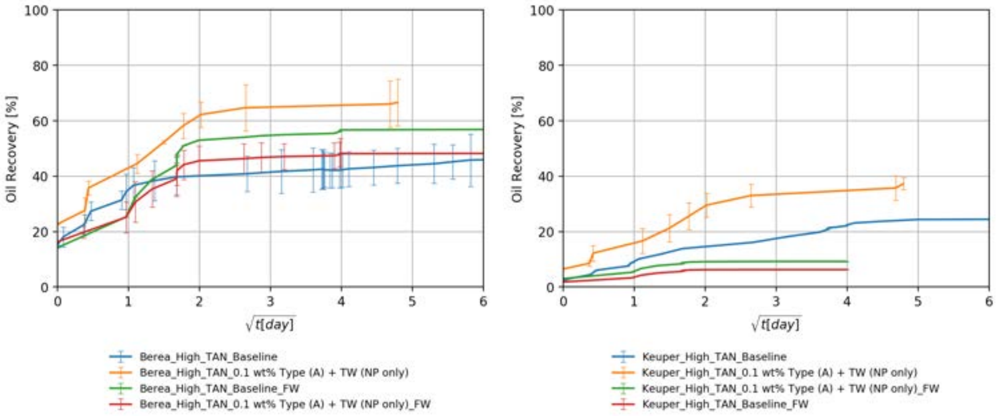

(A) Berea

(B) Keuper

FIGURE 5.16: Oil recovery from core plugs using nanomaterials

5.3.5 The Effect of Alkali

To study the impact of alkali on the recovery process, 3000 ppm of Na_2CO_3 were combined with nanomaterials.

Berea-High TAN Oil

Figure 5.17 shows that alkali per se boosted the recovery by 23%. This can be explained by acid-alkali reaction and the generation of in-situ surfactant. The combination of alkali and nanomaterial *B* resulted in significant improvement in recovery. The high imbibition rate with high ultimate recovery suggests a strong rock fluid interaction. Dean-Stark revealed that the imbibed water volume is lower than monitored during the Amott test, which supports the assumption that the produced volume is macroemulsion. This can be linked to the low IFT, which facilitates spontaneous emulsification. This also explains some abnormally high recoveries ($>$ 100% of OOIP) in some core plugs.

The capillary diffusion coefficient was reduced in this case by a factor of 5% (9.38E-09 vs. 9.88E-09 for the baseline). However, the IFT was 19 times lower ($0.15\,\mathrm{mN\,m^{-1}}$ vs. $8.40\,\mathrm{mN\,m^{-1}}$). This suggests that a major wettability alteration has taken place.

Nanomaterial *A* combined with alkali did not improve the ultimate recovery despite the significant IFT reduction. Imbibition rate was low in this case due to the substantially low IFT. Nevertheless, the ultimate recovery falls close to the baseline.

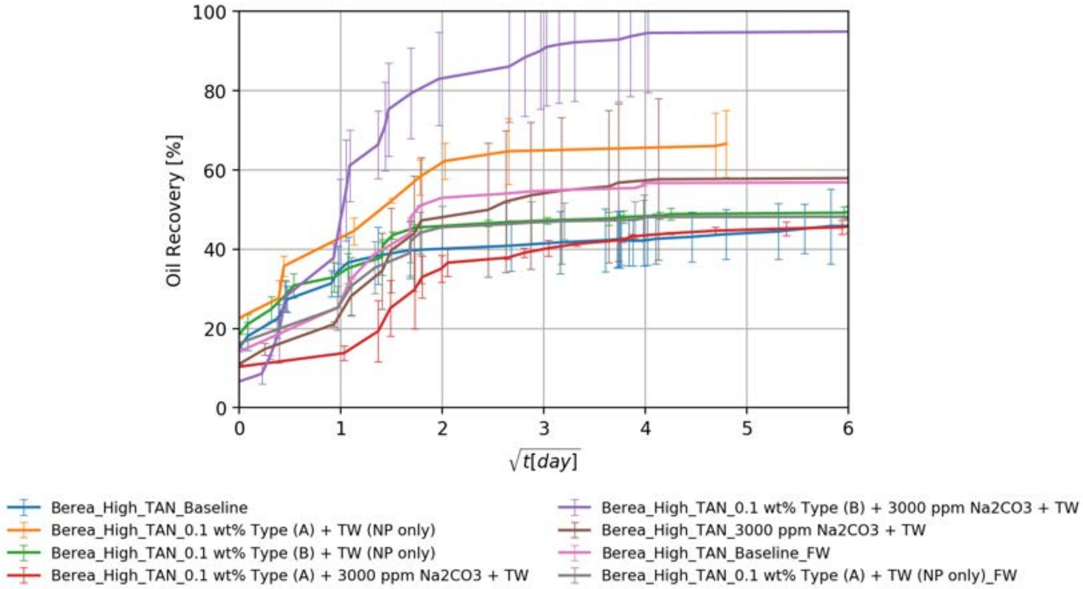

FIGURE 5.17: Oil recovery from Berea cores - High TAN oil

Berea-Low TAN Oil

Figure 5.18 shows that despite the positive impact of alkali and nanomaterials on IFT as well as on emulsion stabilization did not result in a recovery enhancement. The highest ultimate recovery was achieved using alkali alone (86.8% of OOIP). Since the enhancements observed during fluid-fluid interactions did not result in additional recovery, we can attribute that to a major rock-fluid interaction. The synergy between alkali and nanomaterials which was observed in in the experiments using high TAN oil and Berea cores (section 5.3.5) was imperceptible.

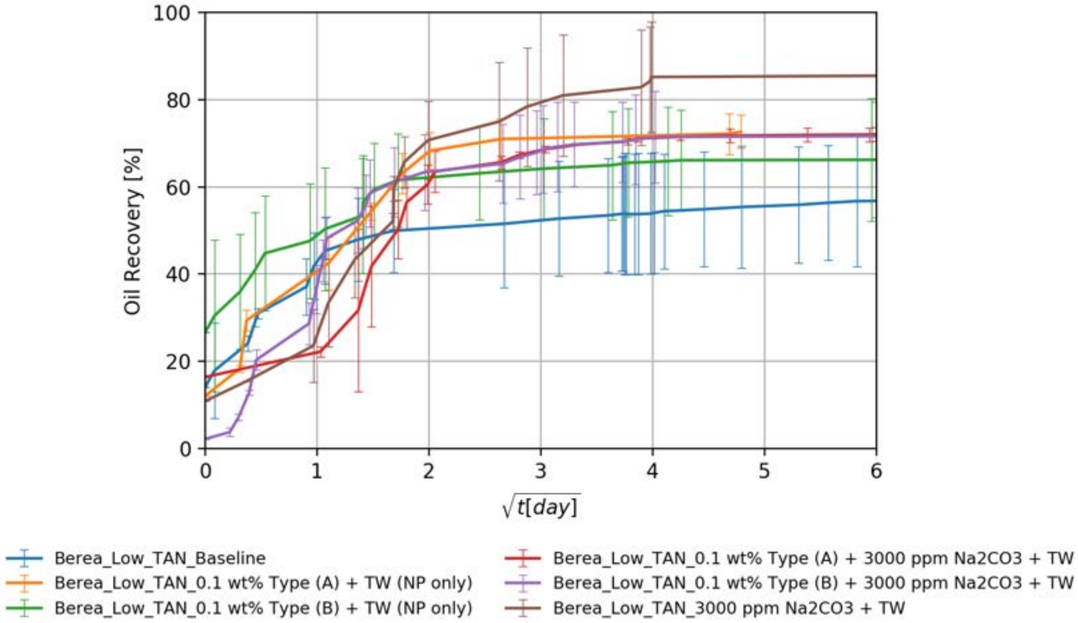

FIGURE 5.18: Oil recovery from Berea cores - Low TAN oil

Table 5.3 summarizes all the ultimate recoveries (as a percent of OOIP) from Berea core plugs using the different EOR formulations.

TABLE 5.3: Summary of oil ultimate recoveries in Berea core plugs

Brine	**Oil**	**AVG [%]**	STD	**Oil**	**AVG [%]**	STD
Baseline(TW)	High TAN	47.2	8.4	Low TAN	57.1	3.8
0.1 wt% TypeA + TW	High TAN	67.1	0.15	Low TAN	72.0	0.85
0.1 wt% TypeB + TW	High TAN	50.2	1.5	Low TAN	66.3	10.6
3000 ppm Na_2CO_3 + TW	High TAN	59.7	23.1	Low TAN	71.5	11.1
0.1 wt% TypeA + 3000 ppm Na_2CO_3 + TW	High TAN	45.8	1.7	Low TAN	72.9	1.6
0.1 wt% TypeB + 3000 ppm Na_2CO_3 + TW	High TAN	97.7	16.0	Low TAN	86.8	9.3

Keuper-High TAN Oil

Figure 5.19 shows a significant increase in ultimate recovery after introducing alkali to the EOR fluid. Alkali reaction with acidic components and the generated soap is responsible for the IFT reduction seen in figure 5.1b and consequently high ultimate recovery.

In some cases the ultimate recovery exceeded 100% of OOIP which is attributed to the spontaneous emulsification of the oil. This was confirmed by Dean-Stark extraction since the extracted water volume was less that the recorded imbibed volume added to the initial WIP.

It is difficult to evaluate the role of nanomaterials since the recoveries with alkaline fluids fall close to each other. For this purpose, further investigations should be carried out (contact angle measurements, core floods, etc.)

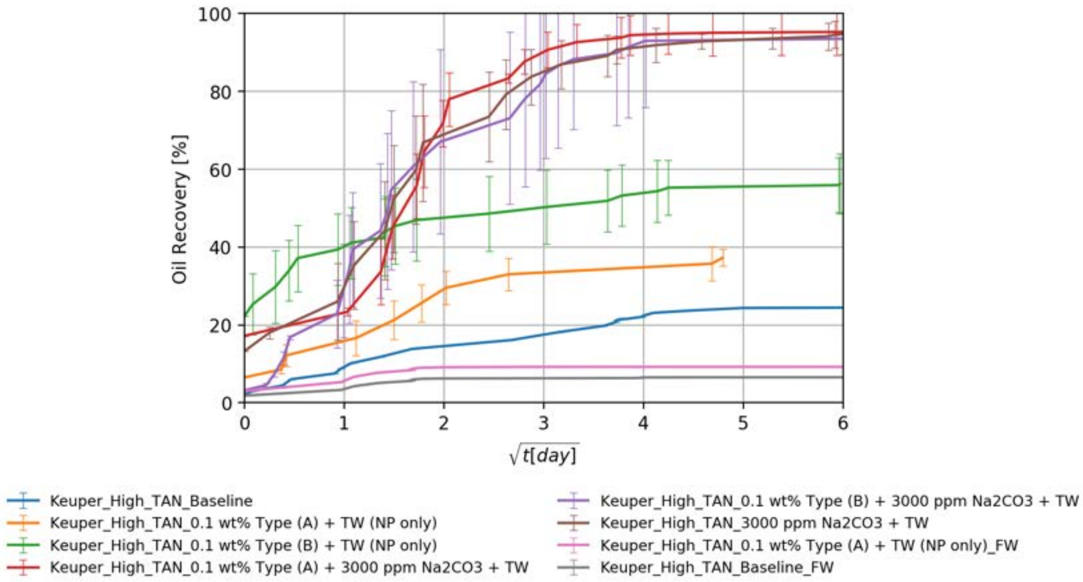

FIGURE 5.19: Oil recovery from Keuper cores - High TAN oil

Keuper-Low TAN Oil

Despite the low TAN number, the utilization of alkali enhanced the recovery as demonstrated in figure 5.20. After introducing the nanomaterials to the alkaline EOR fluid, the recovery was significantly boosted. This is a very good indicator of the synergy between alkali and nanomaterials. Some of these synergistic effects were observed during fluid-fluid interactions in sections 5.1 and 5.2.

Nanomaterial *A* performed better due to neutral surface charge and the affinity of clay to adsorb SiNP coated with more neutral polymers (Omurlu et al. 2016)

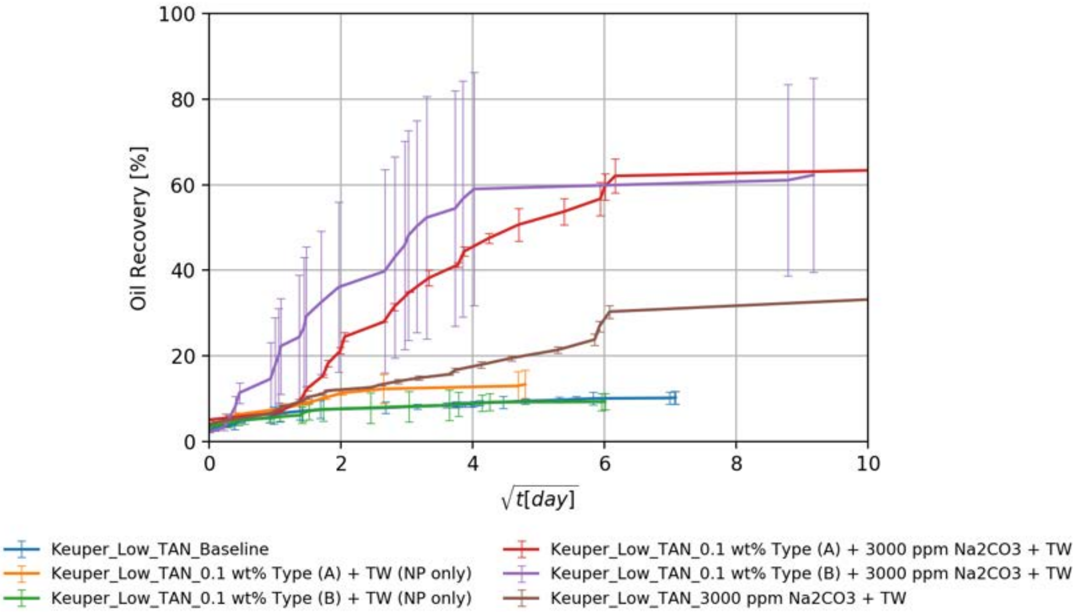

FIGURE 5.20: Oil recovery from Keuper cores - Low TAN oil

Table 5.4 summarizes all the ultimate recoveries (as a percent of OOIP) from Keuper core plugs using the different EOR formulations.

TABLE 5.4: Summary of oil ultimate recoveries in Keuper core plugs

Brine	**Oil**	**AVG [%]**	STD	**Oil**	**AVG [%]**	STD
Baseline(TW)	High TAN	44.8	-	Low TAN	10.3	1.5
0.1 wt% TypeA + TW	High TAN	41.1	2.2	Low TAN	13.8	3.4
0.1 wt% TypeB + TW	High TAN	57.0	7.7	Low TAN	9.3	2.0
3000 ppm Na_2CO_3 + TW	High TAN	95.3	2.6	Low TAN	41.0	15.1
0.1 wt% TypeA + 3000 ppm Na_2CO_3 + TW	High TAN	95.4	5.9	Low TAN	72.2	5.9
0.1 wt% TypeB + 3000 ppm Na_2CO_3 + TW	High TAN	97.5	19.0	Low TAN	66.8	22.7

5.4 Dean-Stark Extraction

Table 5.5 summarizes the results of Dean-Stark extraction. By and large, the results were in accordance with the estimated recoveries. However, in core plugs, which were submerged in alkali and nanomaterials, the extracted water volumes were less than estimated. This was accompanied by high recoveries (exceeded 100% of OOIP) in some cases. This can be explained by the spontaneous emulsification during the recovery process. This leads to overestimation of the recoveries since the readings corresponds for emulsion volume rather than pure oil volume.

TABLE 5.5: Dean-Stark results

Core	*Rock*	*Oil*	*Brine*	PV(mL)	S_{wi}(%)	V_{wi}(mL)	S_{or}(%)	$V_w imbibed$(mL)	$V_w afterSI$(mL)	$S_w afterSI$(%)	DSV_w(mL)	DSS_{wi}(%)	ΔV_w(mL)
$5-114$	*Berea*	$High_T AN$	*Baseline*	10.7	20.2	2.1	47.0	3.5	5.6	53.0	5.6	52.5	0.0
$5-147$	*Berea*	$High_T AN$	*Baseline*	10.5	15.9	1.7	39.3	4.7	6.4	60.7	5.9	56.3	0.5
$5-113$	*Berea*	$High_T AN$	$0.1wt\%TypeB + TW(NPonly)$	11.2	13.0	1.5	42.3	5.0	6.5	57.7	5.2	46.4	1.3
$5-040$	*Berea*	$High_T AN$	$0.1wt\%TypeB + TW(NPonly)$	10.6	13.9	1.5	43.7	4.5	6.0	56.3	5.2	49.0	0.8
$5-206$	*Berea*	$High_T AN$	$0.1wt\%TypeA + 3000ppmNa2CO3 + TW$	11.0	16.9	1.9	44.0	4.3	6.2	56.0	6.6	60.1	-0.4
$5-212$	*Berea*	$High_T AN$	$0.1wt\%TypeA + 3000ppmNa2CO3 + TW$	10.9	21.7	2.4	43.3	3.8	6.2	56.7	6.8	62.6	-0.6
$5-130$	*Berea*	$High_T AN$	$3000ppmNa2CO3 + TW$	10.7	19.1	2.0	27.6	5.7	7.7	72.4	6.2	58.0	1.5
$5-067$	*Berea*	$High_T AN$	$3000ppmNa2CO3 + TW$	11.0	30.5	3.3	45.8	2.6	5.9	54.2	6.4	58.3	-0.5
$5-184$	*Berea*	$Low_T AN$	*Baseline*	10.9	14.4	1.6	45.3	4.4	6.0	54.7	5.6	51.3	0.4
$5-179$	*Berea*	$Low_T AN$	*Baseline*	10.8	22.8	2.5	25.4	5.6	8.1	74.6	6.4	59.2	1.7
$5-203$	*Berea*	$Low_T AN$	$0.1wt\%TypeB + TW(NPonly)$	10.9	24.1	2.6	32.7	4.7	7.3	67.3	7.0	64.3	0.3
$5-178$	*Berea*	$Low_T AN$	$0.1wt\%TypeB + TW(NPonly)$	10.8	23.8	2.6	18.5	6.2	8.8	81.5	6.0	55.8	2.8
$5-210$	*Berea*	$Low_T AN$	$0.1wt\%TypeA + 3000ppmNa2CO3 + TW$	10.7	19.2	2.0	21.7	6.3	8.3	78.3	6.6	61.9	1.7
$5-211$	*Berea*	$Low_T AN$	$0.1wt\%TypeA + 3000ppmNa2CO3 + TW$	10.9	29.8	3.2	20.4	5.4	8.6	79.6	6.8	62.7	1.8
$K103$	*Keuper*	$High_T AN$	*Baseline*	11.3	16.7	1.9	66.5	1.9	3.8	33.5	6.8	60.2	-3.0
$K88$	*Keuper*	$High_T AN$	$0.1wt\%TypeB + TW(NPonly)$	11.4	17.5	2.0	31.0	5.9	7.9	69.0	6.0	52.4	1.9
$K81$	*Keuper*	$High_T AN$	$0.1wt\%TypeB + TW(NPonly)$	11.5	22.2	2.6	37.7	4.6	7.2	62.3	5.8	50.5	1.4
$K124$	*Keuper*	$High_T AN$	$0.1wt\%TypeA + 3000ppmNa2CO3 + TW$	10.9	15.6	1.7	7.5	8.4	10.1	92.5	9.6	87.9	0.5
$K110$	*Keuper*	$High_T AN$	$0.1wt\%TypeA + 3000ppmNa2CO3 + TW$	12.4	18.8	2.3	0.4	10.0	12.3	99.6	9.4	76.0	2.9
$K119$	*Keuper*	$High_T AN$	$3000ppmNa2CO3 + TW$	12.1	28.6	3.5	2.0	8.4	11.9	98.0	8.4	69.4	3.5
$K113$	*Keuper*	$High_T AN$	$3000ppmNa2CO3 + TW$	11.6	28.7	3.3	5.5	7.6	10.9	94.5	7.5	64.9	3.4
$K123$	*Keuper*	$Low_T AN$	*Baseline*	11.2	21.3	2.4	69.8	1.0	3.4	30.2	1.3	11.3	2.1
$K111$	*Keuper*	$Low_T AN$	*Baseline*	11.8	17.9	2.1	74.5	0.9	3.0	25.5	0.8	7.1	2.2
$K120$	*Keuper*	$Low_T AN$	$0.1wt\%TypeB + TW(NPonly)$	10.8	22.8	2.5	68.9	0.9	3.4	31.1	1.2	11.1	2.2
$K99$	*Keuper*	$Low_T AN$	$0.1wt\%TypeA + 3000ppmNa2CO3 + TW$	11.6	25.4	2.9	28.0	5.4	8.3	72.0	5.5	47.5	2.8
$K115$	*Keuper*	$Low_T AN$	$0.1wt\%TypeA + 3000ppmNa2CO3 + TW$	11.8	24.1	2.8	32.7	5.1	7.9	67.3	5.2	44.0	2.7
$K65$	*Keuper*	$Low_T AN$	$3000ppmNa2CO3 + TW$	13.3	8.6	1.1	69.6	2.9	4.0	30.4	3.0	22.5	1.0
$K14$	*Keuper*	$Low_T AN$	$3000ppmNa2CO3 + TW$	12.8	30.6	3.9	51.4	2.3	6.2	48.6	2.4	18.8	3.8

5.5 Numerical Analysis

5.5.1 Inverse Bond Number

the fundamentals of inverse Bond number were discussed thoroughly in section 2.7.3. This study aims to influence N_B^{-1} by lowering IFT in the oil/brine system.

The Shape of Recovery Curve

Figure 5.21 shows the ultimate recovery curve of two Berea cores saturated with low TAN oil. Core (5-179) was submerged in softened injection brine (TW) while (5-122) was submerged in alkaline nanomaterial (0.1 wt% Type B + 3000 ppm Na2CO3 + TW). Since the IFT was reduced, the recovery was slower (lower imbibition rate) while a rapid imbibition can be observed in case of high IFT (5-179). Lowering IFT results in weakening the capillary forces that are significant for counter current imbibition, which was noticed during baseline experiments. Gravitational forces are more effective in case of low inverse Bond number, which results in sufficient hydrostatic pressure behind oil droplets to detach them before snap-off takes place. Gravitational forces are significant for concurrent spontaneous imbibition (Al-Quraishi 2004).

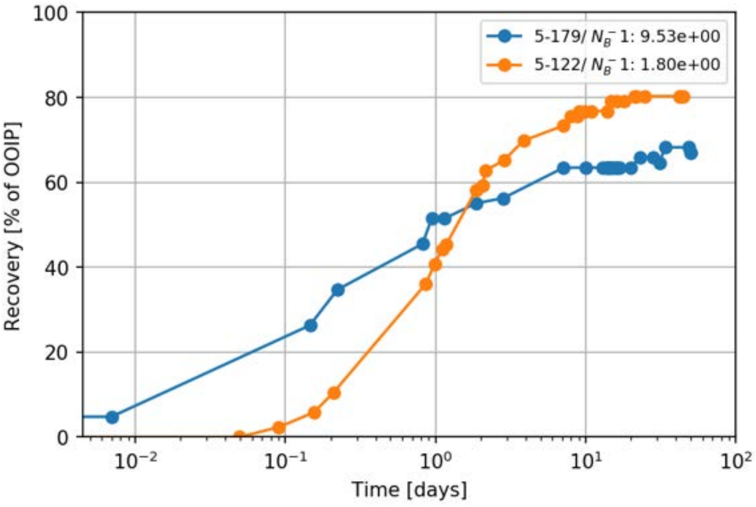

FIGURE 5.21: Recovery curve comparison for different values of N_B^-1

Recovery vs Inv. Bond Number

Figure 5.22 depicts the results of from previous works, which investigated low IFT imbibition together with the results obtained from this study.

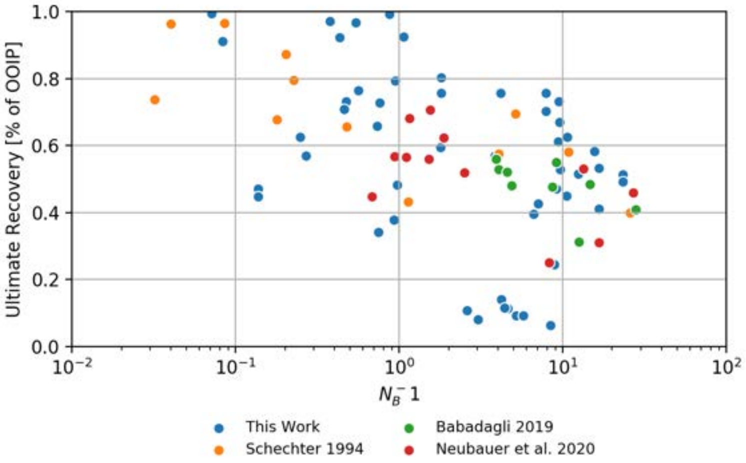

FIGURE 5.22: Oil recovery vs N_B^-1 - comparison with previously done works

There is a general trend showing that the ultimate recovery increases when N_B^-1 decreases. However, no systematic trend can be recognized since the data is obtained from different rock/oil systems.

In figure 5.23 the ultimate recoveries vs N_B^-1 for the different rock/oil systems are plotted.Except for Berea- high TAN oil case, an exponential relationship delivered the best fit, which is in consistency with the literature (Babadagli 2005), (Neubauer et al. 2020).

This analysis does not take the wettability effect into account. Hence, in cases were IFT was lowered and imbibition rate increased, a wettability alteration process must have taken place (Babadagli 2005).

5.5.2 Capillary Diffusion Coefficient

By fitting the obtained normalized oil saturation values to the equation 2.24, A constant D_c can be estimated using a *Non-Linear Least-Squares* fitting algorithm [5].

Example

Figure 5.24 shows that with a constant capillary diffusion coefficient a reasonable fit has been achieved. Mismatches occurred mainly due to the shaking process and spikes in read-off values. the core *5-184* was submerged in softened injection brine (Baseline) while core *5-122* was submerged in brine containing 0.1 wt% type (*B*) and 3000 ppm of Na_2CO_3. By looking at 5.1 we can see that IFT was reduced 98%. Under a fixed wettability state, imbibition kinetics should be lowered by the same magnitude. However, capillary diffusion coefficient is in *5-122* slightly lower than *5-184*. IFT reduction suggests a weaker capillarity and thus slower imbibition.

---

[5] See `https://lmfit.github.io/lmfit-py/`

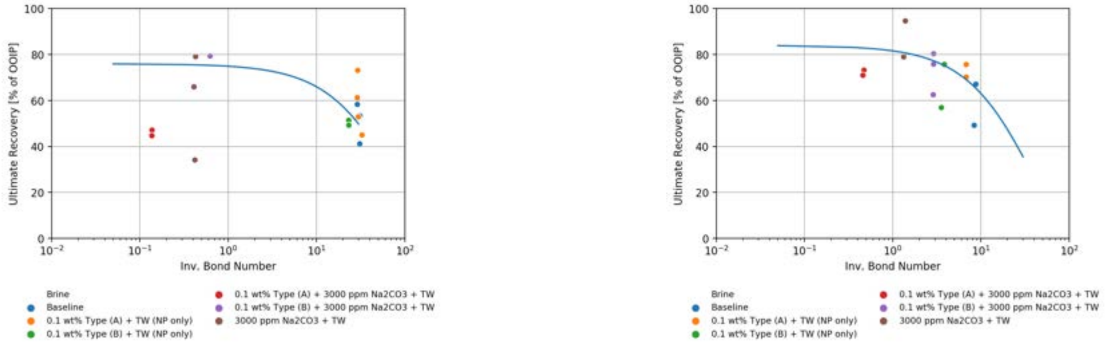

(A) Berea - High TAN oil

(B) Berea - Low TAN oil

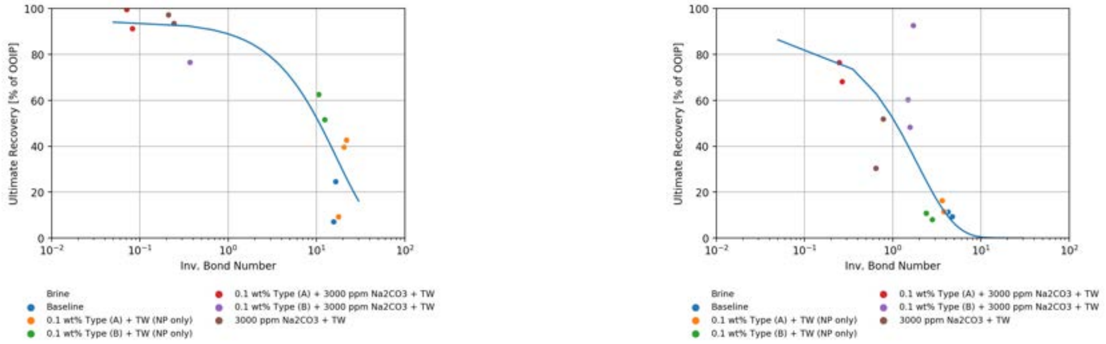

(C) Keuper- High TAN oil

(D) Keuper - Low TAN oil

FIGURE 5.23: Ultimate recovery vs $N_B^{-}1$

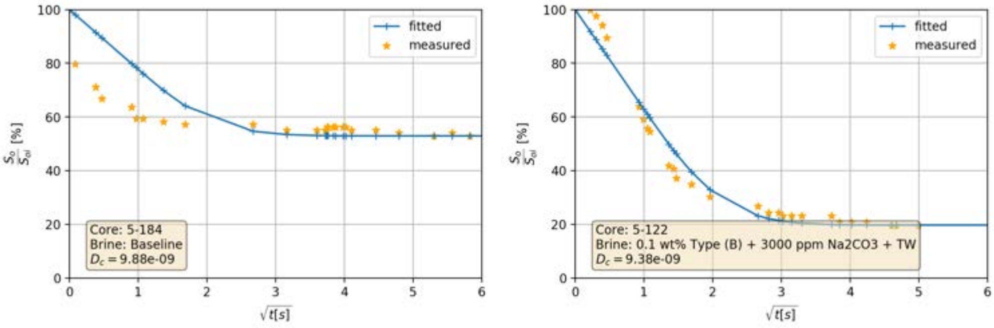

(A) 5-184

(B) 5-122

FIGURE 5.24: Relative oil Saturation vs. square root of time

TABLE 5.6: Results of computations performed on each core

	Core	Rock	D_c	N_B^-1	IFT	Oil	Brine	S_{or}	Recovery	IFTreduction[%]	$D_c$change[%]
0	5 − 114	Berea	9.88E − 09	30.92	8.40	High_TAN	Baseline	47.0	41.1	0.00%	0.00%
1	5 − 147	Berea	9.88E − 09	31.05	8.40	High_TAN	Baseline	39.3	53.3	0.00%	0.00%
2	5 − 184	Berea	9.88E − 09	8.39	3.40	Low_TAN	Baseline	43.5	49.2	0.00%	0.00%
3	5 − 179	Berea	9.88E − 09	8.76	3.40	Low_TAN	Baseline	25.4	67.1	0.00%	0.00%
4	K108	Keuper	1.10E − 08	16.54	8.40	High_TAN	Baseline	65.3	24.5	0.00%	0.00%
5	K123	Keuper	9.88E − 09	4.24	3.40	Low_TAN	Baseline	69.8	11.4	0.00%	0.00%
6	K111	Keuper	9.88E − 09	4.74	3.40	Low_TAN	Baseline	74.5	9.3	0.00%	0.00%
7	5 − 204	Berea	1.61E − 08	29.33	8.30	High_TAN	0.1wt%Type(A) + TW(NPonly)	18.3	73.1	1.19%	−62.74%
8	5 − 181	Berea	1.62E − 08	28.98	8.30	High_TAN	0.1wt%Type(A) + TW(NPonly)	27.0	61.2	1.19%	−63.86%
9	5 − 126	Berea	1.60E − 08	6.82	2.60	Low_TAN	0.1wt%Type(A) + TW(NPonly)	18.6	75.6	23.53%	−62.15%
10	5 − 213	Berea	1.61E − 08	6.82	2.60	Low_TAN	0.1wt%Type(A) + TW(NPonly)	22.0	70.2	23.53%	−62.53%
11	K135	Keuper	1.59E − 08	21.92	8.30	High_TAN	0.1wt%Type(A) + TW(NPonly)	42.4	42.6	1.19%	−43.86%
12	K126	Keuper	1.58E − 08	20.55	8.30	High_TAN	0.1wt%Type(A) + TW(NPonly)	51.0	39.6	1.19%	−42.77%
13	K112	Keuper	1.59E − 08	3.64	2.60	Low_TAN	0.1wt%Type(A) + TW(NPonly)	66.9	16.3	23.53%	−61.14%
14	K80	Keuper	1.61E − 08	3.81	2.60	Low_TAN	0.1wt%Type(A) + TW(NPonly)	69.7	11.5	23.53%	−62.99%
15	5 − 113	Berea	1.56E − 08	23.21	5.30	High_TAN	0.1wt%Type(B) + TW(NPonly)	42.3	51.3	36.90%	−57.39%
16	5 − 040	Berea	1.55E − 08	23.26	5.30	High_TAN	0.1wt%Type(B) + TW(NPonly)	43.7	49.2	36.90%	−57.19%
17	5 − 203	Berea	1.56E − 08	3.57	1.26	Low_TAN	0.1wt%Type(B) + TW(NPonly)	32.7	56.9	62.94%	−57.49%
18	5 − 178	Berea	1.56E − 08	3.85	1.26	Low_TAN	0.1wt%Type(B) + TW(NPonly)	18.5	75.7	62.94%	−57.70%
19	K88	Keuper	1.56E − 08	10.61	5.30	High_TAN	0.1wt%Type(B) + TW(NPonly)	31.0	62.5	36.90%	−41.04%
20	K81	Keuper	1.55E − 08	12.44	5.30	High_TAN	0.1wt%Type(B) + TW(NPonly)	37.7	51.5	36.90%	−40.62%
21	K134	Keuper	1.55E − 08	2.82	1.26	Low_TAN	0.1wt%Type(B) + TW(NPonly)	73.4	8.0	62.94%	−56.55%
22	K120	Keuper	1.55E − 08	2.41	1.26	Low_TAN	0.1wt%Type(B) + TW(NPonly)	68.9	10.8	62.94%	−57.13%
23	5 − 206	Berea	1.55E − 08	0.14	0.04	High_TAN	0.1wt%Type(A) + 3000ppmNa2CO3 + TW	44.0	47.1	99.54%	−56.60%
24	5 − 212	Berea	1.56E − 08	0.14	0.04	High_TAN	0.1wt%Type(A) + 3000ppmNa2CO3 + TW	43.3	44.7	99.54%	−57.36%
25	5 − 210	Berea	1.55E − 08	0.47	0.18	Low_TAN	0.1wt%Type(A) + 3000ppmNa2CO3 + TW	21.7	73.2	94.76%	−57.01%
26	5 − 211	Berea	1.56E − 08	0.46	0.18	Low_TAN	0.1wt%Type(A) + 3000ppmNa2CO3 + TW	20.4	70.9	94.76%	−57.59%
27	K124	Keuper	1.55E − 08	0.08	0.04	High_TAN	0.1wt%Type(A) + 3000ppmNa2CO3 + TW	7.5	91.2	99.54%	−40.91%
28	K110	Keuper	1.55E − 08	0.07	0.04	High_TAN	0.1wt%Type(A) + 3000ppmNa2CO3 + TW	0.4	99.5	99.54%	−40.47%
29	K99	Keuper	1.52E − 08	0.25	0.18	Low_TAN	0.1wt%Type(A) + 3000ppmNa2CO3 + TW	17.6	76.4	94.76%	−54.25%
30	K115	Keuper	1.53E − 08	0.27	0.18	Low_TAN	0.1wt%Type(A) + 3000ppmNa2CO3 + TW	24.2	68.1	94.76%	−54.49%
31	5 − 163	Berea	9.38E − 09	0.63	0.15	High_TAN	0.1wt%Type(B) + 3000ppmNa2CO3 + TW	−4.9	108.1	98.21%	5.07%
32	5 − 186	Berea	9.38E − 09	0.63	0.15	High_TAN	0.1wt%Type(B) + 3000ppmNa2CO3 + TW	13.6	79.3	98.21%	5.07%
33	5 − 124	Berea	9.38E − 09	2.90	1.00	Low_TAN	0.1wt%Type(B) + 3000ppmNa2CO3 + TW	18.0	75.8	70.59%	5.07%
34	5 − 122	Berea	9.38E − 09	2.91	1.00	Low_TAN	0.1wt%Type(B) + 3000ppmNa2CO3 + TW	15.5	80.3	70.59%	5.07%
35	K106	Keuper	9.38E − 09	0.37	0.15	High_TAN	0.1wt%Type(B) + 3000ppmNa2CO3 + TW	20.2	76.5	98.21%	14.95%
36	K131	Keuper	9.38E − 09	1.72	1.00	Low_TAN	0.1wt%Type(B) + 3000ppmNa2CO3 + TW	5.1	92.5	70.59%	5.07%
37	K122	Keuper	9.38E − 09	1.57	1.00	Low_TAN	0.1wt%Type(B) + 3000ppmNa2CO3 + TW	36.1	48.2	70.59%	5.07%
38	5 − 067	Berea	1.56E − 08	0.42	0.11	High_TAN	3000ppmNa2CO3 + TW	45.8	34.1	98.69%	−57.49%
39	5 − 130	Berea	1.55E − 08	0.41	0.11	High_TAN	3000ppmNa2CO3 + TW	27.6	65.9	98.69%	−56.94%
40	K119	Keuper	1.55E − 08	0.21	0.11	High_TAN	3000ppmNa2CO3 + TW	2.0	97.2	98.69%	−40.11%
41	K113	Keuper	1.54E − 08	0.24	0.11	High_TAN	3000ppmNa2CO3 + TW	4.7	93.4	98.69%	−39.67%
42	K65	Keuper	1.53E − 08	0.65	0.55	Low_TAN	3000ppmNa2CO3 + TW	63.6	30.4	83.82%	−54.40%
43	K14	Keuper	1.51E − 08	0.78	0.55	Low_TAN	3000ppmNa2CO3 + TW	33.4	51.8	83.82%	−53.20%
44	5 − 225	Berea	1.55E − 08	1.39	0.55	Low_TAN	3000ppmNa2CO3 + TW	3.9	94.6	83.82%	−57.20%
45	5 − 201	Berea	1.56E − 08	1.33	0.55	Low_TAN	3000ppmNa2CO3 + TW	17.9	78.9	83.82%	−57.55%
46	K130	Keuper	1.24E − 08	0.36	0.15	High_TAN	0.1wt%Type(B) + 3000ppmNa2CO3 + TW	−6.2	108.9	98.21%	−12.58%
47	K139	Keuper	1.24E − 08	0.28	0.15	High_TAN	0.1wt%Type(B) + 3000ppmNa2CO3 + TW	−5.5	108.0	98.21%	−12.58%
48	K121	Keuper	1.24E − 08	1.49	1.00	Low_TAN	0.1wt%Type(B) + 3000ppmNa2CO3 + TW	35.5	60.2	70.59%	−25.65%
49	5 − 191	Berea	1.24E − 08	2.88	1.00	Low_TAN	0.1wt%Type(B) + 3000ppmNa2CO3 + TW	35.3	62.5	70.59%	−25.65%
50	5 − 185	Berea	1.24E − 08	0.57	0.15	High_TAN	0.1wt%Type(B) + 3000ppmNa2CO3 + TW	−3.3	106.0	98.21%	−25.65%
51	5 − 129	Berea	1.55E − 08	0.43	0.11	High_TAN	3000ppmNa2CO3 + TW	15.1	79.1	98.69%	−57.14%
52	5 − 086	Berea	1.57E − 08	29.02	8.40	High_TAN	Baseline	32.1	58.3	0.00%	−58.45%
53	5 − 082	Berea	1.57E − 08	32.78	8.30	High_TAN	0.1wt%Type(A) + TW(NPonly)	47.9	45.0	1.19%	−58.82%
54	5 − 097	Berea	1.57E − 08	29.76	8.30	High_TAN	0.1wt%Type(A) + TW(NPonly)	34.8	52.9	1.19%	−58.87%
55	K23	Keuper	1.58E − 08	17.82	8.30	High_TAN	0.1wt%Type(A) + TW(NPonly)	76.4	9.2	1.19%	−42.79%
56	K33	Keuper	1.57E − 08	15.68	8.40	High_TAN	Baseline	88.6	7.1	0.00%	−41.89%

Wettability and Diffusion

Table 5.6 summarizes the results of $N^{-}1_B$ calculations. As mentioned earlier, $N^{-}1_B$ is insensitive to wettability changes. In case of a stable wettability state, a reduction in IFT should result in slower imbibition and thus reduction in D_c in the same magnitude. The reduction in D_c can be seen only in the cores submerged in 0.1 $wt\%$ $Type\ B\ +$ 3000 $ppm\ Na2CO3\ +\ TW$. However, for the other EOR fluids, imbibition kinetics were accelerated despite the IFT reduction. This can be attributed to wettability alteration towards water wet, which results in rapid imbibition of the aqueous phase into the core. Other works that investigated SI using nanomaterials also reported an increase in imbibition rate (Wang et al. 2017).

By taking a closer look into the table 5.6, we can draw the following conclusions:

It can be seen that nanomaterial A induced an acceleration of the imbibition (in case of Berea with high TAN oil, D_c was increased by 62% using nanomaterial (A) compared to 57% with nanomaterial (B)). By adding 30000 ppm of Na_2CO_3, IFT was lowered. Consequently, imbibition kinetics were decelerated compared to the case of nanomaterials only. However, D_c is still higher than the base case except the combinations with nanomaterial (B).

Chapter 6

Final Conclusions

In this chapter, the conclusions drawn in the course of this study are summarized based on the the experimental methods and presented in a way that addresses the research objective.

6.1 Summary

6.1.1 Interfacial Tension

The following points were concluded from the relatively short measurement period. However, nanomaterials are expected to be more effective within a larger time scale since they are less liable to degradation.

- Nanomaterials were very effective in terms of IFT reduction as standalone EOR agents. With high TAN oil, IFT was lowered from 8.3 to 0.039 to $\mathrm{mN\,m^{-1}}$ after combining nanomaterial (A) and 3000 ppm of Na_2CO_3
- The magnitude of IFT reduction by nanomaterials is highly dependent on its surface modification
- Combining nanomaterials with alkali can result in synergistic IFT reduction especially after optimizing the surface charge of the utilized nanomaterials
- The TAN of the oil plays a substantial role when alkali is used

6.1.2 Phase Behavior

The phase behavior experiment could provide an idea on the effect of nanomaterials on the emulsion stability but they can be hardly linked to the Amott tests since the conditions of energy input are not the same in both experiments.
The main points are:

- The effect of TAN becomes detrimental since the emulsification process is mainly driven by the alkali-acid reaction
- Nanomaterials alone were not able to generate a significant volume of emulsions
- The emulsions generated using alkali and nanomaterials were very stable compared to those which were generated using alkali

- EOR formulations with lower IFT resulted in better emulsification
- The effect of nanomaterial's surface charge was more notable with high TAN oil

6.1.3 Spontaneous Imbibition

In Amott test the conclusions are grouped based on each parameter, which was varied throughout the experiment

The Influence of Rock Type

- In Berea core plugs and in the absence of alkali, ultimate recoveries were higher with low TAN oil
- This can be linked to the oil viscosity and the lower content of asphaltene and resins
- With Keuper core samples, the opposite behavior was observed and the ultimate recovery with high TAN oil were always higher
- The presence of clay minerals in Keuper core plugs together with the high content of polar components in high TAN oil promotes more oil-wetness. Hence, the wettability alteration becomes very effective in the recovery process
- The complex wetting behavior in the rock-fluid system is still to be investigated

The Influence of Nanomaterials

- In Berea core plugs, nanomaterials with more neutrally charged surface performed better as a standalone EOR agent. This is in accordance with IFT and ζ-potential measurements
- In Keuper core plugs, the comparison becomes more complex due to rock heterogeneity and the presence of clay minerals

The Influence of Alkali

- In some cases, alkali exhibited a synergistic effect with nanomaterials which resulted in high ultimate recoveries (e.g. 97.7% of OOIP in Berea-high TAN oil case)
- In general, nanomaterial *B* performed better with alkali
- The IFT reduction by alkali and nanomaterials is vital for spontaneous imbibition but it cannot serve as the only explanation for the ultimate recovery (e.g. nanomaterial *A* + 3000 ppm Na_2CO_3 with high TAN oil in Berea core plugs)
- The recoveries might differ from those expected from fluid-fluid interaction due to complex rock-fluid interactions especially in cases with alkaline EOR formulations
- The high ultimate recoveries can be attributed to different mechanisms but mainly to IFT reduction and wettability alteration towards water-wet

The Influence of Divalent Cations

- In Berea core plugs, the baseline in the core plugs saturated with synthetic formation brine (rich of divalent cations) was slightly higher than the one in core plugs saturated with softened injection brine
- Introducing nanomaterials to the softened injection brine did not result in additional recovery
- In Keuper core plugs saturated with synthetic formation brine, the addition of nanomaterials achieved slightly higher recovery
- Colloidal stability in the presence of divalent cations should be deeper investigated

6.1.4 Numerical analysis

Inverse Bond Number

Unlike modified inverse Bond number, the classical inverse Bond number does not take the wettability state into account but it is still a useful tool that links the gravity and capillary forces together. Contact angle measurements would help optimizing this calculation.
The following points were concluded:

- The impact of IFT reduction on the recovery under spontaneous imbibition is well-captured by inverse Bond number
- An exponential relationship between inverse Bond number and ultimate recovery was fitted for each oil-rock system
- The obtained results were in agreement with the ones from previous literature

Capillary Diffusion Coefficient

The capillary diffusion coefficient of the imbibing aqueous phase is an important indicator of the imbibition kinetics. However, dividing the diffusion process into early time and late time would have been more informative.

- A reasonable fit was obtained using a constant capillary diffusion coefficient
- Wettability alteration was indicated via a change in capillary diffusion coefficient
- The imbibition kinetics are very dependent on the wettability state of the studied sample

6.2 Overall Conclusion

In general, nanomaterials had a positive impact on many EOR-related parameters. Once combined with alkali, this impact was more significant and cannot be solely attributed to one effect but rather a firm synergy.

The surface modification of the particles is a determinant factor in the recovery process. A neutrally charged surface was more effective in IFT reduction once combined with alkali whereas a more negatively-charged surface performed better as standalone. During spontaneous imbibition, the surface charge of pore walls comes also into play. The presence of cationic iron oxides might have promoted a better adsorption of negatively charged particles onto the surface. Hence, a more prominent rock-fluid interaction.

In other words, the electrostatic interactions between the elements in a rock-fluid system are the decisive factor during a nano-EOR process and any synergy between other EOR agents and nanomaterials should consider this factor.

Inverse Bond number linked the additional recovery to IFT reduction in oil/brine systems without considering the wettability state. However, an analysis of diffusion mechanism and some of the high recovery rates revealed that a substantial wettability alteration was taking place.

Some of these improvements especially in phase behavior should be closer inspected. Better emulsification may not necessarily lead to higher recovery. It might also lead to clustering of the oil or low mobility of the emulsion phase. The same applies for the wettability state. A drainage in a strongly water-wet medium is mainly achieved by oil-filling and snap-off which might influence the relative permeability at pore scale.

Although this work showed promising ultimate recoveries, the future work should include deeper investigations in terms of downscaling to pore scale and upscaling towards field scale and cannot provide a conclusive answer.

6.3 Future Work

- Perform contact angle measurements to quantitatively capture the wettability alteration and determine the initial wettability state
- Preform core floods and microfluidic experiments to study the particle retention and the dynamic behavior of nanofluids in the reservoir
- Investigate the recovery in secondary and tertiary mode
- Study the phase behavior using μCT to determine droplet size and better understand the mechanisms contributing to emulsion stabilization
- Perform Amott test under CT scanner in order to understand the imbibition kinetics and better determine the diffusion coefficient
- Assess the utilization of nanomaterials from a HSE point of view

Bibliography

Abd, Abdul Salam, Elsiddig Elhafyan, Abdul Rafey Siddiqui, Wajdi Alnoush, Martin J. Blunt, and Nayef Alyafei (2019). “A review of the phenomenon of counter-current spontaneous imbibition: Analysis and data interpretation”. In: *Journal of Petroleum Science and Engineering* 180. PII: S0920410519305200, pp. 456–470. ISSN: 09204105. DOI: `10.1016/j.petrol.2019.05.066`.

Aboofazeli, Reza (2010). “Nanometric-scaled emulsions (nanoemulsions)”. eng. In: *Iranian Journal of Pharmaceutical Research : IJPR* 9.4. Journal Article Editorial Journal Article, pp. 325–326. ISSN: 1735-0328. eprint: `24381596`.

Ahmed, Afaque, Ismail Mohd Saaid, Abdelazim Abbas Ahmed, Rashidah M. Pilus, and Mirza Khurram Baig (2019). “Evaluating the potential of surface-modified silica nanoparticles using internal olefin sulfonate for enhanced oil recovery”. In: *Petroleum Science* 8.2. PII: 404, p. 49. ISSN: 1672-5107. DOI: `10.1007/s12182-019-00404-1`.

Ahmed, Tarek H. (2010). *Reservoir engineering handbook*. eng. 4. ed. Amsterdam: Elsevier/GPP Gulf Professional Publ. 1454 pp. ISBN: 9781856178037. URL: `http://search.ebscohost.com/login.aspx?direct=true&scope=site&db=nlebk&db=nlabk&AN=334590`.

Al-Quraishi, A. A. (2004). “Oil Recovery by Dynamic Imbibition in Low Tension Aqueous Systems”. In: *Oil & Gas Science and Technology* 59.3. PII: alquraishi_vol59n3, pp. 267–273. ISSN: 1294-4475. DOI: `10.2516/ogst:2004019`.

Ali, Jagar A., Kamal Kolo, Abbas Khaksar Manshad, and Amir H. Mohammadi (2018). “Recent advances in application of nanotechnology in chemical enhanced oil recovery: Effects of nanoparticles on wettability alteration, interfacial tension reduction, and flooding”. In: *Egyptian Journal of Petroleum* 27.4. PII: S1110062118301405, pp. 1371–1383. ISSN: 11100621. DOI: `10.1016/j.ejpe.2018.09.006`.

Almahfood, Mustafa and Baojun Bai (2018). “The synergistic effects of nanoparticle-surfactant nanofluids in EOR applications”. In: *Journal of Petroleum Science and Engineering* 171. PII: S0920410518306053, pp. 196–210. ISSN: 09204105. DOI: `10.1016/j.petrol.2018.07.030`.

Alvarez-Berrios, Merlis P., Lisa M. Aponte-Reyes, Lissette M. Aponte-Cruz, Paula Loman-Cortes, and Juan L. Vivero-Escoto (2018). “Effect of the surface charge of silica nanoparticles on oil recovery: wettability alteration of sandstone cores and imbibition experiments”. In: *International Nano Letters* 8.3. PII: 243, pp. 181–188. ISSN: 2008-9295. DOI: `10.1007/s40089-018-0243-5`.

Alyafei, Nayef and Martin J. Blunt (2018). “Estimation of relative permeability and capillary pressure from mass imbibition experiments”. In: *Advances in Water Resources* 115. PII: S0309170817309582, pp. 88–94. ISSN: 03091708. DOI: `10.1016/j.advwatres.2018.03.003`.

Andersen, Pål Ø., Yangyang Qiao, Dag Chun Standnes, and Steinar Evje (2019). "Cocurrent Spontaneous Imbibition in Porous Media With the Dynamics of Viscous Coupling and Capillary Backpressure". In: *SPE Journal* 24.01, pp. 158–177. ISSN: 1086-055X. DOI: 10.2118/190267-PA.

Anton Paar (2020). *Density meter: DMA 5000 M :: Anton-Paar.com*. URL: \url{https://www.anton-paar.com/corp-en/products/details/density-meter-dmatm-5000-m/} (visited on 02/23/2020).

Arab, Danial, Apostolos Kantzas, and Steven L. Bryant (2018). "Nanoparticle stabilized oil in water emulsions: A critical review". In: *Journal of Petroleum Science and Engineering* 163. PII: S0920410517310549, pp. 217–242. ISSN: 09204105. DOI: 10.1016/j.petrol.2017.12.091.

Babadagli, T. (2005). "Analysis of Oil Recovery by Spontaneous Imbibition of Surfactant Solution". In: *Oil & Gas Science and Technology* 60.4. PII: babadagli_vol60n4, pp. 697–710. ISSN: 1294-4475. DOI: 10.2516/ogst:2005049.

Bear, Jacob (2013). *Dynamics of Fluids in Porous Media*. eng. Reprint. Originally published: New York: American Elsevier. Pub. Co., 1972. Originally published in series: Environmental science series (New York, 1972-). With corrections. New York: Dover Publ. 1512 pp. ISBN: 9780486656755. URL: \url{http://gbv.eblib.com/patron/FullRecord.aspx?p=1894909}.

Berg, Robert R. (1970). "Method for determining permeability from reservoir rock properties". In: *TRANS* 1970.VOL. 20, pp. 303–317. URL: \url{https://pascal-francis.inist.fr/vibad/index.php?action=getRecordDetail&idt=GEODEBRGM71091580}.

Bila, Alberto, Jan Åge Stensen, and Ole Torsæter (2019). "Experimental Investigation of Polymer-Coated Silica Nanoparticles for Enhanced Oil Recovery". eng. In: *Nanomaterials (Basel, Switzerland)* 9.6. Journal Article. ISSN: 2079-4991. DOI: 10.3390/nano9060822. eprint: 31159232.

Binks, B. P. and S. O. Lumsdon (2000). "Influence of Particle Wettability on the Type and Stability of Surfactant-Free Emulsions †". In: *Langmuir* 16.23, pp. 8622–8631. ISSN: 0743-7463. DOI: 10.1021/la000189s.

Binks, Bernard P. (2002). "Particles as surfactants—similarities and differences". In: *Current Opinion in Colloid & Interface Science* 7.1-2. PII: S1359029402000080, pp. 21–41. ISSN: 13590294. DOI: 10.1016/S1359-0294(02)00008-0.

Binks, Bernard P. and Jhonny A. Rodrigues (2007). "Enhanced stabilization of emulsions due to surfactant-induced nanoparticle flocculation". eng. In: *Langmuir : the ACS journal of surfaces and colloids* 23.14. Journal Article, pp. 7436–7439. DOI: 10.1021/la700597k. eprint: 17536846.

Blunt, Martin J. (2017a). *Multiphase flow in permeable media. A pore-scale perspective*. eng. Cambridge: Cambridge University Press. 482 pp. ISBN: 9781316145098. DOI: 10.1017/9781316145098.

— (2017b). *The Imperial College Lectures in Petroleum Engineering. Volume 2: Reservoir engineering*. eng. Vol. volume 2. The Imperial College Lectures in Petroleum Engineering. Blunt, Martin J. (VerfasserIn). Singapore: World Scientific. 388 pp. ISBN: 9781786342096.

Buckley, J. S. (1995). "Asphaltene Precipitation and Crude Oil Wetting". In: *SPE Advanced Technology Series* 3.01, pp. 53–59. ISSN: 1076-0148. DOI: 10.2118/26675-PA.

— (1998). "Wetting Alteration of Solid Surfaces by Crude Oils and Their Asphaltenes". In: *Revue de l'Institut Français du Pétrole* 53.3. PII: buckley_v53n3, pp. 303–312. ISSN: 0020-2274. DOI: `10.2516/ogst:1998026`.

Chen, Haihui, Hongfu Fan, Yi Zhang, Xingguang Xu, Long Liu, and Qingfeng Hou (2018). "Investigations on the driving forces of the fluorocarbon surfactant-assisted spontaneous imbibition using thermogravimetric analysis (TGA)". In: *RSC Advances* 8.67, pp. 38196–38203. DOI: `10.1039/c8ra08423h`.

Chengara, Anoop, Alex D. Nikolov, Darsh T. Wasan, Andrij Trokhymchuk, and Douglas Henderson (2004). "Spreading of nanofluids driven by the structural disjoining pressure gradient". eng. In: *Journal of colloid and interface science* 280.1. Journal Article, pp. 192–201. ISSN: 0021-9797. DOI: `10.1016/j.jcis.2004.07.005`. eprint: `15476790`.

Chevalier, T., J. Labaume, A. Delbos, T. Clemens, V. M. Waeger, B. Bourbiaux, and M. Fleury (2019). "A novel experimental approach for studying spontaneous imbibition processes with alkaline solutions". In: *E3S Web of Conferences* 89. Nicot, B. (Editor) PII: e3sconf_sca2018_04004, p. 04004. DOI: `10.1051/e3sconf/20198904004`.

Corredor, Laura M., Ehsan Aliabadian, Maen Husein, Zhangxin Chen, Brij Maini, and Uttandaraman Sundararaj (2019). "Heavy oil recovery by surface modified silica nanoparticle/HPAM nanofluids". In: *Fuel* 252. PII: S0016236119307112, pp. 622–634. ISSN: 00162361. DOI: `10.1016/j.fuel.2019.04.145`.

Crank, John (1979). *The mathematics of diffusion*. eng. 2. ed., reprinted. Oxford science publications. Oxford: Oxford Univ. Press. 414 pp. ISBN: 0198534116.

Delshad, Mojdeh, Choongyong Han, Faiz Koyassan Veedu, and Gary Arnold Pope (2011). "A Simplified Model for Simulations of Alkaline-Surfactant-Polymer Floods". In: *SPE Reservoir Simulation Symposium*. SPE Reservoir Simulation Symposium (SPE, Jan. 1, 2011). Ed. by SPE. The Woodlands, Texas, USA: Society of Petroleum Engineers, p. 17. ISBN: 978-1-55563-324-0. DOI: `10.2118/142105-MS`.

Denney, Dennis (2011). "Nanosized Particles for Enhanced Oil Recovery". In: *Journal of Petroleum Technology* 63.01, pp. 54–56. ISSN: 0149-2136. DOI: `10.2118/0111-0054-JPT`.

Donaldson, Erle C. and Waqi Alam (2010). *Wettability*. eng. Houston, Tex: Gulf Pub. Co. 336 pp. ISBN: 9781933762296. URL: `\url{http://www.sciencedirect.com/science/book/9781933762296}`.

Enerdata (2019). *World Energy Consumption Statistics*. en. Enerdata. URL: `\url{https://yearbook.enerdata.net/total-energy/world-consumption-statistics.html}` (visited on 08/10/2019).

EVONIK (n.d.). *AEROSIL® fumed silica. Product datasheet*. Copyright: Copyright Evonik Industries AG - all rights reserved. URL: `\url{https://products-re.evonik.com/lpa-productfinder/page/productsbytext/detail.html?channel=aerosil&pid=1830&lang=en}` (visited on 12/06/2019).

Ezekwe, Nnaemeka (2011). *Petroleum reservoir engineering practice*. London: Prentice Hall. 1 volume. ISBN: 0133807428.

Falode, Olugbenga and Edo Manuel (2014). "Wettability Effects on Capillary Pressure, Relative Permeability, and Irredcucible Saturation Using Porous Plate". In: *Journal of Petroleum Engineering* 2014. PII: 465418, pp. 1–12. ISSN: 2314-5005. DOI: `10.1155/2014/465418`.

Firozjaii, Ali Mohsenatabar and Hamid Reza Saghafi (2019). “Review on chemical enhanced oil recovery using polymer flooding: Fundamentals, experimental and numerical simulation”. In: *Petroleum*. PII: S2405656119300434. ISSN: 24056561. DOI: `10.1016/j.petlm.2019.09.003`.

Ganie, Kenny, Ahmad Kamal Idris, Dzeti Farhah Mohshim, Wan Rosli Wan Sulaiman, Ismail Mohd Saaid, and Azlinda Abdul Malik (2019). “A review on the wettability alteration mechanism in condensate banking removal”. In: *Journal of Petroleum Science and Engineering* 183. PII: S0920410519308526, p. 106431. ISSN: 09204105. DOI: `10.1016/j.petrol.2019.106431`.

Gbadamosi, Afeez O., Radzuan Junin, Muhammad A. Manan, Augustine Agi, and Adeyinka S. Yusuff (2019). “An overview of chemical enhanced oil recovery: recent advances and prospects”. In: *International Nano Letters* 9.3. PII: 272, pp. 171–202. ISSN: 2008-9295. DOI: `10.1007/s40089-019-0272-8`.

Gennes, Pierre-Gilles de, Françoise Brochard-Wyart, and David Quéré (2004). *Capillarity and Wetting Phenomena*. New York, NY: Springer New York. ISBN: 978-1-4419-1833-8. DOI: `10.1007/978-0-387-21656-0`.

Green, Don W. and G. Paul Willhite (2008). *Enhanced oil recovery*. eng. [4. Nachdr.] Vol. 6. SPE textbook series. Richardson, Tex.: Henry L. Doherty Memorial Fund of AIME Society of Petroleum Engineers. 545 pp. ISBN: 9781555630775.

Haagh, M. E. J., I. Siretanu, M. H. G. Duits, and F. Mugele (2017). “Salinity-Dependent Contact Angle Alteration in Oil/Brine/Silicate Systems: the Critical Role of Divalent Cations”. eng. In: *Langmuir : the ACS journal of surfaces and colloids* 33.14. Journal Article, pp. 3349–3357. DOI: `10.1021/acs.langmuir.6b04470`. eprint: `28332396`.

Haugen, Å., M. A. Fernø, G. Mason, and N. R. Morrow (2014). “Capillary pressure and relative permeability estimated from a single spontaneous imbibition test”. In: *Journal of Petroleum Science and Engineering* 115. PII: S0920410514000242, pp. 66–77. ISSN: 09204105. DOI: `10.1016/j.petrol.2014.02.001`.

Healy, Robert N., Ronald L. Reed, and Clarence W. Carpenter (1975). “A Laboratory Study of Microemulsion Flooding (includes associated papers 6395 and 6396)”. In: *Society of Petroleum Engineers Journal* 15.01, pp. 87–103. ISSN: 0197-7520. DOI: `10.2118/4752-PA`.

Hornyak, Gábor Louis (2009). *Fundamentals of nanotechnology*. eng. Boca Raton, Fla.: CRC Press/Taylor & Francis. 780 pp. ISBN: 9781420048032.

Huh, Chun, Hugh Daigle, Valentina Prigiobbe, and Masa Prodanovic (2019). *Practical nanotechnology for petroleum engineers*. Huh, Chun, (author.) Daigle, Hugh, (author.) Prigiobbe, Valentina, (author.) Prodanovic, Masa, (author.) Boca Raton: Taylor & Francis a CRC title part of the Taylor & Francis imprint a member of the Taylor & Francis Group the academic division of T&F Informa plc. pages cm. ISBN: 9780815381495.

Jiang, Renfeng, Kewen Li, and Roland Horne (2017). “A Mechanism Study of Wettability and Interfacial Tension for EOR Using Silica Nanoparticles”. In: *SPE Annual Technical Conference and Exhibition*. SPE Annual Technical Conference and Exhibition (San Antonio, Texas, USA, Oct. 9, 2017). Ed. by SPE. Society of Petroleum Engineers. DOI: `10.2118/187096-MS`.

Juarez-Morejon, J. L., H. Bertin, A. Omari, G. Hamon, C. Cottin, G. Bourdarot, and D. Morel (2017). “Spontaneous Imbibition as Indicator of Wettability Change During

Polymer Flooding". In: *IOR 2017 - 19th European Symposium on Improved Oil Recovery*. Ed. by EAGE. Proceedings. EAGE Publications BVNetherlands. DOI: `10.3997/2214-4609.201700334`.

Kamkar, Milad, Parisa Bazazi, Aadithya Kannan, Vineeth Chandran Suja, Seyed Hossein Hejazi, Gerald G. Fuller, and Uttandaraman Sundararaj (2020). "Polymeric-Nanofluids Stabilized Emulsions: Interfacial versus Bulk Rheology". In: *Journal of colloid and interface science*. ISSN: 0021-9797. DOI: `10.1016/j.jcis.2020.04.105`.

Kantzas, A., M. Pow, K. Allsopp, and D. Marentette (1997). "Co-Current And Counter-Current Imbibition Analysis For Tight Fractured Carbonate Gas Reservoirs". In: *Technical Meeting / Petroleum Conference of The South Saskatchewan Section*. Ed. by SPE. Petroleum Society of Canada. DOI: `10.2118/97-181`.

Kazempour, Mahdi, Eduardo J. Manrique, Vladimir Alvarado, Jieyuan Zhang, and Michael Lantz (2013). "Role of active clays on alkaline–surfactant–polymer formulation performance in sandstone formations". In: *Fuel* 104, pp. 593–606. ISSN: 00162361. DOI: `10.1016/j.fuel.2012.04.034`.

Khajehpour, Maryam, S. Reza Etminan, Jon Goldman, Fred Wassmuth, and Steven Bryant (2018). "Nanoparticles as Foam Stabilizer for Steam-Foam Process". In: *SPE Journal* 23.06, pp. 2232–2242. ISSN: 1086-055X. DOI: `10.2118/179826-PA`.

Kim, Ijung, Andrew J. Worthen, Mohammad Lotfollahi, Keith P. Johnston, David A. DiCarlo, and Chun Huh (2016). "Nanoparticle-Stabilized Emulsions for Improved Mobility Control for Adverse-mobility Waterflooding". In: DOI: `10.2118/179644-MS`.

Kim, Kyoung-Min, Hye Min Kim, Won-Jae Lee, Chang-Woo Lee, Tae-il Kim, Jong-Kwon Lee, Jayoung Jeong, Seung-Min Paek, and Jae-Min Oh (2014). "Surface treatment of silica nanoparticles for stable and charge-controlled colloidal silica". eng. In: *International journal of nanomedicine* 9 Suppl 2, pp. 29–40. DOI: `10.2147/IJN.S57922`.

Kondiparty, Kirti, Alex Nikolov, Stanley Wu, and Darsh Wasan (2011). "Wetting and spreading of nanofluids on solid surfaces driven by the structural disjoining pressure: statics analysis and experiments". eng. In: *Langmuir : the ACS journal of surfaces and colloids* 27, pp. 3324–3335. DOI: `10.1021/la104204b`.

Krüss Scientific (2018). *Spinning Drop Tensiometer SDT - KRÜSS GmbH*. en. URL: `\url{https://www.kruss-scientific.com/products/tensiometers/spinning-drop-tensiometer-sdt/}` (visited on 01/03/2020).

Kuang, Wendi, Soheil Saraji, and Mohammad Piri (2018). "A systematic experimental investigation on the synergistic effects of aqueous nanofluids on interfacial properties and their implications for enhanced oil recovery". In: *Fuel* 220, pp. 849–870. ISSN: 00162361. DOI: `10.1016/j.fuel.2018.01.102`.

Kumar, Narendra, Tushar Gaur, and Ajay Mandal (2017). "Characterization of SPN Pickering emulsions for application in enhanced oil recovery". In: *Journal of Industrial and Engineering Chemistry* 54, pp. 304–315. ISSN: 1226086X. DOI: `10.1016/j.jiec.2017.06.005`.

Kumar, Rahul, Eric Khoi Dao, and Kishore K. Mohanty (2010). "Emulsion Flooding of Heavy Oil". In: *SPE Improved Oil Recovery Symposium*. SPE Improved Oil Recovery Symposium (Tulsa, Oklahoma, USA, Apr. 24, 2010). Ed. by SPE. Society of Petroleum Engineers. DOI: `10.2118/129914-MS`.

Lake, Larry W. (1989). *Enhanced oil recovery*. eng. Englewood Cliffs, NJ: Prentice Hall. 550 pp. ISBN: 0132816016.

León-Pabón, John-Alexander, Tito-Javier Mejía-Pilonieta, Luis-Felipe Carrillo-Moreno, Hernando Buendía-Lombana, José-Francisco Zapata, and Carlos-Andrés Díaz-Prada (2014). "EXPERIMENTAL COMPARISON FOR THE CALCULATION OF ROCK WETTABILITY USING THE AMOTT-HARVEY METHOD AND A NEW VISUAL METHOD". In: *CT&F - Ciencia, Tecnología y Futuro* 5, pp. 5–22. ISSN: 0122-5383.

Li, Shidong, Daniel Dan, Hon Chung Lau, Nanji J. Hadia, Ole Torsæter, and Ludger P. Stubbs (2019a). "Investigation of Wettability Alteration by Silica Nanoparticles Through Advanced Surface-Wetting Visualization Techniques". In: *SPE Annual Technical Conference and Exhibition*. SPE Annual Technical Conference and Exhibition (Calgary, Alberta, Canada, Sept. 23, 2019). Ed. by SPE. Society of Petroleum Engineers. DOI: 10.2118/196192-MS.

Li, Shidong, Ole Torsæter, Hon Chung Lau, Nanji J. Hadia, and Ludger P. Stubbs (2019b). "The Impact of Nanoparticle Adsorption on Transport and Wettability Alteration in Water-Wet Berea Sandstone: An Experimental Study". In: *Frontiers in Physics* 7, P1476. DOI: 10.3389/fphy.2019.00074.

Liesegang, Moritz, Ralf Milke, Christine Kranz, and Gregor Neusser (2017). "Silica nanoparticle aggregation in calcite replacement reactions". eng. In: *Scientific reports* 7.1. Journal Article Research Support, Non-U.S. Gov't Journal Article Research Support, Non-U.S. Gov't, p. 14550. DOI: 10.1038/s41598-017-06458-8. eprint: 29109392.

Linstrom, Peter (2020). *NIST Chemistry WebBook, NIST Standard Reference Database 69*. DOI: 10.18434/T4D303. URL: \url{https://webbook.nist.gov/cgi/fluid.cgi?ID=C124389&Action=Page}.

Lüftenegger, Markus and Torsten Clemens (2017). "Chromatography Effects in Alkali Surfactant Polymer Flooding". In: *SPE Europec featured at 79th EAGE Conference and Exhibition*. SPE Europec featured at 79th EAGE Conference and Exhibition (Paris, France, June 12, 2017). Ed. by SPE. Society of Petroleum Engineers. DOI: 10.2118/185793-MS.

Lyons, William (2009). *Working Guide to Reservoir Engineering*. eng. 1. Aufl. s.l.: Elsevier professional. 0 pp. ISBN: 978-1-85617-824-2. URL: \url{http://search.ebscohost.com/login.aspx?direct=true&scope=site&db=nlebk&db=nlabk&AN=298006}.

Ma, C. and R. A. Eggleton (1999). "Cation Exchange Capacity of Kaolinite". In: *Clays and Clay Minerals* 47, pp. 174–180. ISSN: 0009-8604. DOI: 10.1346/CCMN.1999.0470207.

Magnabosco, Giulia, Iryna Polishchuk, Francesco Palomba, Enrico Rampazzo, Luca Prodi, Joanna Aizenberg, Boaz Pokroy, and Giuseppe Falini (2019). "Effect of Surface Chemistry on Incorporation of Nanoparticles within Calcite Single Crystals". In: *Crystal Growth & Design* 19.8, pp. 4429–4435. ISSN: 1528-7483. DOI: 10.1021/acs.cgd.9b00208.

McPhee, Colin, Jules Reed, and Izaskun Zubizarreta (2015). *Core analysis. A best practice guide*. eng. Vol. volume 64. Developments in petroleum science. McPhee, Colin (VerfasserIn) Reed, Jules (VerfasserIn) Zubizarreta, Izaskun (VerfasserIn) McPhee, Colin (VerfasserIn) Reed, Jules (VerfasserIn) Zubizarreta, Izaskun (VerfasserIn). Amsterdam: Elsevier. 829 pp. ISBN: 9780444636577. URL: \url{http://www.sciencedirect.com/}.

Meng, Qingbang, Huiqing Liu, and Jing Wang (2017). “A critical review on fundamental mechanisms of spontaneous imbibition and the impact of boundary condition, fluid viscosity and wettability”. In: *Advances in Geo-Energy Research* 1, pp. 1–17. ISSN: 22079963. DOI: 10.26804/ager.2017.01.01.

Metin, Cigdem O., Larry W. Lake, Caetano R. Miranda, and Quoc P. Nguyen (2011). “Stability of aqueous silica nanoparticle dispersions”. In: *Journal of Nanoparticle Research* 13, pp. 839–850. ISSN: 1388-0764. DOI: 10.1007/s11051-010-0085-1.

Mohnot, S. M., J. H. Bae, and W. L. Foley (1987). “Study of Mineral/Alkali Reactions”. In: *SPE Reservoir Engineering* 2.04. ISSN: 0885-9248. DOI: 10.2118/13032-PA.

Morrow, Norman R. and Geoffrey Mason (2001). “Recovery of oil by spontaneous imbibition”. In: *Current Opinion in Colloid & Interface Science* 6, pp. 321–337. ISSN: 13590294. DOI: 10.1016/S1359-0294(01)00100-5.

Nanoscience Instruments (2020). *Surface Free Energy*. URL: \url{https://www.nanoscience.com/techniques/tensiometry/surface-free-energy/} (visited on 04/23/2020).

Narr, Wayne (2011). *Characterization of naturally fractured reservoirs*. eng. Society of Petroleum Engineers (U.S.) and ebrary, Inc. URL: \url{http://site.ebrary.com/lib/alltitles/docDetail.action?docID=10619559}.

Negin, Chegenizadeh, Saeedi Ali, and Quan Xie (2017). “Most common surfactants employed in chemical enhanced oil recovery”. In: *Petroleum* 3, pp. 197–211. ISSN: 24056561. DOI: 10.1016/j.petlm.2016.11.007.

Neubauer, Elisabeth, Rafael E. Hincapie, Torsten Clemens, and Maximilian Cornelius (2020). “Selection Of Nanomaterials As Emulsion Stabilizers In Alkali-polymer EOR Of High Tan Number Oil”. In: *SPE Improved Oil Recovery Conference*. SPE Improved Oil Recovery Conference (Tulsa, Oklahoma). Ed. by SPE. SPE-200411-MS. SPE.

Nooruddin, Hasan A. and Martin J. Blunt (2016). “Analytical and numerical investigations of spontaneous imbibition in porous media”. en. In: *Water Resources Research* 52, pp. 7284–7310. ISSN: 00431397. DOI: 10.1002/2015WR018451. URL: \url{https://agupubs.onlinelibrary.wiley.com/doi/full/10.1002/2015WR018451}.

Ohshima, Hiroyuki (2012). *Electrical phenomena at interfaces and biointerfaces. Fundamentals and applications in nano-, bio-, and environmental sciences*. eng. Hoboken: Wiley. 850 pp. ISBN: 9781118135419. DOI: 10.1002/9781118135440. URL: \url{http://site.ebrary.com/lib/alltitles/docDetail.action?docID=10529303}.

Omurlu, Cigdem, H. Pham, and Q. P. Nguyen (2016). “Interaction of surface-modified silica nanoparticles with clay minerals”. In: *Applied Nanoscience* 6, pp. 1167–1173. ISSN: 2190-5509. DOI: 10.1007/s13204-016-0534-y.

PanTerra (2020). *Equipment Sales and Laboratory Design - PanTerra*. URL: \url{https://www.panterra.nl/services/equipment-sales-laboratory-design/} (visited on 03/20/2020).

Perazzo, Antonio, Giovanna Tomaiuolo, Valentina Preziosi, and Stefano Guido (2018). “Emulsions in porous media: From single droplet behavior to applications for oil recovery”. eng. In: *Advances in colloid and interface science* 256, pp. 305–325. DOI: 10.1016/j.cis.2018.03.002.

Peters, Ekwere J. (2012). *Advanced petrophysics*. eng. Austin, Tex.: Live Oak. 268 pp. ISBN: 9781936909476.

Pham, Hieu and Quoc P. Nguyen (2014). “Effect of silica nanoparticles on clay swelling and aqueous stability of nanoparticle dispersions”. eng. In: *Journal of Nanoparticle Research* 16, p. 2137. ISSN: 1388-0764. DOI: `10.1007/s11051-013-2137-9`.

Pickering, Spencer Umfreville (1907). “CXCVI.—Emulsions”. In: *J. Chem. Soc., Trans.* 91.0, pp. 2001–2021. ISSN: 0368-1645. DOI: `10.1039/CT9079102001`.

Pinder, George Francis and William Guerin Gray (2008). *Essentials of multiphase flow and transport in porous media*. eng. Hoboken, NJ: Wiley-Interscience. ISBN: 9780470317624. DOI: `10.1002/9780470380802`. URL: `\url{http://site.ebrary.com/lib/alltitles/docDetail.action?docID=10250340}`.

Raffa, Patrizio and Pablo Druetta (2019). *Chemical enhanced oil recovery. Advances in polymer flooding and nanotechnology*. In English. De Gruyter STEM. Raffa, Patrizio (Verfasser.) Druetta, Pablo (Verfasser.) Raffa, Patrizio, (author.) Druetta, Pablo, (author.) Berlin and Boston: De Gruyter. 1 online resource. ISBN: 3110640252.

Rognmo, A. U., S. Heldal, and M. A. Fernø (2018). “Silica nanoparticles to stabilize CO2-foam for improved CO2 utilization: Enhanced CO2 storage and oil recovery from mature oil reservoirs”. In: *Fuel* 216, pp. 621–626. ISSN: 00162361. DOI: `10.1016/j.fuel.2017.11.144`.

Rostami, Peyman, Mohammad Sharifi, Babak Aminshahidy, and Jalal Fahimpour (2019). “The effect of nanoparticles on wettability alteration for enhanced oil recovery: micromodel experimental studies and CFD simulation”. In: *Petroleum Science* 16, pp. 859–873. ISSN: 1672-5107. DOI: `10.1007/s12182-019-0312-z`.

Rücker, M. et al. (2019). “The Effect of Mixed Wettability on Pore–Scale Flow Regimes Based on a Flooding Experiment in Ketton Limestone”. In: *Geophysical Research Letters* 46.6, pp. 3225–3234. ISSN: 0094-8276. DOI: `\url{10.1029/2018GL081784}`.

Samanta, Abhijit, Keka Ojha, and Ajay Mandal (2011). “Interactions between Acidic Crude Oil and Alkali and Their Effects on Enhanced Oil Recovery”. In: *Energy & Fuels* 25, pp. 1642–1649. ISSN: 0887-0624. DOI: `10.1021/ef101729f`.

Sayyouh, M. H., A. S. Dahab, and A. E. Omar (1990). “Effect of clay content on wettability of sandstone reservoirs”. In: *Journal of Petroleum Science and Engineering* 4, pp. 119–125. ISSN: 09204105. DOI: `10.1016/0920-4105(90)90020-4`.

Schechter, D.S, D. Zhou, and F.M Orr (1994). “Low IFT drainage and imbibition”. In: *Journal of Petroleum Science and Engineering* 11, pp. 283–300. ISSN: 09204105. DOI: `10.1016/0920-4105(94)90047-7`.

Schön, Jürgen H. and A. Dasgupta (2015). *Physical properties of rocks. Fundamentals and principles of petrophysics*. eng. 2nd. ed. Vol. Volume 65. Developments in petroleum science. Amsterdam u. a.: Elsevier. 497 pp. ISBN: 9780081004043.

Schumi, Bettina, Torsten Clemens, Jonas Wegner, Leonhard Ganzer, Anton Kaiser, Rafael E. Hincapie, and Verena Leitenmüller (2019). “Alkali Co-Solvent Polymer Flooding of High TAN Number Oil: Using Phase Experiments, Micro-Models and Corefloods for Injection Agent Selection”. In: *SPE Europec featured at 81st EAGE Conference and Exhibition*. SPE Europec featured at 81st EAGE Conference and Exhibition (London, England, UK, June 3, 2019). Ed. by SPE. Society of Petroleum Engineers. DOI: `10.2118/195504-MS`.

Shamekhi, Hani, Apostolos Kantzas, Jonathan Luke Bryan, and Shi Su (2013). “Insights into Heavy Oil Recovery by Surfactant, Polymer and ASP Flooding”. In:

SPE Heavy Oil Conference-Canada. SPE Heavy Oil Conference-Canada (Calgary, Alberta, Canada, June 11, 2013). Ed. by SPE. Society of Petroleum Engineers. DOI: 10.2118/165440-MS.

ShamsiJazeyi, Hadi, Clarence A. Miller, Michael S. Wong, James M. Tour, and Rafael Verduzco (2014). "Polymer-coated nanoparticles for enhanced oil recovery". In: *Journal of Applied Polymer Science* 131, n/a–n/a. ISSN: 00218995. DOI: 10.1002/app.40576.

Sharma, M. K. and Shah D. O. (1985). "Introduction to Macro- and Microemulsions". In: *ACS Symposium Series; American Chemical Society* 272, pp. 1–18. DOI: 10.1021/bk-1985-0272.ch001. URL: \url{http://pubs.acs.org/doi/abs/10.1021/bk-1985-0272.ch001}.

Sharma, M. M., L. K. Jang, and T. F. Yen (1989). "Transient Interfacial Tension Behavior of Crude-Oil/Caustic Interfaces". In: *SPE Reservoir Engineering* 4.02, pp. 228–236. ISSN: 0885-9248. DOI: 10.2118/12669-PA.

Sharma, Tushar, Stefan Iglauer, and Jitendra S. Sangwai (2016). "Silica Nanofluids in an Oilfield Polymer Polyacrylamide: Interfacial Properties, Wettability Alteration, and Applications for Chemical Enhanced Oil Recovery". In: *Industrial & Engineering Chemistry Research* 55, pp. 12387–12397. ISSN: 0888-5885. DOI: 10.1021/acs.iecr.6b03299.

Sharma, Tushar, G. Suresh Kumar, Bo Hyun Chon, and Jitendra S. Sangwai (2015). "Thermal stability of oil-in-water Pickering emulsion in the presence of nanoparticle, surfactant, and polymer". In: *Journal of Industrial and Engineering Chemistry* 22, pp. 324–334. ISSN: 1226086X. DOI: 10.1016/j.jiec.2014.07.026.

Sheng, James (2011). *Modern chemical enhanced oil recovery. Theory and practice*. Amsterdam, Boston, and Burlington, Mass.: Elsevier and Gulf Professional Pub. 1 online resource. ISBN: 9781856177450.

— (2015a). "Status of Alkaline Flooding Technology". In: pp. 44–50.

Sheng, James J. (2013). *Enhanced oil recovery. Field case studies*. eng. Amsterdam: Elsevier/GPP Gulf Professional Publ. 685 pp. ISBN: 9780123865465.

— (2015b). "Investigation of alkaline–crude oil reaction". In: *Petroleum* 1, pp. 31–39. ISSN: 24056561. DOI: 10.1016/j.petlm.2015.04.004.

Singh, Robin and Kishore K. Mohanty (2017). "Foam flow in a layered, heterogeneous porous medium: A visualization study". In: *Fuel* 197, pp. 58–69. ISSN: 00162361. DOI: 10.1016/j.fuel.2017.02.019.

Sofla, Saeed Jafari Daghlian, Lesley Anne James, and Yahui Zhang (2019). "Toward a mechanistic understanding of wettability alteration in reservoir rocks using silica nanoparticles". In: *E3S Web of Conferences* 89, p. 03004. DOI: 10.1051/e3sconf/20198903004.

Sofla, Saeed Jafari Daghlian, Lesley Anne James, and Yahui Zhang (2019). "Understanding the behavior of H+-protected silica nanoparticles at the oil-water interface for enhanced oil recovery (EOR) applications". In: *Journal of Molecular Liquids* 274, pp. 98–114. ISSN: 01677322. DOI: 10.1016/j.molliq.2018.09.049.

Somerton, W. H. and C. J. Radke (1983). "Role of Clays in the Enhanced Recovery of Petroleum From Some California Sands". In: *Journal of Petroleum Technology* 35.03, pp. 643–654. ISSN: 0149-2136. DOI: 10.2118/8845-PA.

Spanos, Nikos and Petros G. Koutsoukos (1998). “Kinetics of Precipitation of Calcium Carbonate in Alkaline pH at Constant Supersaturation. Spontaneous and Seeded Growth”. In: *The Journal of Physical Chemistry B* 102, pp. 6679–6684. ISSN: 1520-6106. DOI: 10.1021/jp981171h.

Speight, James G. (2016). *Introduction to enhanced recovery methods for heavy oil and tar sands*. eng. Second edition. Speight, James G. (VerfasserIn). Cambridge, MA: Gulf Professional Publishing is an imprint of Elsevier. ISBN: 9780128499061. URL: \url{http://www.sciencedirect.com/science/book/9780128499061}.

Standnes, Dag Chun (2004). “Analysis of oil recovery rates for spontaneous imbibition of aqueous surfactant solutions into preferential oil-wet carbonates by estimation of capillary diffusivity coefficients”. In: *Colloids and Surfaces A: Physicochemical and Engineering Aspects* 251, pp. 93–101. ISSN: 09277757. DOI: 10.1016/j.colsurfa.2004.09.013.

Sun, Xiaofei, Yanyu Zhang, Guangpeng Chen, and Zhiyong Gai (2017). “Application of Nanoparticles in Enhanced Oil Recovery: A Critical Review of Recent Progress”. In: *Energies* 10, p. 345. DOI: 10.3390/en10030345.

Taghavi, Sayed Mohammad, Mahdiye Momenpour, Maryam Azarian, Mohammad Ahmadian, Faramarz Souri, Sayed Ali Taghavi, Marzieh Sadeghain, and Mohsen Karchani (2013). “Effects of Nanoparticles on the Environment and Outdoor Workplaces”. eng. In: *Electronic physician* 5.4. Journal Article Review, pp. 706–712. ISSN: 2008-5842. DOI: \url{10.14661/2013.706-712}. eprint: 26120406.

Tiab, Djebbar and Erle C. Donaldson (2012). *Petrophysics. Theory and practice of measuring reservoir rock and fluid transport properties*. 3rd ed. Amsterdam and Boston: Gulf Professional Pub. xx, 950. ISBN: 9780123838483.

Torsæter, Ole and Manoochehr Abtahi (2003). *Experimental reservoir engineering. laboratory workbook*. 1st ed. This book is intended primarily as a text in the course SIG4015 Reservoir Property Determination by Core Analysis and Well Testing at the Norwegian University of Science and Technology. Part of this course introduces the basic laboratory equipment and procedures used in core analysis and the theoretical aspects of the parameters. The book also includes detailed description of laboratory exercises suitable for student work. NTNU. URL: \url{https://www.spec2000.net/downloads/LabManual.pdf}.

van Oss, Carel Jan (2008). “The Extended DLVO Theory”. In: *The properties of water and their role in colloidal and biological systems*. Ed. by Carel J. van Oss. 1. ed. Vol. 16. Interface Science and Technology 16. Amsterdam: Elsevier/Acad. Press, pp. 31–48. ISBN: 9780123743039. DOI: 10.1016/S1573-4285(08)00203-2.

Vatanparast, Hamid, Farshid Shahabi, Alireza Bahramian, Aliyar Javadi, and Reinhard Miller (May 2018). “The Role of Electrostatic Repulsion on Increasing Surface Activity of Anionic Surfactants in the Presence of Hydrophilic Silica Nanoparticles”. In: *Scientific Reports* 8.1. DOI: 10.1038/s41598-018-25493-7. URL: https://doi.org/10.1038/s41598-018-25493-7.

Viades-Trejo, Josefina and Jesús Gracia-Fadrique (2007). “Spinning drop method. From Young–Laplace to Vonnegut”. In: *Colloids and Surfaces A: Physicochemical and Engineering Aspects* 302, pp. 549–552. ISSN: 09277757. DOI: 10.1016/j.colsurfa.2007.03.033.

Wang, Xiao, Senbo Xiao, Zhiliang Zhang, and Jianying He (2017). "Effect of Nanoparticles on Spontaneous Imbibition of Water into Ultraconfined Reservoir Capillary by Molecular Dynamics Simulation". In: *Energies* 10, p. 506. DOI: 10.3390/en10040506.

Wasan, Darsh T. and Alex D. Nikolov (2003). "Spreading of nanofluids on solids". eng. In: *Nature* 423, pp. 156–159. ISSN: 0028-0836. DOI: 10.1038/nature01591.

Winsor, P. A. (1956). "P. A. Winsor, Solvent Properties of Amphiphilic Compounds. Butterworths Scientific Publications. London, 207 S. mit zahlr. Tabb. u. Abb. Preis £ 40.—". In: *Fette, Seifen, Anstrichmittel* 58, pp. 1103–1104. ISSN: 0015038X. DOI: 10.1002/lipi.19560581222.

Xin, Xiankang, Gaoming Yu, Zhangxin Chen, Keliu Wu, Xiaohu Dong, and Zhouyuan Zhu (2018). "Effect of Polymer Degradation on Polymer Flooding in Heterogeneous Reservoirs". eng. In: *Polymers* 10. DOI: 10.3390/polym10080857.

Xu, Derong, Baojun Bai, Hairong Wu, Jirui Hou, Ziyu Meng, Renxian Sun, Zhe Li, Yao Lu, and Wanli Kang (2019). "Mechanisms of imbibition enhanced oil recovery in low permeability reservoirs: Effect of IFT reduction and wettability alteration". In: *Fuel* 244, pp. 110–119. ISSN: 00162361. DOI: 10.1016/j.fuel.2019.01.118.

Yang, Ling and Daniel J. Watts (2005). "Particle surface characteristics may play an important role in phytotoxicity of alumina nanoparticles". eng. In: *Toxicology letters* 158.2. Journal Article Research Support, Non-U.S. Gov't, pp. 122–132. ISSN: 0378-4274. DOI: \url{10.1016/j.toxlet.2005.03.003}. eprint: 16039401.

Yeganeh, Mohsen, Jessica Hegner, Eric Lewandowski, Aruna Mohan, Larry W. Lake, Dan Cherney, Arben Jusufi, and Aditya Jaishankar (2016). "Capillary Desaturation Curve Fundamentals". In: *SPE Improved Oil Recovery Conference*. SPE. SPE Improved Oil Recovery Conference (Tulsa, Oklahoma, USA, Apr. 11, 2016). Ed. by SPE. Society of Petroleum Engineers. DOI: 10.2118/179574-MS.

Yekeen, Nurudeen, Muhammad A. Manan, Ahmad Kamal Idris, Eswaran Padmanabhan, Radzuan Junin, Ali Mohamed Samin, Afeez O. Gbadamosi, and Ifeanyi Oguamah (2018). "A comprehensive review of experimental studies of nanoparticles-stabilized foam for enhanced oil recovery". In: *Journal of Petroleum Science and Engineering* 164, pp. 43–74. ISSN: 09204105. DOI: 10.1016/j.petrol.2018.01.035.

Youssef, Souhail, Yannick Peysson, Daniela Bauer, and Daniela Vizika (2015). "Capillary Desaturation Curve Prediction Using 3D Microtomography Images". In: *SCA*.

Yu, Jiapeng and Hao Wang (2012). "Thin-film phase change driven by disjoining pressure difference". In: *Heat and Mass Transfer* 48, pp. 1135–1140. ISSN: 0947-7411. DOI: 10.1007/s00231-012-0967-0.

Zhou, D., L. Jia, J. Kamath, and A.R Kovscek (2002). "Scaling of counter-current imbibition processes in low-permeability porous media". In: *Journal of Petroleum Science and Engineering* 33, pp. 61–74. ISSN: 09204105. DOI: 10.1016/S0920-4105(01)00176-0.